

Alma Mater Studiorum – Università di Bologna

DOTTORATO DI RICERCA IN  
Biologia Cellulare e Molecolare

Ciclo XXXII

Settore Concorsuale: 03/C1

Settore Scientifico Disciplinare: CHIM/06

**AMPLIFICATION STRATEGIES IN DNA BASED  
BIOSENSORS FOR MIRNA DETECTION**

**Presentata da: Andrea Miti**

**Coordinatore Dottorato**

**Prof. Giovanni Capranico**

**Supervisore**

**Dott. Giampaolo Zuccheri**

**Esame finale anno 2020**

# **Amplification strategies in DNA based biosensors for miRNA detection**

## Abstract

DNA biosensors have attracted great attention in the last years thanks to the application perspectives in many fields such as environmental analysis, food safety and diagnostics. The versatility of DNA as tool can be exploited to build nanotechnological devices, improving the detection of a broad variety of analytes in real time, thanks to the implementation on the proper technological platforms. Nowadays, new diagnostic tools are required for the sensitive detection of biomarkers in human samples, towards the replacement or the integration of common lab-based detection methods. MicroRNAs are very interesting biomarkers for many reasons: their role and deregulation in pathological processes, their specific expression, and their stability in body fluids. The challenge in their detection is related to their short sequences (20-23 nt), their low concentration and the high sequence homology between different miRNAs. Common lab-based techniques often struggle in efficiently detecting them because of the preparation required, the complex instrumentation needed and the lack of sensitivity. Moreover, these techniques are not conceptually adaptable to a fast diagnosis and point-of-care applications. DNA based biosensors represent a valid alternative to these techniques, providing new detection methods able to support the common analytical strategies or replace them. In this class of sensors, DNA is employed as bioreceptor and it interacts directly with the specific nucleic acid target, returning a signal, potentially with a reduced time of analysis. Biosensors in general can provide high sensitivity and many examples are reported about biosensors working in complex media, avoiding samples purifications. The peculiar features of DNA allow the design of a specific processes that can enhance the sensitivity and the general performances of the detection. DNA nanotechnology can furnish new tools to improve the sensitivity and the recognition mechanisms of such sensors. We worked towards the development and the application of new strategies and nanotechnological tools to improve the sensitivity of DNA based biosensors for miRNA detection. Hybridization Chain Reaction is an isothermal amplification process based on the self-assembly of DNA strands in solution. HCR can be used to improve DNA based biosensors leading to an enhanced response upon target detection. In our lab, we have experience in the design of DNA assemblies, and we designed HCR amplification to detect specific miRNAs. After the characterization in solution, we worked towards the implementation on electrochemical sensing platform and in sensing based on Localized Surface Plasmon Resonance in order to evaluate the enhancement in sensitivity reachable with HCR. Although electrochemical detection has still to be improved and optimization of the electrochemical setup is required, we proved the effect of the self-assembling reaction. Better results were obtained in the LSPR setup that allowed performing the detection of the target in real time and in a label-free manner. Using the LSPR detection we were able to detect the target miR-17 in buffer with a limit of detection of 1 nM, and we improved it to 1 pM using HCR.

In parallel, we designed an alternative detection method employing a triple helix probe, involving a double hybridization chain reaction able to induce the formation of bigger nanostructure to induce a greater amplification. The aim was to investigate new methods to further improve the sensitivity of DNA based biosensors. This was done by exploiting the two triple helix forming strands, both used to induce a response after target detection, in a strategy never reported in literature. In principle, this strategy would allow the combination of different transduction methods and the adaptation to multiplexed detection. We demonstrated the working principle of this method and performed preliminary experiments in electrochemical detection of microRNAs. In line with our aim, during the work, we explored alternative strategies to enhance the response of DNA based biosensors, for instance investigating the possibility to employ DNA templated Ag/Pt nanoclusters in sensing applications. We were able to characterize their formation and work on the application in sensing thanks to a collaboration.

# Index

<b>ABSTRACT</b> .....	<b>3</b>
<b>SHORT CV</b> .....	ERRORE. IL SEGNALIBRO NON È DEFINITO.
<b>INDEX</b> .....	<b>5</b>
<b>1 INTRODUCTION</b> .....	<b>8</b>
1.1 MICRORNAS AS BIOMARKERS .....	8
1.1.1 <i>MicroRNA detection</i> .....	10
1.2 BIOSENSORS .....	11
1.3 ELECTROCHEMICAL BIOSENSORS .....	13
1.3.1 <i>Electrochemical techniques for biosensing</i> .....	14
1.4 SURFACE PLASMON RESONANCE (SPR) .....	16
1.5 METAL NANOPARTICLES IN BIOSENSING .....	17
1.5.1 <i>Gold nanoparticles</i> .....	18
1.5.2 <i>Localized Surface Plasmon Resonance (LSPR)</i> .....	19
1.5.3 <i>DNA templated Silver/Pt nanoclusters</i> .....	21
1.6 DNA NANOTECHNOLOGY AND BIOSENSING .....	22
1.6.1 <i>Structural DNA nanotechnology in biosensing</i> .....	22
1.6.2 <i>Dynamic DNA nanotechnology in biosensing</i> .....	23
1.6.3 <i>Alternative DNA structures as DNA probes</i> .....	25
1.7 HYBRIDIZATION CHAIN REACTION .....	26
1.7.1 <i>HCR in biosensing</i> .....	27
<b>2 AIM OF THE STUDY</b> .....	<b>31</b>
<b>3 MATERIALS AND METHODS</b> .....	<b>32</b>
3.1 REAGENTS AND BUFFERS .....	32
3.2 DESIGN OF THE OLIGONUCLEOTIDES .....	32
3.2.1 <i>Design of the sequences for direct HCR reaction</i> .....	33
3.2.2 <i>Design of the sequences for triplex HCR</i> .....	34
3.3 CHARACTERIZATION OF THE DIRECT HCR IN SOLUTION .....	36
3.3.1 <i>Characterization of the product of direct HCR through electrophoresis gel analysis</i> .....	36
3.3.2 <i>Characterization of the product of direct HCR through Atomic Force Microscopy</i> .....	36
3.4 CHARACTERIZATION OF THE TRIPLEX HCR IN SOLUTION .....	37
3.4.1 <i>Characterization of the triple helix in gel electrophoresis</i> .....	37
3.4.2 <i>Circular Dichroism characterization of the triple helix probe</i> .....	37
3.4.3 <i>Characterization of the triplex HCR in solution</i> .....	38
3.5 ELECTROCHEMICAL SETUP .....	38
3.5.1 <i>Preparation of the and functionalization of the TSGs (electrode surfaces)</i> .....	39
3.5.2 <i>Electrochemical measurements</i> .....	40
3.5.3 <i>Electrochemical detection of microRNA sequences through direct HCR</i> .....	40
3.5.4 <i>Electrochemical detection of microRNA sequences through triple helix-controlled HCR</i> .....	40

3.5.5	<i>Analysis of data obtained in electrochemistry</i> .....	41
3.6	LSPR .....	41
3.6.1	<i>Preparation of the LSPR Chips</i> .....	42
3.6.2	<i>Functionalization of the LSPR chips</i> .....	43
3.6.3	<i>LSPR measurements and detection</i> .....	43
3.6.4	<i>Analysis of the LSPR data</i> .....	44
3.7	DNA TEMPLATED MIXED PLATINUM-SILVER NANOCCLUSERS: SYNTHESIS AND CHARACTERIZATION.....	45
<b>4</b>	<b>RESULTS AND DISCUSSION</b> .....	<b>46</b>
4.1	DIRECT HYBRIDIZATION CHAIN REACTION.....	48
4.1.1	<i>Design of direct HCR based detection</i> .....	48
4.1.2	<i>The product of the direct Hybridization Chain Reaction in solution</i> .....	51
4.1.3	<i>The rate of the hybridization chain reaction</i> .....	53
4.1.4	<i>The effect of temperature on the hybridization chain reaction</i> .....	54
4.1.5	<i>The specificity of the direct HCR</i> .....	55
4.1.6	<i>Effect of BSA on direct HCR in solution</i> .....	56
4.1.7	<i>Sensitivity</i> .....	57
4.1.8	<i>Conclusions and observations</i> .....	58
4.2	IMPLEMENTATION OF THE DIRECT HCR ON ELECTROCHEMICAL DETECTION .....	58
4.2.1	<i>Characterization and functionalization of the electrodes</i> .....	58
4.2.2	<i>Detection of miRNA and direct Hybridization Chain Reaction on surface</i> .....	60
4.2.3	<i>Conclusions and observations</i> .....	63
4.3	LSPR BASED DETECTION .....	64
4.3.1	<i>Characterization of the chips</i> .....	66
4.3.2	<i>Detection of miR-17</i> .....	67
4.3.3	<i>Specificity for the detection of miR-17 in the LSPR setup</i> .....	69
4.3.4	<i>Sensitivity of the LSPR-based method without HCR</i> .....	70
4.3.5	<i>Hybridization Chain Reaction in LSPR</i> .....	72
4.3.6	<i>Conclusions and observations</i> .....	77
4.4	TRIPLEX-TRIGGERED HCR.....	79
4.4.1	<i>Design of the sequences of the triplex-triggered HCR</i> .....	81
4.4.2	<i>Characterization of the DNA triple helix probe</i> .....	82
4.4.3	<i>"Sticky" Hybridization Chain Reactions</i> .....	87
4.4.4	<i>miRNA detection</i> .....	90
4.4.5	<i>Electrochemical detection using the triple helix probe</i> .....	92
4.4.6	<i>Conclusions and observations</i> .....	94
4.5	METALLIC NANOPARTICLES AND NANOCCLUSERS AS BIOSENSING TOOLS .....	95
4.5.1	<i>Synthesis and characterization of the DNA templated Ag/Pt nanoclusters</i> .....	96
4.5.2	<i>Spectroscopic analysis of the DNA-templated Ag/Pt nanoclusters</i> .....	96
4.5.3	<i>Morphological characterization of the DNA templated Ag/Pt nanoclusters</i> .....	98
4.5.4	<i>Catalytic activity of the DNA templated Ag/Pt nanoclusters</i> .....	99
4.5.5	<i>Conclusions and observations</i> .....	100

<b>5</b>	<b>CONCLUSIONS .....</b>	<b>101</b>
<b>6</b>	<b>REFERENCES.....</b>	<b>103</b>
<b>APPENDIX.....</b>	<b>ERRORE. IL SEGNALIBRO NON È DEFINITO.</b>	

# 1 Introduction

There is a great interest in the development of new methods for the sensitive and specific detection of nucleic acids biomarkers. DNA based biosensors can be implemented in original and alternative ways for this purpose. During the introduction, we will focus on the needs of innovative analytical tools. We will present an overview of the main biosensing strategies for the detection of biomarkers and especially of nucleic acids, presenting the state of the art and concentrating the attention on short nucleic acids such as microRNAs. We will explain why they are so interesting as biomarkers, its importance and the challenge in the detection, giving some hints about the techniques employed with this purpose. We will present some of the nanotechnological tools we decided to take into account for the development of such devices, introducing DNA nanotechnology and metal nanoparticles.

## 1.1 MicroRNAs as biomarkers

MicroRNAs are small, conserved, endogenous, non-coding RNAs expressed in plants, animals and some viruses. These RNAs are coded in the nucleus through transcription of nuclear DNA, and they can be 20-23 nucleotides in length. They have regulatory roles for the level of expression of genes at transcriptional and post-transcriptional level. Complexed in the RISC protein complex, the miRNA performs its task, able to recognize the mRNA target and lead to its degradation or silencing (O'Brien et al., 2018). In general, in physiological conditions, miRNAs are involved in complex cellular networks with feedback mechanisms which ensure the efficiency of many important biological processes. Researchers proved, and widely reported, the involvement of miRNAs in the main cellular process, such as development, differentiation, apoptosis, proliferation, migration, signal transduction and metabolism (Vidigal and Ventura, 2015, Chandra et al., 2017, Hwang and Mendell, 2006). It is not surprising that, in pathological conditions, the concentration and the activity of microRNAs may be affected (Chandra et al., 2017, Mendell and Olson, 2012, Sayed and Abdellatif, 2011). For instance, many miRNAs are deregulated during tumorigenesis and tumor progression (Calin and Croce, 2006, Sethi et al., 2014, Farazi et al., 2011). The loss or gain of function of specific microRNAs can lead to the increase in the cell plasticity, dedifferentiation and oncogenic transformation. The deregulation of a small group of microRNAs could be enough to induce the progression towards neoplastic transformation of few cells. The detection of the concentration and activities in cells and tissue would provide an important tool towards early and efficient diagnosis of specific pathologies. MiRNAs are very interesting as biomarkers also because they can be released from cells in body fluids such as blood, saliva and urine (Bianchi et al., 2012, Li et al., 2019, Turchinovich et al., 2011).

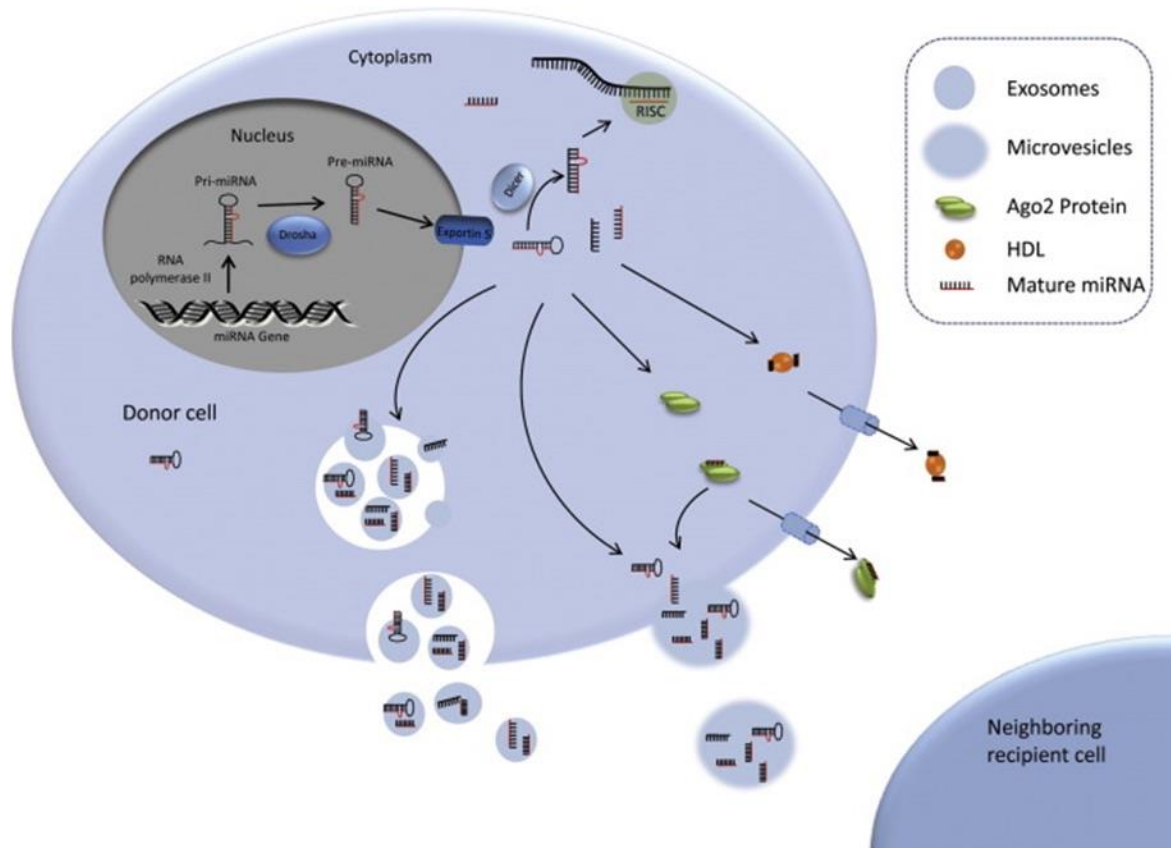


Fig1.1. Scheme of the biogenesis and release of microRNAs by cells. MicroRNAs are coded and in the nucleus as pre-miRNA and then exported in the nucleus where further maturation processes lead to the formation of the mature miRNAs. miRNAs are then complexed in RISC complex or other proteins. miRNAs can then be released either complexed in proteins, in vesicles such as exosomes but also in free forms in exosomes. Reprinted from Sohel 2016 (Image licensed under the Creative Commons Attribution-NonCommercial-NoDerivatives 4.0 International).

MiRNAs may act as hormones, able to regulate the expression of target genes in cells elsewhere in the body. Mechanisms leading to these processes need to be further characterized, but it is proposed that miRNAs could be released after cell damage, inflammation or necrosis, related to pathological conditions (Chen et al., 2008b, Arroyo et al., 2011, Mitchell et al., 2008). The secretion can take place through the formation of vesicles such as exosomes, apoptotic bodies (Zernecke et al., 2009), complexed with lipoproteins (HDL) or RNA binding proteins. Researchers reported the correlation between specific miRNAs in blood and tumor progression (Calin and Croce, 2006, Chen et al., 2008b, Mitchell et al., 2008). Their presence in higher or lower concentration can be used to get information about the status of a pathogenic process for follow-up or diagnosis. Knowing the complexity of the biological networks and the individual biological differences, a more efficient diagnostic strategy should focus on the determination of a group (a signature) of miRNAs informative for the pathological outcome. For instance, in literature many groups of miRNAs are reported as deregulated in patients affected by cancer, but there is a big challenge in finding overlapping evidences because of the lack of standardization and robust methods for their identification. In the case of lung cancer, many signature of miRNAs have been validated (Abd-El-Fattah et al., 2013, Aushev et al., 2013, Bianchi et al., 2012, Geng et al., 2014,

Heegaard et al., 2012, Hennessey et al., 2012, Keller et al., 2011, Qin et al., 2015, Rabinowits et al., 2009). Bianchi and its group identified a group of 34 circulating miRNAs in serum, allowing the assignment of the onset probability of lung cancer in asymptomatic patients (Bianchi et al., 2011). Their work shows how any group of five of these miRNAs are enough to obtain reliable information about the status of the disease. A parallel study performed by Boeri's group revealed a conceptually comparable group of miRNAs also in asymptomatic patients, including 13 miRNAs. Five of these miRNAs are present in Bianchi's diagnostic signature, with the same direction of variation (over or under expression) (Boeri et al., 2011). Known that specific "signature" can be defined and validated. Even if the standardization is one of the main issues, it is undoubtful that the development of new detection methods, with better performances, would guarantee new precious tools towards the diagnosis based on miRNAs, also in combination with existing techniques.

### **1.1.1 MicroRNA detection**

As mentioned before, microRNAs have perfect features as biomarkers: 1) they are well conserved in the genome 2) they are expressed in tissue-specific manner 3) even a low alteration in their concentration can be considered informative 4) microRNAs are very stable in body fluids. Beside the standardization problems, there are problems due to their short length (20-23 nt), their low concentration and the high similarity between different miRNAs. The most common techniques for the detection of microRNAs are northern blot, microarrays, Next Generation Sequencing (NGS) and quantitative real-time PCR (Graybill and Bailey, 2016). NGS allows the generation of a large amount of data from parallel sequencing in a single reaction, and it emerged as one the favorite system for the analysis of the expression of microRNAs. This technique is able to discriminate differences of one base between miRNAs, and the analysis of large number of samples is possible in weeks. The common techniques often are time consuming, expensive, the sample need preparation steps and transfers all over the analysis. The manipulation of the sample leads to higher variability or degradation, affecting the sensitivity. Table 1-1 resumes some features of these techniques, pointing out also at the cost and the time needed for the analysis.

Table 1-1. Common techniques for microRNAs detection and characterization. Reprinted (adapted) with permission from Graybill & Bailey 2016 (Graybill and Bailey, 2016). Copyright (2016) American Chemical Society.

Summary of the common techniques	qRT-PCR	Microarrays	Next Generation Sequencing
<b>Time to result</b>	hours	days	weeks
<b>Cost</b>	\$\$	\$	\$\$\$
<b>Biochemical processing</b>	ligation with T4 (SYBR Green) Annealing of primers	no ligation steps	ligate barcode
<b>Input</b>	low (ng)	large (ng- $\mu$ g)	large (ng- $\mu$ g)
<b>Drawbacks</b>	results need validation long time to result	single plex	do not always need global view

Different microRNAs can act in different ways during the same preparation procedure. In techniques requiring enzymes, such as ligase or polymerase in PCR-based techniques and NGS, the results strongly depend on the purity of the sample or the different method used for the separation. Beside the short length, microRNAs can show great variation in the CG content, affecting the detection efficiency. Alternative techniques could help to overcome the main limitations of these methods, towards the development of easy to use devices allowing faster point of care analysis of nucleic acids (Bellassai and Spoto, 2016, Tavallaie et al., 2015). Biosensors represent a valid alternative, thanks to a broad variety of nanotechnological tools such as Nano and Micro structured surfaces, nanoparticles, self-assembled biomolecules layers, alternative amplification strategies and implementation on different transducers (Tian et al., 2015).

## 1.2 Biosensors

Biosensors are analytical tools, in principle able to bring a big improvement to the detection and quantification of biomarkers such as miRNAs. Biosensors are mainly composed by two elements: the bioreceptor and the transducer. 1) The bioreceptor is responsible for the specificity in the interaction with a target molecule in a complex medium. A large variety of biological elements can be used, such as enzymes, antibodies, nucleic acids, entire cells, tissues, proteins or even cellular receptors (Patel et al., 2016). Antibodies, and DNA have been widely employed in the realization of many immunosensors and DNA based biosensors respectively, for their high specificity and ability to recognize a wide range of analytes (Ronkainen et al., 2010). 2) The transducer is an element designed to convert the capture to a measurable physical signal, such as a fluorescent, electrochemical or even a colorimetric response (Patel et al., 2016). In some biosensors, a signal

processing system is also present, depending on the transduction method and the technology in use. This is required to process the output responses returned by the transducer and show it in an interpretable form.

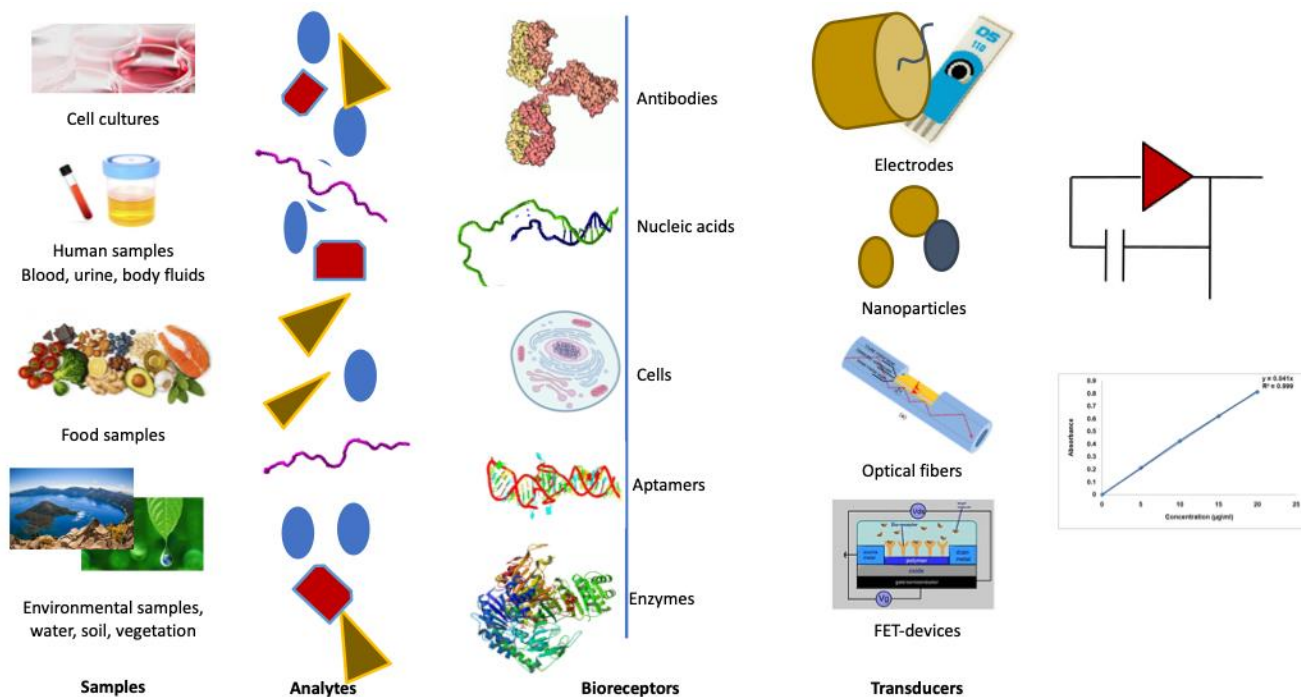


Fig 1-1. Scheme of applications and components of existing biosensors.

In principle, the response can be generated in real time and it is related to the presence of the target and its concentration. Their applications are studied in a wide variety of fields, such as environmental analysis, cells, body fluids, and food industry, allowing real time analysis with low limit of detection and better performances (Malhotra et al., 2005, Perez-Lopez and Merkoci, 2011). Scientific community and the high market demand are always pushing for new strategies to improve these devices and implement them for point of care detection of biomarkers. In combination with microfluidics and miniaturization, it would be possible to design lab-on-chip devices, where different process for sample preparation and analysis are integrated in the same instrument. This allows skipping time-consuming processes and expensive lab facilities without transfers of the samples, contaminations and waste of reagents (Foudeh et al., 2012, Estevez et al., 2012). Nanotechnology helps facing these challenges, providing new tools towards miniaturization of the components, analysis of small volumes of samples with high resolution and efficiency and fine functionalization of materials. We will focus in the next sections on some of the transduction methods applied to biosensing and on some applications in the detection of nucleic acids with DNA based biosensors. This class of biosensors can be very selective and sensitive thanks to the complementarity rules in the formation of base pairs, beside their cheap realization and simple interfacing with a variety of transducing elements (Teles and Fonseca, 2008).

### 1.3 Electrochemical biosensors

Electrochemical biosensors show remarkably high sensitivity, potentially cheap instrumentation is available, and they can be easily implemented in miniaturized devices. Their versatility allows multiplexation and portability for point-of-care analysis of different compounds simultaneously (Abi et al., 2018, Cagnin et al., 2009, Ronkainen et al., 2010, Wang, 2006). An electrochemical reaction involves the flow of charges at the interface between an electrolyte (a species in solution) and a conductive surface, also called electrode.

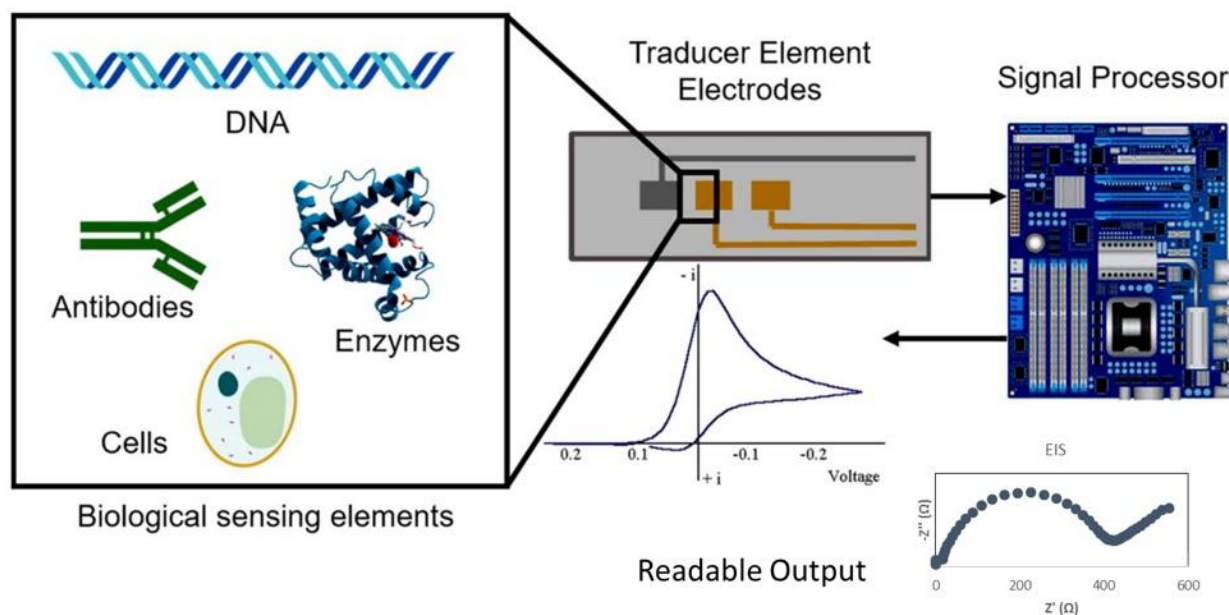


Fig 1-2. Scheme of a general electrochemical biosensor. Readapted from Hernandez-Vargas et al., 2018 (image licensed under Creative Commons license Attribution 4.0 International).

Electrochemical biosensing exploits these kind of phenomena to convert a molecular process to a signal related to the concentration of a specific analyte (Ronkainen et al., 2010). In biocatalytic, electrochemical biosensors the analytes are substrates of a chemical reaction that is catalyzed by the bioreceptor. This is the case of enzymes, or entire cells employed as recognition elements, able to generate an electrochemically detectable product or signal (Wang, 2006). The glucose monitoring devices are the most successful biocatalytic electrochemical sensors (Wang, 2008). These sensors can be realized employing glucose oxidase or glucose dehydrogenase enzymes, able to catalyze, in presence of glucose, a redox reaction that is an electrochemically readable charge transfer. Affinity electrochemical biosensors are instead based just on the specific interaction between the analyte and the receptor. The interaction does not lead to the signal production by itself, but the interaction is converted into a signal response. There are two main possibilities to get information from this interaction: 1) using electroactive labels detectable after the target recognition or 2) detecting some changes in the electrical properties at the interface

between the surface and the medium. A great variety of electrochemical biosensors has been developed using a broad range of molecules, antibodies, nucleic acids, aptamers (Ronkainen et al., 2010, Abi et al., 2018, Navani and Li, 2006). In DNA based biosensors, DNA can be easily immobilized through covalent bond on the electrodes using thiol-gold affinity and electrical parameters can be measured when a hybridization occurs on surface. DNA based electrochemical biosensors could detect in real time nucleic acids biomarkers in the diagnosis of infections, cancer, and other diseases. In addition, aptamers can be developed and implemented on electrochemical sensing for a large variety of analytes with different strategies (Navani and Li, 2006, Song et al., 2008). Nucleic acid based electrochemical biosensors are witnessing an increasing progress with big efforts to obtain innovative nucleic acid based electrochemical sensors with improved performances (Abi et al., 2018, Cagnin et al., 2009, Sassolas et al., 2008).

### **1.3.1 Electrochemical techniques for biosensing**

Electrochemistry includes many techniques for the investigation of conductive surfaces and detection of analytes. In general, an electrochemical biosensor is part of an electrochemical cell, allowing us monitoring of the occurring phenomena. A typical three-electrode electrochemical cell is composed by three elements: a working electrode, usually a conductive and stable material such as gold; a reference electrode often consisting in a silver component coated with a silver chloride AgCl layer (Ag/AgCl); a counter or auxiliary electrode, such as a platinum wire. The phenomena that we want to measure take place at the working electrode. The charges flow through the counter and the working electrode, while the reference maintain its half-cell potential allowing the control of the overall potential applied to the cell. Voltammetry and amperometry are techniques based on the simple application of a potential versus a reference electrode, while the current is measured. The voltage step generates a current due to the electrolysis mediated by an oxidation or reduction at the working electrode. The response is dependent on the rate of mass transport to the conductive surface. Voltammetry is a class of electrochemical methods where the potential at working electrode is varied while the current is measured. Many techniques are included in this group. Some of those, employed in biosensing, are linear sweep voltammetry, cyclic voltammetry, Square wave voltammetry and differential pulse voltammetry. In cyclic voltammetry (CV), the potential is scanned in a defined potential range back and forth and it is used to monitor reversible reactions. In linear sweep voltammetry (LSV), the potential is scanned just in one direction to get the oxidation or reduction current peak of the analyzed species. In presence of electroactive molecules, the oxidation and reduction current are sampled, and the current intensity would be proportional to the concentration of the analyte. Differential pulse voltammetry (DPV) and square wave voltammetry (SWV) are voltammetric techniques where the potential is varied with regular voltage pulses or applying square wave and staircase potential.

This peculiar potential step lead to the reduction of the non-faradaic component of the current enhancing the sensitivity. Hexamminoruthenium (III) (RuHex) and Methylene Blue (MB) are common electrochemical labels used in DNA based biosensors and they are detectable with voltammetric methods, either covalently bound to the DNA probe or added later after target detection (Liu et al., 2014, Liu et al., 2017, Ferapontova, 2018). Also intercalating electroactive molecules can be used as labels: Hoechst is for example used in nucleic acid detection and measured through voltammetric techniques upon incubation on the electrode surface (Sufen et al., 2002, Zhao et al., 2012). Electrochemical impedance spectroscopy (EIS) is also an interesting technique for biosensing applications (Bahadir and Sezginurk, 2016). Impedance is a generalized term referring to resistance, including other parameters affecting the charge transfer, such as mass transfer and capacitance. It consists on the measurement of the resistive and capacitive properties of materials, after a perturbation of the system, by applying a small amplitude sinusoidal AC excitation typically in the range of 2-10 mV. The frequency of such oscillation is varied in a wide range of values to obtain a spectrum of impedance in stationary conditions. The currents generated are monitored in order to obtain information about the components of the impedance. Depending on the frequency value, impedance can sample electron transfer at high frequency and mass transfer at low frequencies. EIS is a label-free technique and its application is convenient for affinity sensors, where the binding of the target molecule on the immobilized bioreceptor can produce small changes in the impedance related and proportional to the concentration of the analyte. Impedimetric sensors have been widely proposed in literature in DNA based biosensing but also in other fields (Bahadir and Sezginurk, 2016, Bertok et al., 2019, Daniels and Pourmand, 2007).

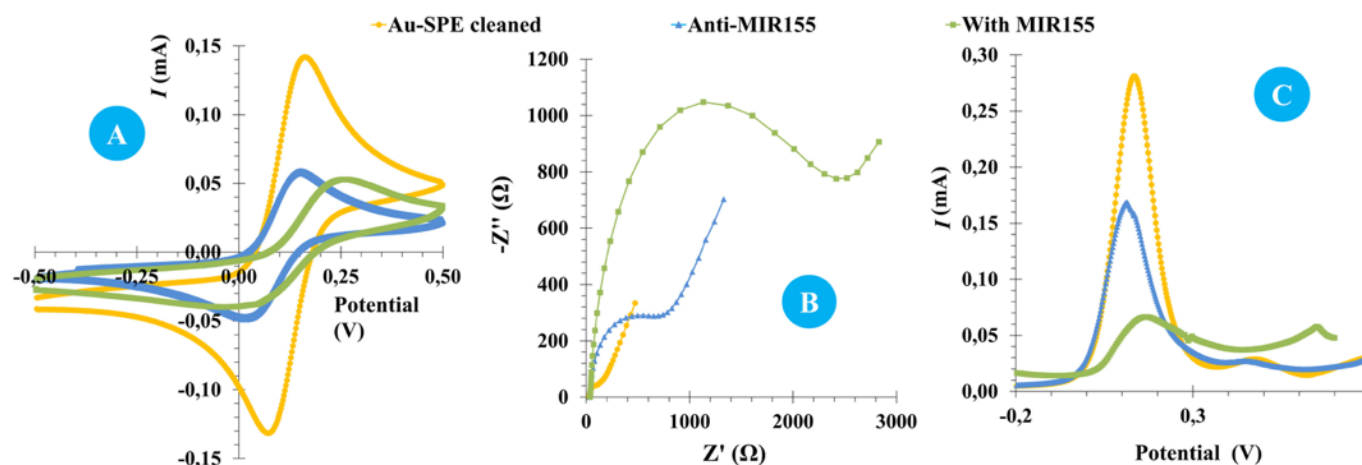


Fig 1-3. Electrochemical detection of miR-155 proposed by Cardoso et al, comparing the detection using Cyclic Voltammetry (A), Electrochemical Impedance Spectroscopy (B) and Square Wave Voltammetry (C). (Readapted from (Cardoso et al., 2016). (Image Under Creative Commons License Attribution-NonCommercial-NoDerivatives 4.0 International).

Voltammetric and Impedance based technique have been also compared by Cardoso and coworkers, proposing a simple detection method for miR-155 in breast cancer samples, reaching a limit of detection close to the attomolar range (Cardoso et al., 2016).

## 1.4 Surface Plasmon Resonance (SPR)

Surface Plasmon Resonance (SPR) is a label-free technique, which came out in the last decades as a suitable and reliable platform for biosensing applications (Nguyen et al., 2015, Hoa et al., 2007). Surface plasmon resonance is a phenomenon occurring when an incident light hits a noble metal surface, for instance gold surface. When the incidence angle assumes a certain value (SPR angle), at a fixed wavelength, the light energy excites the electrons at the interface of the metal layer, allowing resonance. The oscillations of the electrons due to the energy coupling are called plasmons, and they propagate on the metal surface. The oscillation of the plasmons returns an evanescent electric field with a range of about 300 nm from the boundary between the metal surface and the solution. In a standard commercial SPR sensor, the incident light is directed on the sensing surface using a glass prism with high reflective index. When these conditions are satisfied, the resonance effect can be observed as a drop in the reflected light at the SPR angle (Fig 1-4).

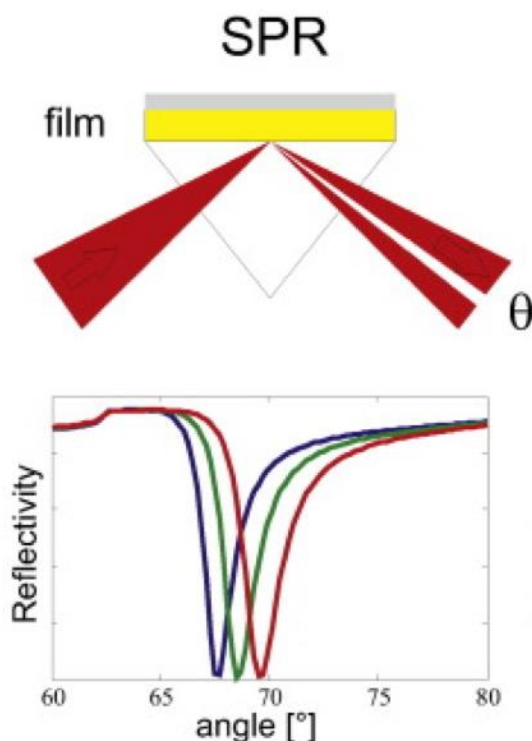


Fig 1-4. Scheme of the working principle of SPR. Readapted from Jacqueline Jatschka, 2016 (licensed under Creative Commons Attribution 4.0 International).

The coupling conditions depend also on the refractive index of the medium at the interface and these change when the refractive index at the interface changes. Even a small variation leads to

a perturbation of the resonance conditions, and therefore the SPR angle. The refractive index can change for example upon the binding of a specific target to a bioreceptor immobilized on the metal surface. The change in the refractive index can be observed in real time by monitoring the shift of the SPR angle over time, while flowing the sample on the sensing surface. SPR based methods are very interesting for biosensing applications because it could very sensitive and it is label-free. These are basically sensitive to mass changes nearby the surface. SPR is already used for the screening and detection of analytes or to investigate the interaction between proteins (Mariani and Minunni, 2014, Nguyen et al., 2015).

## **1.5 Metal nanoparticles in biosensing**

Metal nanoparticles (MNPs) are an important tool offered by nanotechnology for a broad variety of applications (Malekzad et al., 2017). Metal nanoparticles show many advantageous features making them very interesting as possible transducers elements in biosensors. Especially noble metal nanoparticles, such as silver, gold and platinum NPs attracted great attention and they have been widely studied. Their unique properties are related to the material but also strongly related to their dimensions (Wu et al., 2011). Objects with dimensions up to 100 nm are considered nanoparticles, and at this scale, there is an increased surface/volume ratio, influencing indeed their physical chemical properties. Metallic nanoparticles received in the last decades great popularity, also thanks to the uniform and sharp size distribution reachable in chemical synthesis. Beside the advantages offered by their dimensions, they can be easily functionalized, modified to be exploited to bind ligands, drugs, antibodies and DNA. The role of metal nanoparticles in biosensing can be assigned depending on the physical or electrochemical changes occurring upon target detection. NPs can act as platforms for immobilization (Guo et al., 2014, Turkmen et al., 2014), enhancers of the electron transfer (Li et al., 2010), catalyze chemiluminescent reaction in presence of substrates (Tian et al., 2009, Chaichi and Ehsani, 2016), amplify changes in refractive index in SPR based sensors (Sugawa et al., 2015, Zhang et al., 2014) and amplify changes in mass (Yan et al., 2015). For these reasons we took into account the employment of metal nanoparticles as signal transducers and enhancer in our detection methods. With smaller sizes, also metal nanoclusters are interesting objects for biosensing applications. Their dimensions can be perfectly controlled it can usually reach 2 nm and they also have unique electrical, optical, magnetic and reactivity properties (Li et al., 2014, Shang et al., 2011, Wang et al., 2016b, Zheng et al., 2017). They are often biocompatible, and they can be easily combined in biosensing with a great variety of biomolecules.

## 1.5.1 Gold nanoparticles

Gold nanoparticles (AuNPs) have been widely employed in biosensing and many other bionanotechnological applications, for their specific properties, the large variety of synthesis methods and ease of functionalization (Herizchi et al., 2016, Tiwari et al., 2011). In addition to the properties discussed above concerning metal nanoparticles in general, AuNPs show excellent biocompatibility and low toxicity, with a broad spectrum of possible applications (Yeh et al., 2012). In electrochemistry, they allow fast electron transfer between a wide range of electroactive materials and species on the surface, enhancing the conductivity (Pingarron et al., 2008). Optical properties include surface plasmon resonance (SPR) (Csaki et al., 2018), mentioned in previous sections, and fluorescence modulation (Kang et al., 2011). Gold nanoparticles can provide in general a very versatile platform for molecular assemblies involving antibodies, oligonucleotides and proteins for biosensing purposes, also implementable for visual detection of biomolecules (Cao et al., 2011, Li et al., 2010).

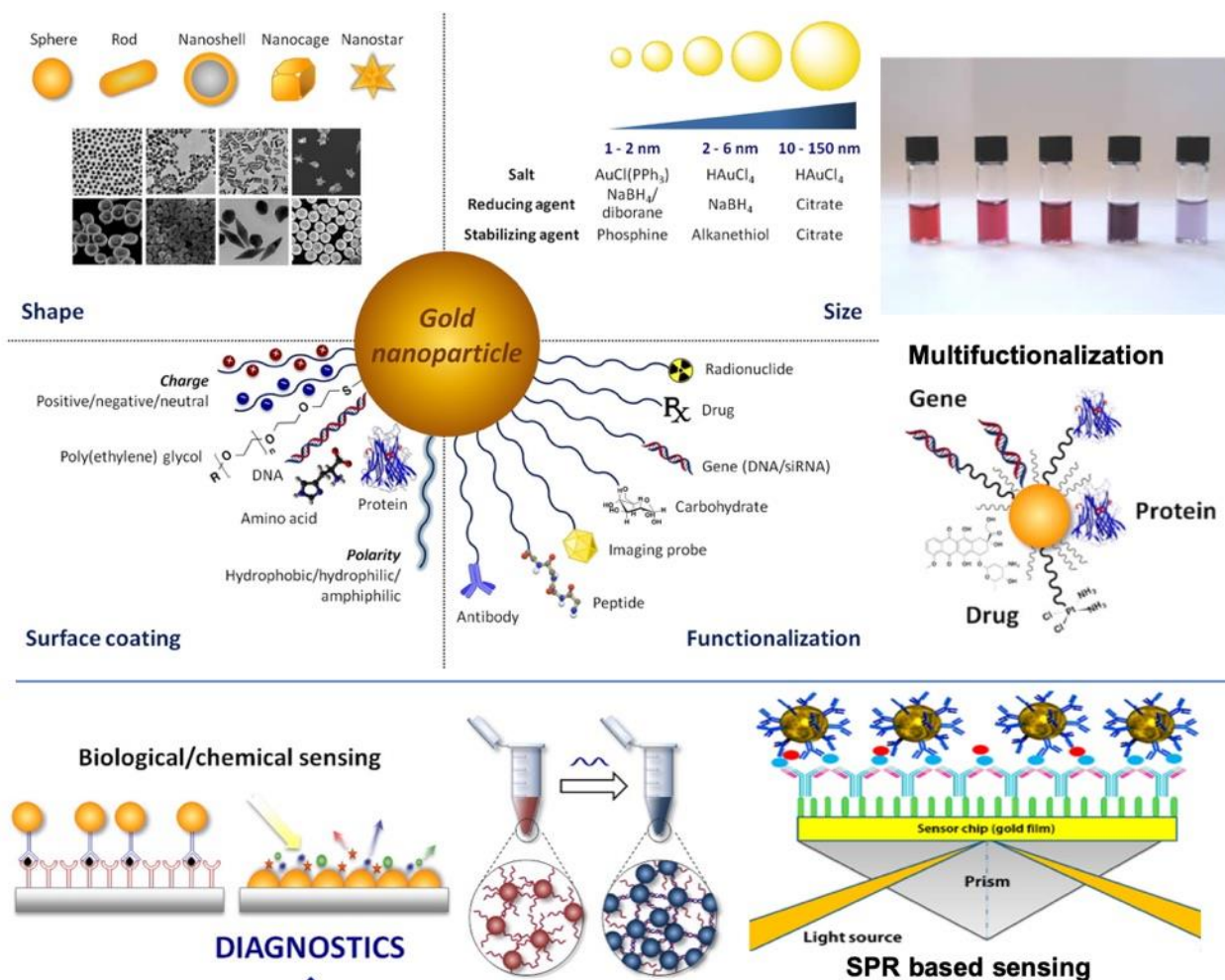


Fig 1-5. Gold nanoparticles properties and applications. Adapted from Her, Jaffray, & Allen 2017 (Her et al., 2017) Image licensed by Elsevier and Copyright Clearance Center (License number 4698271265307, 4698280074473).

DNA can be covalently or not covalently immobilized on the gold nanoparticles and used for DNA based sensing of molecules. In DNA based biosensors, due to the surface-to-volume ratio, the amount of hybridized target DNA can be greatly increased, and so it is possible for many other molecules. Fang and coworkers were able to increase the immobilized oligonucleotides probes on gold electrodes by 10 fold compared to bare gold electrode (Cai et al., 2001). Researchers also experimented multi-biofunctionalized gold nanoparticles. A barcode assay was proposed by Mirkin and coworkers, immobilizing barcode oligonucleotides and target-specific antibodies on gold nanoparticles (Tang et al., 2007). In combination with antibody-functionalized magnetic microparticles, the target is detected with a sandwich-like method. Also examples of the combination of aptamer-functionalized gold nanoparticles to spectroscopically detect small molecules and cancer cells (Yeh et al., 2012). DNA based biosensors can take advantage of non-covalent interaction between nucleic acids and gold nanoparticles to modulate a response. The interaction of nucleic acids with modified or unmodified metal nanoparticles can affect their optical properties, giving the chance to generate a spectroscopically detectable signal thanks to plasmonic phenomena.

### **1.5.2 Localized Surface Plasmon Resonance (LSPR)**

The field of plasmonics also experimented the application of metal and metal-hybrid nanostructures with unique optical properties, due to the strong interaction of their charge carriers (electrons) with an incident light. This phenomenon is called LSPR, localized surface plasmon resonance (Willets and Van Duyne, 2007). As for SPR, the effect of LSPR is based on delocalized charges in noble metal objects but these objects have dimensions smaller than the wavelength of light. An external electromagnetic field (the light) induces, at a specific fixed wavelength, the oscillation of the conduction electrons with a subsequent excitation of localized surface plasmons, allowing the resonance. Unlike SPR, in LSPR, the localized plasmons in the metal nanostructures, for examples metal nanoparticles, can be excited directly by an incident light, without any constrain about the incident angel. This make the realization of LSPR based devices simpler. The coupling of energy is observable as a drop in the transmitted light, which is a peak in the absorbance of the nanoparticles (Fig 1-6) (Jung et al., 1998). When resonance occurs, an evanescent field takes place around the nanoparticles. The plasmonic optical response, such as the color of the colloidal solution, is related to the material, the geometry, the shape and the dimension (Lee and El-Sayed, 2006). As for SPR, changes in the refractive index around the nanoparticles affects the coupling conditions resulting in a shift of the absorbance peak. In general, bulk sensitivity of gold nanoparticles is positively correlated to the diameter, but it is usually lower than SPR based system with metal thin coats.

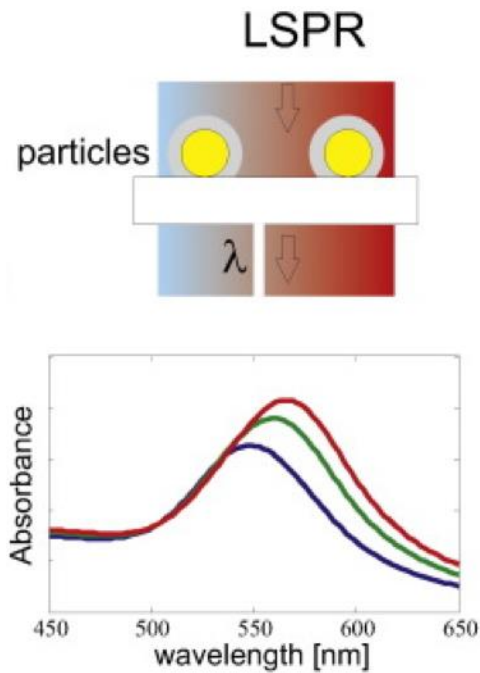


Fig 1-6. Scheme of the working principle of LSPR. Readapted from Jacqueline Jatschka, 2016 (licensed under Creative Commons Attribution 4.0 International).

The sensitivity to changes in the refractive index in the surrounding media allow the employment of LSPR in sensing applications based on spherical gold nanoparticles but also non-spherical metal nanostructures with peculiar shapes, such as prisms, nanorods, showing in general high sensitivity (Chen et al., 2008a). As for SPR, molecules binding on the surface can be detected, as the covalent immobilization of the probe and the interaction with specific analytes. LSPR is even more addressable to biosensing purposes for the simplicity of the components and the easier fabrication. In principle, a change in the plasmonic effect could be observed by naked eye, otherwise, for more complex setup, a simple light source and a spectrophotometer can be used. Synthesis of metal nanostructures and nanoparticles is easier, in a bottom up approach, compared to the fabrication of gold layers for SPR chips. Moreover, the shape and the dimensions of the nanoparticles can be fully controlled. Many examples of the employment of LSPR for biosensing purposes are present in literature (Csaki et al., 2018). The sensing principle was widely confirmed through several model systems involving synthetic oligonucleotides as probes (Schneider et al., 2013, Spadavecchia et al., 2013). DNA based sensors with LSPR detection methods have been used to detect microbial DNA or RNA and other DNA based biomarkers after PCR amplification, returning higher selectivity and specificity (Fong and Yung, 2013, Kim et al., 2011, Wang et al., 2012, Parab et al., 2010, Soares et al., 2014). LSPR methods were also applied to miRNA detection, for example combining BCA (bio-bar-code amplification) on nanoparticles and LNA as probe (Dong et al., 2015). LSPR has been proved to return good performances also without amplification in real samples. Joshi et al proposed a method for the detection of circulating

and exosomal miRNAs in plasma from pancreatic cancer patients (Joshi et al., 2014, Joshi et al., 2015).

### 1.5.3 DNA templated Silver/Pt nanoclusters

As previously anticipated, metal nanoclusters are smaller than nanoparticles, usually less than 2 nm and they show a broad variety of functionalities and interesting electronic, optical and chemical properties, such as enhanced conductivity, plasmon resonance, fluorescence and catalytic activity (Wilcoxon and Abrams, 2006). In the context of DNA nanotechnology and DNA based biosensors, these objects are very interesting since some metal nanoclusters can be synthesized on a DNA template in a controllable manner (Chen et al., 2018). For example, AgNCs can be specifically synthesized on C-rich DNA sequences (Fig 1-7). DNA templated AgNCs and AuNCs are widely reported in literature as fluorescent labels in biosensing applications (Latorre et al., 2013, Zheng et al., 2017). In addition, the catalytic activity of metal nanoclusters, made them effective transducers in biosensing purposes as (Chang et al., 2016, Li et al., 2016, Wang et al., 2016b).

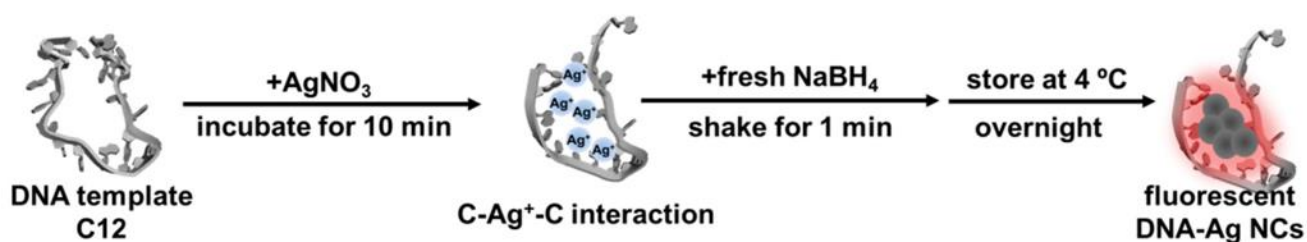


Fig 1-7. Steps for the formation of silver nanoclusters on DNA templates. Readapted from Teng et al 2018 (Teng et al., 2018). (image under Creative Commons Attribution 4.0 International license).

The catalytic activity of metallic nanoclusters is significantly affected by the surface composition. For instance silver nanoclusters show poor catalytic activity as enzyme-mimicking transducers (Zheng et al., 2014a), compared to other metal such as Platinum (Pt), which possess a unique peroxidase activity (Gao et al., 2013). Platinum nanoclusters can be also formed on DNA, as shown by Higuchi et al that used DNA-Pt complexes to establish a colorimetric assay for thrombin (Higuchi et al., 2008, Matsuoka et al., 2007). However, the preparation of DNA templated Pt nanoclusters is complex and the Pt clusters form on the DNA in unspecific manner, leading to loss in stability of the system in terms of sensitivity and specificity. Mixed Ag/Pt bimetallic nanoclusters with peroxidase-like catalytic activity were recently proposed for the colorimetric detection of analytes (Wu et al., 2016, Zheng et al., 2014a). They provide a strategy to produce in one-step Ag/Pt bimetallic nanoclusters on DNA: AgNCs are formed in presence of a reducer such as NaBH<sub>4</sub> on C-rich sequences thanks to affinity for Ag(I) while Pt(0) would grow on the surface of the AgNCs because of a galvanic replacement reaction. DNA encapsulate the newly

formed cluster, keeping its size to few nanometers. Ag/Pt nanoclusters do not show fluorescence, but they have strong peroxidase like activity. We recently published with the group of Dr. Hosseini of the University Of Teheran (IRAN) and thanks to the PhD work of Hanie Ahmadzade Kermani, a bioassay to detect methyl-transferase activity in biological samples (Kermani et al., 2018). The methylation of cytosines in specific DNA C-rich sequences can affect the actuation or the catalytic activity of these metal nanoclusters, allowing the detection of the enzymatic activity.

## **1.6 DNA nanotechnology and biosensing**

DNA nanotechnology can give a great contribution to DNA based biosensors by enhancing their performances and sensitivity (Chao et al., 2016). DNA nanotechnology is a branch of nanotechnology in which DNA found alternative uses related to its peculiar properties for structural but also functional purposes (Chen et al., 2015b, Seeman, 2007). DNA is no more just the stable and ordered source of genetic information, but it becomes custodian of another kind of programmable information, addressable in building functional nanodevices and nanostructures. New tools are available thanks to the structural and dynamical properties of the DNA as biopolymer. The pioneering work of Nadrian Seeman (Seeman, 2007, Seeman, 2010a), in the last decades, highlighted these new way to look at the DNA, opening the doors to new applications in many fields. Nano-objects made of DNA can be precisely built exploiting the peculiar features of nucleic acids: resistance, flexibility, but most of all the programmability. DNA is a smart material, and DNA strands can be designed to build up process in the nanoscale providing simple building blocks able to self-organize. David Yu Zhang and Georg Seelig proposed a general classification of DNA nanotechnology, distinguishing structural DNA nanotechnology and dynamical DNA nanotechnology (Seelig et al., 2006, Zhang and Seelig, 2011).

### **1.6.1 Structural DNA nanotechnology in biosensing**

Structural DNA nanotechnology involves the use of DNA for its structural properties in a 'bottom up' approach. This branch of DNA nanotechnology involves the construction of specific two and three-dimensional nanostructures, suitable to be controlled in their shape, complexity, dimensions, starting from individual DNA strands. The principle is simply based on hybridization (Chen et al., 2015b, Zhang and Seelig, 2011). This is the case of DNA origami and tetrahedrons, where long DNA molecules are deigned to interact in aqueous solution to form spontaneously more complex nano-objects (Seeman, 2010b, Zadegan and Norton, 2012, Sadowski et al., 2014). The programmability of DNA allows the precise ordering of elements on surface. This is very useful in some biosensing applications where the distribution and arrangement of the sensing

nanocomponents could be important. For instance DNA origami have been employed to localize and order nanoplasmonic antennas, such as gold nanoparticles on surface or in solution to enhance their optical properties (Lermusiaux and Funston, 2018, Ou et al., 2018, Zhou et al., 2014). Miao et al designed a detection method using DNA tetrahedrons to regulate the density of the probe on the electrode surface for electrochemical detection of microRNAs. Other examples are present in literature about the employment of these structures within different detection strategies for DNA and microRNA sensing (Lu et al., 2019, Wang et al., 2019).

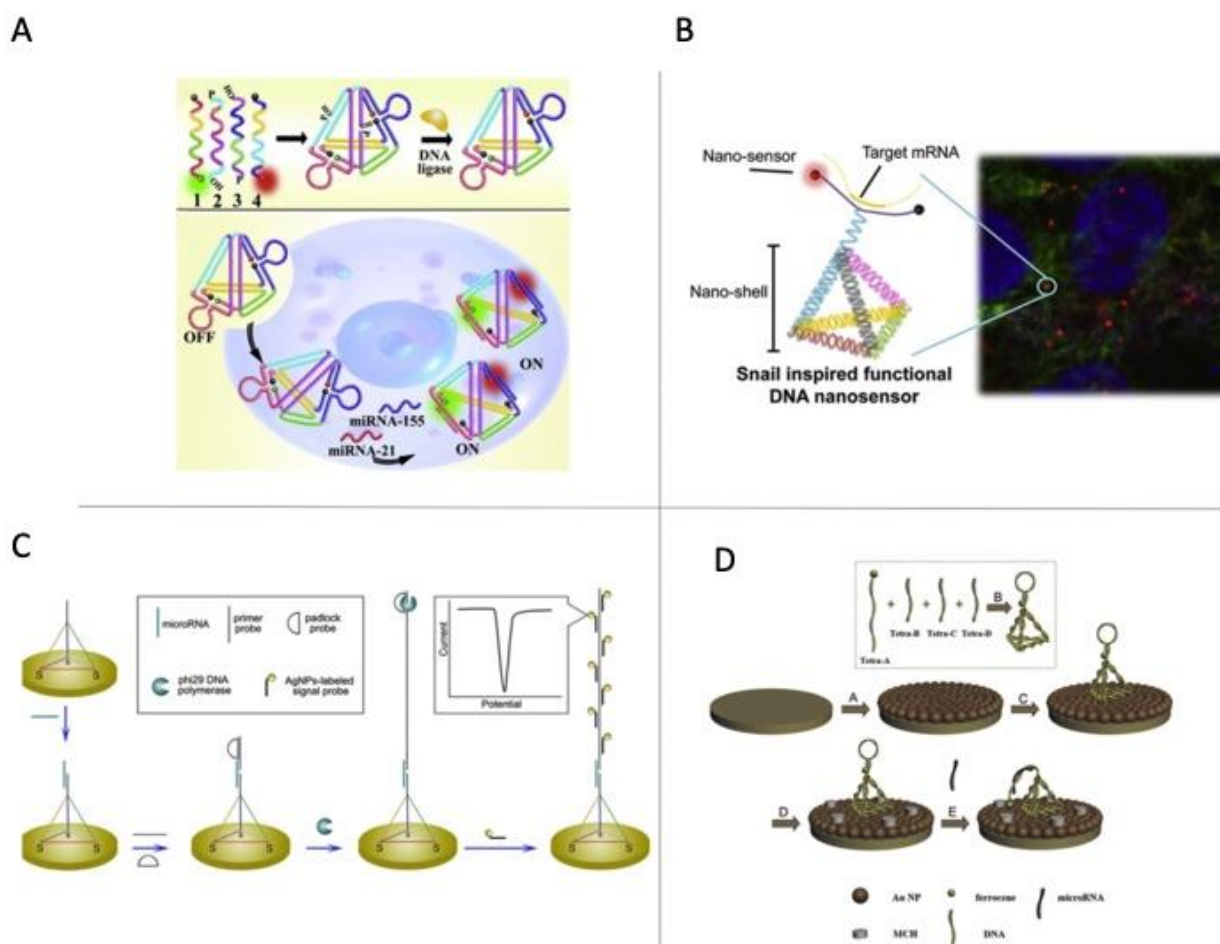


Fig 1-8. Examples of DNA nanotechnology used in biosensing, specially tetrahedrons. A) A multicolor encoded based DNA tetrahedron for multiplexed detecting of miRNAs in living cells. B) Scheme of a DNA tetrahedron-based assay for sensing mRNA in living cells. C) An ultrasensitive electrochemical assay of microRNA based on DNA tetrahedron on gold electrodes. D) An electrochemical assay to detect lung cancer-related microRNAs. Readapted from with permission from Ebrahimi et al (Ebrahimi et al., 2019). Image licensed by Elsevier and Copyright Clearance Center (License number 4698280432904).

### 1.6.2 Dynamic DNA nanotechnology in biosensing

DNA is suitable to design and control dynamical process (Zhang and Seelig, 2011). In such processes, the attention would not be focused on the equilibrium end-state but on the non-equilibrium dynamics. For instance, the toehold mediated strand displacement (TMSD) is a process that may be involved in programming dynamical systems based on DNA (Srinivas et al., 2013). This is an isothermal process, in which one DNA single strand is able to displace a second

strand complexed in a double helix with a third one. If the double strand DNA has a short single stranded overhanging toehold, a longer and fully complementary strand would start interacting on the toehold and continue in the hybridization displacing the shorter strand (Fig 1-9).

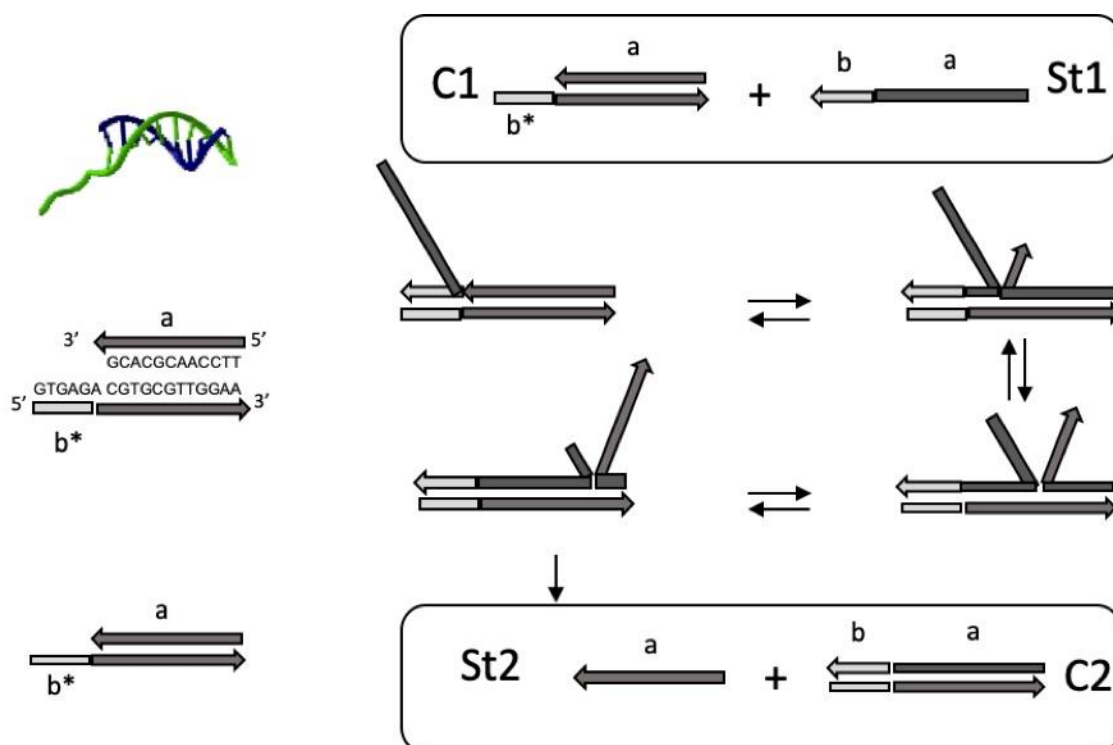


Fig 1-9. Scheme showing the principle of the Toehold Mediated Strand Displacement. Complex C1 has a toehold (b\*). St1 strand can interact on b\* and start displacing the shorter strand. The entire process leads to the release of St2 and the formation of the full-hybridized complex C2.

The favored interaction is the most thermodynamically advantageous. The TMSD offers the opportunity to control the kinetics of a DNA rearrangement and interaction, by varying the length and composition of the toehold (Srinivas et al., 2013, Machinek et al., 2014). The realization of switchable dynamic nanodevices combined with isothermal amplifications can enhance the response upon target detection and improve DNA-based detection methods for microRNAs (Zhao et al., 2015, Deng and Gao, 2015, Deng et al., 2017). Isothermal amplifications do not require enzymes and they can replace the common amplification techniques in use. Catalyzed Hairpin Assembly (CHA) involves the spontaneous hybridization between two hairpins thanks to the sequences embedded in the stems. An input strand can initiate the process through toehold mediated strand displacement on one of the hairpins. A second hairpin displaces then the initiating sequence forming a double stranded complex with the first one. The target is then released and it is able to interact with other hairpins in solution (Zang et al., 2015, Zhang et al., 2015b). Another interesting isothermal amplification based on TMSD is Hybridization Chain Reaction (HCR), and it will be deeply introduced in the next sections.

### 1.6.3 Alternative DNA structures as DNA probes

Alternative DNA structures can be also employed in DNA nanotechnology and sensing. Some specific sequences and conditions can force the double helix to assume alternative conformations, such as Z-DNA, hairpins, triple helices, Holliday junctions, G-quadruplex and i-motif (Choi and Majima, 2011) Fig 1-10.

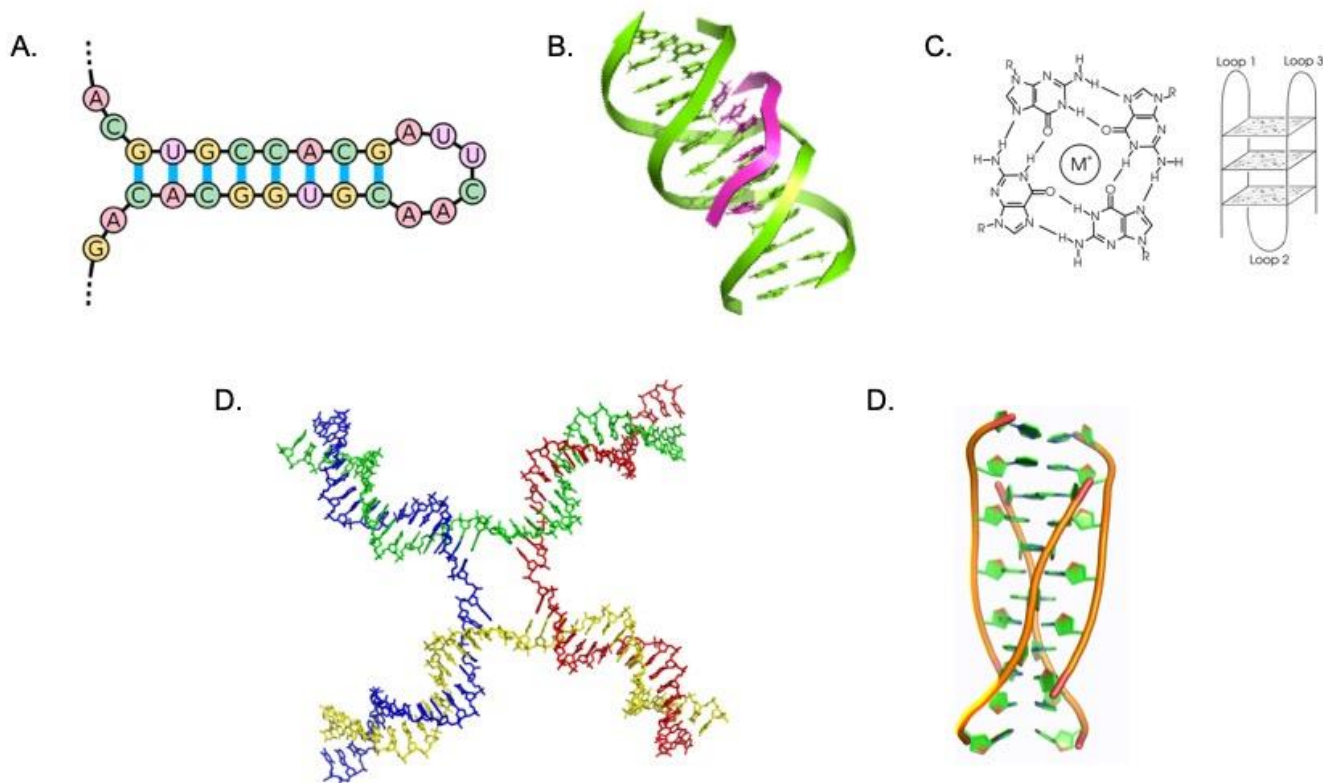


Fig 1-10. Representation of non-B DNA structures. A) Hairpin structure (Creative Commons license Attribution 2.5 Generic); B) Triple helix of DNA (Creative Commons license Attribution-ShareAlike 4.0); C) G-quadruplex (Public domain); D) Holliday junction (Creative Commons license Attribution-ShareAlike 3.0 Unported); E) A-motif (Creative Commons license Attribution-ShareAlike 4.0 International).

These structures can be stabilized by canonical or alternative hydrogen bonds. These can be found also *in vivo*, and they attracted great attention for their biological role and because in some cases related to an increase in genetic instability (Jain et al., 2008, Wang and Vasquez, 2008). Some of these DNA structures are interesting for applications in biosensing, thanks to their tunable stability and programmability. Hairpin-like structures of DNA are formed by two elements: a double stranded stem and a loop in single strand conformation or with alternative base-pairings. In biotechnology, they are widely used to design probes and molecular beacons for specific recognition of nucleic acids (Huang et al., 2014, Stobiecka and Chalupa, 2015). Hairpin-like probes offer the chance to improve the specificity of a sensor, since the recognition has to face a higher energy barrier due to the secondary structure. Another interesting non-B DNA structure is

the triple helix of DNA (Manzini et al., 1990, Xodo, 1995). This is obtained when a double stranded DNA assembles with a third additional strand, termed triple helix forming oligo (TFO), through Hoogsteen interactions. In general, this conformation involves a polypurine-polypyrimidine duplex and a third strand that could be either polypurinic or polypyrimidinic. Depending on the composition of the third strand, triple helices can be classified into parallel triple helix, If the TFO is a polypyrimidinic strand, or antiparallel triple helix when the third strand is a polypurinic strand. These terms referred to the chirality in respect to the purines-rich strand of the double helix. The parallel triplex structure is formed by T-A\*T and C-G\*C+ base pairs, while in the antiparallel triplex structure is stabilized by T-A\*A and C-G\*G. In the parallel triple helix, the formation of the Hoogsteen hydrogen bonds in the C-G\*C+ triad is pH dependent, since cytosines need to be protonated (Brucale et al., 2005). These structure have been broadly studied and widely introduced in many biotechnological applications (Hu et al., 2017). Researchers presented many strategies for DNA-based biosensing employing triple helix probe as recognition element for the specific detection of nucleic acids or other biomolecules (Chen et al., 2017, Du et al., 2014, Wang et al., 2014, Zhang et al., 2016, Zheng et al., 2011, Zheng et al., 2014b). The triple helix structure offers different advantages, such as (I) enhanced sensitivity, (II) improved specificity, (III) same stability of classic molecular beacon with double helix DNA with longer complementary strands.

## 1.7 Hybridization Chain Reaction

Hybridization Chain Reaction (HCR) is a self-assembling reaction involving hairpin-like DNA strands in solution. Dirks and Pierce invented this reaction in 2004 and since their first publication, HCR attracted great attention for possible applications in the development of functional DNA nanosystems (Augspurger et al., 2018, Bi et al., 2017, Dirks and Pierce, 2004b). The reaction involves two species of hairpins in solution in a metastable status: the information for the complementarity needed to build the nanostructure is confined in the stem at the equilibrium in a kinetical and thermodynamic trap until the occurrence of a perturbation.

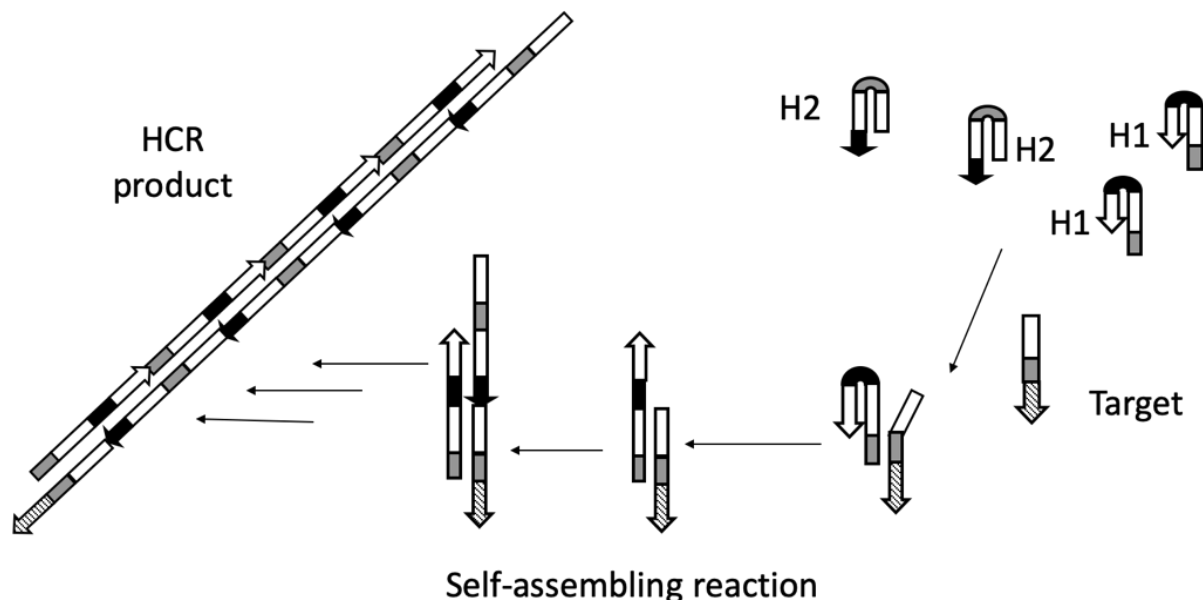


Fig 1-11. Scheme of the Hybridization Chain Reaction.

The hairpins can be designed to interact with a specific sequence or respond to a change affecting their stability. Once triggered, the building process consists in the interaction of the two species of hairpins, able to open each other and assemble in a chain reaction (Fig 1-11). When the first hairpin interacts with the second one, they form a nicked dsDNA with ssDNA “sticky ends”, able to induce the opening of the first hairpin species, perpetuating the toehold mediated strand displacement at the base of the HCR mechanism (Zhang and Seelig, 2011). In the case of nucleic acids as initiators, the target is able to interact with the first hairpin, and this interaction starts with nucleation, through hybridization at the short overhanging toehold and it spreads at the enclosed portion of the sequence. At the end the hairpin would be completely open and hybridized to the trigger sequence. As for the basic TMSD, the toehold is responsible for the hairpin opening and for the polymerization: the length and the base composition would affect both the recognition and the self-assembling reaction (Srinivas et al., 2013). Yung and Ang proposed the rational design of hybridization chain reaction monomers, by focusing on such parameters, CG content, length of stem and the toehold (Ang and Yung, 2016). Once triggered the process continues until the total consumption of the hairpins, or the size of the DNA nanostructure reaches a kinetically limited threshold. The product of the self-assembling reaction is a long nicked DNA nanostructure. The entire process is enzyme-free, completely isothermal and spontaneous.

### 1.7.1 HCR in biosensing

Hybridization Chain Reaction can be designed for the specific detection of a broad variety of analytes, biomolecules, especially nucleic acids (Miti and Zuccheri, 2018). HCR represents an alternative to current amplification methods such as polymerase chain reaction (PCR). Unlike PCR, HCR does not require enzymes or heating/cooling cycles for amplification; on the contrary,

it progresses isothermally, with no additional reagents. In principle, the complex media of the samples do not affect the reaction, allowing direct detection, in tubes and in complex biological samples. There are many examples about the employment of HCR in the detection of endogenous biomarkers in situ (Choi et al., 2014) and also in monitoring the traffic of nucleic acids in living systems (Choi et al., 2016, Wu et al., 2015, Zhang et al., 2015a). The self-assembled product can be detected with different transduction methods such as electrochemical transduction, fluorescent, SPR or other optical techniques (Augspurger et al., 2018). Pierce and Dirks used fluorescence spectroscopy, exploiting the quenching of the fluorescent DNA base analogue 2-aminopurine (2AP) in the DNA stem. They monitored the decrease in fluorescence during the polymerization upon introduction of the target (Dirks and Pierce, 2004b). For enhanced characterization of RNAs, fluorescent labeled hairpins were also utilized for the discrimination of protein biomarkers on exosomes thanks to the employment of a specific aptamer, able to trigger the polymerization after the detection directly on the surface of the exosome (Wan et al., 2017). Towards the implementation for electrochemical detection, it is possible to immobilize directly DNA hairpins on electrodes, and used for HCR amplification on surface after the detection of the target (Chen et al., 2012, Liu et al., 2013b). Application of HCR on such sensors showed good results, providing systems able to reach attomolar quantification of the target (Ge et al., 2014). It is possible to measure the changes in the electrical properties at the surface, such as resistance or capacitance, due to the increased amount of DNA (Spiga et al., 2014, Trifonov et al., 2016). HCR can be also combined with alternative DNA structures enhancing signal and sensitivity (Cai et al., 2014, Li et al., 2017). Specific sequences with known functionalities can be introduced in the hairpins and “activated” once the nanostructure is assembled. Combining HCR with the G-quadruplex the self-assembly of the hairpins can lead to the formation of functional domains on the nanostructures with activated and detectable HRP-like activity (Chen et al., 2015a, Dong et al., 2012, Shimron et al., 2012, Trifonov et al., 2016). Since SPR based detection methods are sensitive to change in the mass at the interface, the target detection can be enhanced through HCR amplification, thanks to a bigger change in the refractive index. This strategy reached a limit of detection close to 10-100 femtomoles in the detection of pathogen DNA (Spiga et al., 2014). Researchers exploited also the formation of active metal nanoclusters with catalytic activity on the HCR products, which are observable for example through electrochemical detection (Yang et al., 2015). Triple helix probes have been also used in combination with HCR in different ways. Idili and coworkers designed and Hybridization chain reaction controlled by pH, exploiting the triple helix formation between the toehold and the stem of the hairpin (Idili et al., 2015). Zheng et al developed a detection method based on triple helix and aptamer technology for the detection of multiple analytes using HCR amplification and surface enhanced raman scattering (SERS) (Zheng et al., 2014b). HCR has been adapted to nanoparticles-based methods in many strategies

and in different biosensing platforms (Augsburger et al., 2018). An easy way to use gold nanoparticles in sensing is going through a colorimetric approach, where the interaction with a target molecule would change physical chemical properties of the nanoparticles and thus the color of the solution of nanoparticles. The presence of the target can lead to aggregation of gold nanoparticles upon HCR polymerization, resulting in a shift to blue-grey color through an LSPR phenomenon. He et al exploited the difference in absorption of ssDNA and dsDNA on gold nanoparticles: gold nanoparticles are kept stable in absence of the target thanks to single stranded portion of the HCR hairpins, adsorbed on the surface. After the addition of the trigger, the hairpins are sequestered to build up the nanostructures and the nanoparticles aggregate producing a colorimetric response due to the salt in solution (Liu et al., 2013a). A similar strategy takes advantage of the electrostatic properties of DNA using positive-charged gold nanoparticles. Miao and coworkers proposed a similar method in which 11 nm sized (+)AuNPs were prepared using CTAB (cetylmethyl ammonium bromide) (Miao et al., 2017). These nanoparticles appeared stable in presence of the hairpins in solution in the proper conditions, but they agglomerate on the HCR nanostructure upon addition of the target miR-21, allowing a detection limit of 6.8 pM. Ma and coworkers proposed a strategy where AuNPs were used as substrate for the immobilization of the HCR product, which was able to protect the nanoparticles from salt-induced aggregation (Ma et al., 2014). Gold nanoparticles were also extensively applied with HCR on electrochemical detection, to enhance the performance of nanoparticle-enhanced DNA detection methods. Positive AuNPs can be used as electroactive label and detected on the electrode upon hybridization chain reaction using differential pulse voltammetry (Li et al., 2015). Other interesting approaches involve the employment of HCR in combination with different alternative amplification strategies. HCR has been matched with target-assisted polymerization nicking reaction (TAPNR), using silver nanoclusters AgNCs as transducer; it was possible to reach a limit of detection of 0.64 fM in the detection of miR-199a (Yang et al., 2015). In this work, C-rich hairpins have been employed. AgNCs can be detected electrochemically through CV or DPV after target recognition. An interesting application of fluorescence based detection was proposed by Xiang et al, who tried to combined HCR and CHA for the detection of oncogenic miRNAs using coupled fluorophores and quenchers on the hairpins, reaching 0.3 fM LOD (Wei et al., 2016). Combination of HCR with G-quadruplex and isothermal exponential amplification (EXPAR), in electrochemical assay allowed the detection of avian influenza A virus with a detection limit of 9.4 fM (Yu et al., 2015). Beside the combination of HCR with other isothermal amplification methods, some researchers attempted to get a higher order polymerization during the HCR, for example designing hyperbranched nanostructures formed through HCR mechanism. Liang et al published a method for the electrochemical detection of microRNAs proposing a 4-hairpins HCR leading to a 'hyperbranched nanostructure' on the electrode surface (Liang et al., 2018). The detection on

surface is performed through electrochemical impedance spectroscopy and voltammetry in presence of Ru(Hex), reaching 11 pM as detection limit. Combining branching and additional isothermal amplification, Jinag et al proposed a similar 4-hairpins HCR method in solution combining branching assembly and CHA with a fluorescent readout, reaching 500 fM limit of detection (Liu et al., 2018). The detection of small molecules and ions through aptamer based sensing can be also implemented with HCR amplification (Augspurger et al., 2018, Bi et al., 2017).

## **2 Aim of the study**

The aim was to develop new detection methods based on DNA and DNA self-assembly for the specific detection of short nucleic acids sequences such as microRNAs. DNA based biosensors are powerful tools, in principle able to greatly improve the diagnosis of biomarkers. We wanted to design new strategies with enhanced sensitivity and adaptability, in order to increase the potential of DNA based biosensors. We faced different approaches to improve DNA based sensing. First, we focused on the use of Hybridization Chain Reaction as isothermal amplification. HCR can enhance the response upon target detection. Part of our purpose was to design an HCR reaction specific for microRNAs and test the implementation on different available biosensing platforms. In parallel, we wanted to propose a new strategy, alternative to the simple HCR, involving a triple helix probe able to trigger a double response upon target detection. We concentrated on the characterization of this method and in proving the working principle, aiming to implement it in biosensing. The second goal, always towards the enhancement of the signal in DNA biosensor, was to explore alternative tools able to improve the sensitivity. With regard to this, we attempted to use metal nanoparticles as labels and transducers.

### 3 Materials and methods

#### 3.1 Reagents and buffers

Reagents and chemicals used during the work presented in this thesis was purchased in general by Sigma Aldrich (Merck) and used without any further purification unless specified. All solutions and buffer were prepared in ultrapure water, resistivity of 18.18 mΩ. Oligonucleotides were purchased from Sigma Aldrich (Merck) and Eurofins Genomics (Germany GmbH, Ebersberg).

#### 3.2 Design of the oligonucleotides

The design of the HCR monomers was performed mostly using NUPACK, a growing software that allows the design and the analysis of the secondary structures of nucleic acids (Zadeh et al., 2011a). Thanks to NUPACK we can predict the thermodynamic stability of DNA strands and their propensity to form complexes on the base of thermodynamic models (Dirks and Pierce, 2004a). NUPACK provides two main tools for the design and theoretical analysis of the specific interacting sequences. 1) The Design tool allows us to generate sequences for one or more strands to get a specific secondary structure or complex at the equilibrium Zadeh et al. (2011b). The type of nucleic acids, temperature and salt concentration can be specified, and it is possible to directly define the secondary structure of each structural motive of the strands to generate based on constrains in structure and sequences. Subsequences are defined as *domains* and the program can be instructed about how to concatenate them to form the final strands. The criteria used in the design of NUPACK try to satisfy both positive and negative paradigms: respectively the optimization of the affinity between strands and the selectivity for the specific interaction. Once generated the sequences, NUPACK returns an *ensemble defect* number, that is the average number of nucleotides uncorrectly paired at the equilibrium, as indicator of the goodness of the design. 2) The Analysis tool allows to perform a theoretical thermodynamic analysis of the interacting sequences in a diluted solution and returns information about the species at the equilibrium in the specified conditions. The newly designed strands can be directly evaluated in the Analysis tool, to check if the correct secondary structures and complexes form at the equilibrium. As in the design section, NUPACK let us specify the type of nucleic acid (DNA or RNA) the temperature, the number of nucleic acids species, their sequences, the concentration of each strand and the size of the formed complexes at the equilibrium ( the maximum number of strands involved in the formation of a complex). It is also possible to choose the energy model and the salt concentration. Using dynamical programs, NUPACK calculates the partition function and the probability of the position of each base at the equilibrium. It also returns the *MFE* structure

(minimum free energy) for each complex and species and their final theoretical concentration at the equilibrium. We selected the sequences on the base of 1) the designed secondary structure, 2) the highest probability to form the expected complex at equilibrium, and 3) theoretical presence of possible unspecific interactions.

### 3.2.1 Design of the sequences for direct HCR reaction

We present the steps of the design performed using NUPACK to generate and analyze the sequences of the hairpins for direct hybridization chain reaction in microRNA detection (Miti and Zuccheri, 2018) (Fig 3-1). All the sequences were treated as DNA strands, and the thermodynamic stability was this evaluated in the same conditions.

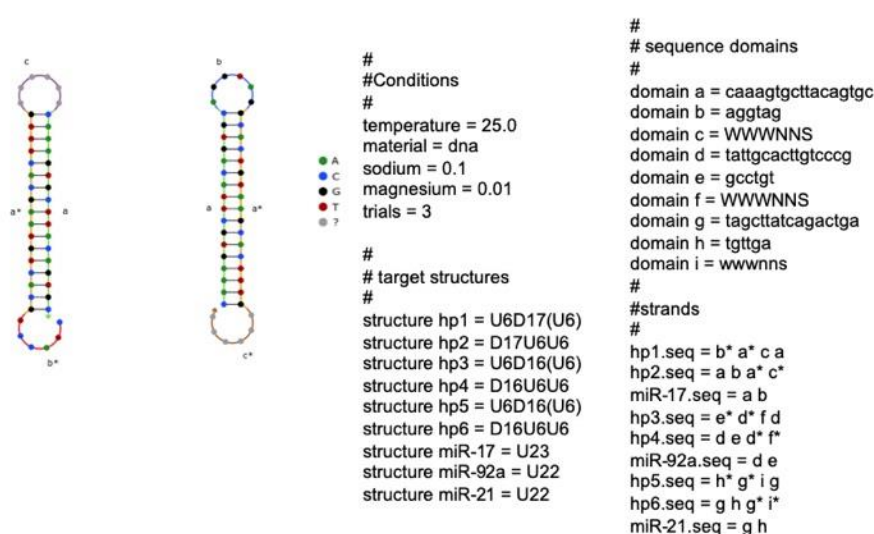


Fig 3-1. Specification of the secondary structure of the individual strands in NUPACK design: 'U' notation means 'single strand' portion, while 'D' means, "double stranded". The information is given in the 5' – 3' direction. Sequence constrains for the generation of hairpins specific for target miR-17. The '\*' notation indicates the complementary strand. 'N' = any base; 'W' = weak binding bases, A or T; 'S' = strong binding bases, C or G; 'K' = keto, G or T; 'M' = aMino, A or C; 'R' = puRine, G or A; 'Y' = pYrimidine, C or T.

1. Theoretical experimental conditions: DNA is specified as material, the temperature value was set at 25 °C (about room temperature) and salt concentration was set at 0.0 M and 0.5 M respectively for the concentration of Mg<sup>2+</sup> and Na<sup>+</sup>, according to the real conditions we chose.
2. Structure description: the structure of each element has been described using parens-dot notation. Three pairs of hairpins have been designed with analogue structure. We kept the length of the toehold and the loop to 6 nt (U6) while the stem had length dependent on the length the target sequence (D16-17).
3. Sequence constrains: here we inserted the specific sequences of the miRNAs as main constrains for the design of the hairpin. Softer constrains about the base composition are

inserted to prevent anomalous structures involving toehold and loop or affecting the polymerization. Additional information was specified to avoid unwanted patterns of bases such as tandem reps of bases.

The generated DNA sequences were analyzed in NUPACK analysis tool, to check the correct theoretical behavior of the designed strands in solution. Temperature was set to 25°C, Mg<sup>2+</sup> to 0 M and Na<sup>+</sup> to 0.5 M. We assessed the secondary structure of the individual strands and the probability to form the required complex, to predict as best as possible the behavior of the sequences in real solutions. The correct functionality of the hairpins in the assembly was tested with the same analysis tool, analyzing the target sequences and hairpins together. The number of strands involved in the formation of the complexes have been set to 3 or to 5, in order to check the theoretical formation of the productive complexes (T-H1-H2) and the capability of the complex to grow interacting with the other hairpins. Attention should be paid about eventual undesired interactions. The analysis was performed setting the concentration of the hairpins to 1 μM and the target in a range between 1 μM or 0.1 μM, towards the investigation of the theoretical behavior at lower concentration of the initiator (the target).

### **3.2.2 Design of the sequences for triplex HCR**

We used NUPACK as shown in section 3.2.1. In order to design the components of the triplex-triggered HCR detection method, we divided the design in two parts: 1) the design of the triple helix probe and subsequently 2) the design of the independent HCR amplifications triggered by the triplex forming strands. We designed the sequences involved in the formation of the triple helix of DNA according to findings in literature (Avino et al., 2002, Gowers and Fox, 1999, Jain et al., 2008, Manzini et al., 1990). Since there is not an available tool for the design of such DNA alternative structure, we treated the probe as a molecular beacon (Fig 3-2).

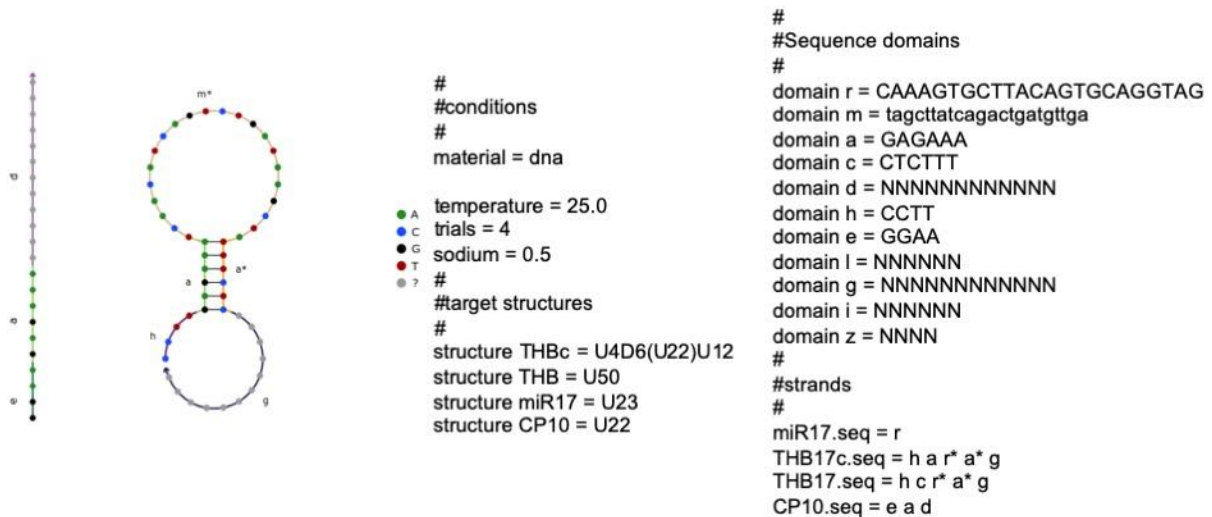


Fig 3-2. Instruction of the design of the triple helix probe. A) Specified structure of the triple helix forming strands; B) design script.

We took into account the referenced differences in stability and carefully considered previously reported triple helix probe applied in biosensing approaches (Wang et al., 2014, Wang et al., 2016a, Zheng et al., 2014b). The selected sequences involved in the formation of the triple helix were inserted in the design, specifying structural and sequence constrains. We designed the monomers for independent HCRs on these sequences as was done for miRNA sequences for the direct HCR in section (Fig 3-3) (Miti and Zuccheri, 2018).

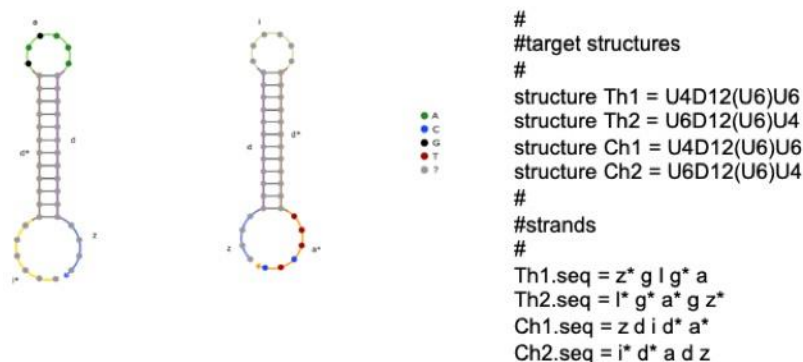


Fig 3-3. Instruction to design the hairpins. A) Structure specified for the pair for hairpins Ch1 and Ch2 for HCR on CP probe.

At the end, the sequences were generated simultaneously with a unique Design script. The sequences were analyzed with NUPACK analysis tool setting 25 °C as temperature and concentration of the reagents set at 1µM or less. The ability of the triple helix forming sequences to trigger the HCRs have been tested independently, checking individual secondary structures, and the formation of multistrand complexes to prevent any undesired interaction. Salt concentration was set to 0 M Mg 2+ and 0.5 M Na+. When necessary, manual adjustment of the constrains were done to optimize the results in analysis.

### **3.3 Characterization of the direct HCR in solution**

DNA oligonucleotides stock solutions (100  $\mu$ M), targets and hairpins, are diluted in PCR tubes in HCR buffer (NaCl 0.5 M, NaH<sub>2</sub>PO<sub>4</sub> 50 mM, pH 6.8), in general at 3-times the final concentration unless specified for more complex experiments. Samples are then subjected to thermal treatment using a Thermocycler (Thermo Scientific, PCR Sprint thermal cycler): 95 °C for 5 min and allowed to cool down to 20°C in 1 h (0.02 °C/second). Stoichiometric amounts of each hairpin were mixed at the proper ratio together by adding then a volume of target solution to the mixture. The reaction is kept at least for 1h at room temperature, unless specified. Reaction product can be characterized directly in gel electrophoresis analysis or atomic force microscopy.

#### **3.3.1 Characterization of the product of direct HCR through electrophoresis gel analysis**

Electrophoresis gel analysis was performed through polyacrylamide gel electrophoresis in TBE 1X buffer unless differently specified. Polyacrylamide gels were prepared at 10 % polyacrylamide in TBE 1X buffer. We mixed buffer to a proper volume of stock acrylamide solution (Acrylamide 40% acrylamide Acrylamide/bis-acrylamide, suitable for electrophoresis, 37.5:1). We added the proper volume of 10% APS (ammonium persulfate, Sigma) solution in ultrapure water and TEMED (N, N, N', N'-Tetramethyl ethylenediamine, Sigma) stock solution to trigger the gel polymerization. Electrophoresis was generally run at room temperature at 5 V/cm for 1 h. 15-wells gels were run 5 V/cm for about 3 hours at controlled temperature, depending on the size of the investigated DNA complexes, the employed running buffer, the temperature and gel density. SYBR Gold (Nucleic Acid Gel Stain, Invitrogen) was then used to visualize the results using a Gel doc (Bio-Rad Gel doc 1000 System).

#### **3.3.2 Characterization of the product of direct HCR through Atomic Force Microscopy**

First the sample were diluted 1/100 in TE 1X (10 mM Tris-HCl, 1 mM EDTA pH 8.0) buffer and loaded on Centrifugal filter units, MWCO 100 kDa Amicon Ultra- 0.5 mL centrifugal filters for centrifugation 8 min at 11 rpm. The samples were then suspended in 200  $\mu$ L of HEPES buffer (10 mM NaCl, 5 mM MgCl<sub>2</sub> pH 7.5) and centrifuged 5 min 11 rpm. We then collected the samples in new tubes, centrifuging 3 min at 1 rpm. Approximately 10  $\mu$ L of the sample were layered on freshly cleaved muscovite mica surface and left adsorbing 5 min. The mica surface was then rinsed with ultrapure water and gently dried with nitrogen. Imaging for atomic force microscopy have been carried out using Bruker Multimode 8 microscope in ScanAsyst Peakforce Tapping mode.

### 3.4 Characterization of the triplex HCR in solution

We investigated the formation of the triple helix probe using polyacrylamide gel electrophoresis and circular dichroism in different conditions.

#### 3.4.1 Characterization of the triple helix in gel electrophoresis

Triple helix forming oligonucleotides were incubated in buffer Na Acetate 20 mM, MgCl<sub>2</sub>, 20 mM NaCl, 50 mM pH 5.0, or Tris buffer 20 mM, MgCl<sub>2</sub> 20 mM, NaCl 50 mM pH 9.0, to assess the formation of the triple helix complex in solution. The oligonucleotides were diluted in the buffer from 100 μM stock solution in water. The mixture was prepared by mixing equal volumes of THB (triple helix beacon) and CP (Capture probe) strands in buffer, to get 1:1 ratio. The mixtures were heated up to 95 °C for 5 min and let cool down till 20°C in 1h (0.02 °C/second) using a thermocycler to allow the annealing. We then incubated at 37°C overnight for subsequent analysis or usage. Polyacrylamide gel electrophoresis 10% was prepared in Acetate buffer pH 5.0 either in Tris buffer pH 9.0 depending on the conditions in study and run in the same buffer.

#### 3.4.2 Circular Dichroism characterization of the triple helix probe

The mixtures containing equimolar CP and THB were prepared in Acetate buffer 20 mM, NaCl 50 mM, MgCl<sub>2</sub> 20 mM pH 5.0 or in Tris buffer 20 mM, NaCl 50 mM, MgCl<sub>2</sub> 20 mM pH 9.0. For both mixture (THB + CP) and individual strands solutions, we adjusted the concentration to get an absorbance at 260 nm between 0.5 and 1. CD experiments were carried out using Jasco J-710 circular dichroism spectropolarimeter, kindly provided by Dr S. Pieraccini (University of Bologna). Scan rate was set to 100 nm/min performing 5 scans per measurement. The spectra were recorded using a 1 cm pathlength cuvette. The obtained CD spectra where in millidegrees θ units. Molar extinction Δε (mdegrees M<sup>-1</sup> cm<sup>-1</sup>) was calculated after the subtraction of buffer signal by using the formula:

$$\Delta\epsilon_{\lambda} = \frac{\theta_{\lambda}}{32,980 \times l \times C}$$

Where *l* is the path length (1 cm) and *C* the concentration in mol/L evaluated from the measured absorbance at 260 nm of each sample. Normalization for each sample was performed on the absorbance at 260 nm.

### 3.4.3 Characterization of the triplex HCR in solution

The triple helix was formed as described in the previous sections but in HCR buffer at pH 5.0. To We followed a protocol similar to that previously explained in the section 3.3. After the incubation of the triple helix mixture, the proper volume of this solution was added to the mixture of the hairpins. Right after that, we added a volume of target solution at the desired concentration. The mixture was then incubated at room temperature for at least 1 h. We characterized the product in polyacrylamide gel electrophoresis and atomic force microscopy, as mentioned in the previous sections.

### 3.5 Electrochemical setup

Electrochemical measurements were carried out using a custom-made electrochemical setup connected to a  $\mu$ Autolab electrochemical workstation (Metrohm Autolab B.V., Utrecht, The Netherlands), using the manufacturer's software NOVA. Two platinum wires were used as counter electrodes with silver wires were coated with silver chloride and used as reference electrodes. The references electrodes were directly prepared in the cell by depositing silver chloride at the surface through anodic reduction in KCl 0.1 M, setting the silver wire as working electrode and flowing a fixed 0.15 mA current for 153 s. As working electrodes, we used gold surfaces commonly referred to as 'templated stripped gold' (TSG), offering flat gold surfaces. The device has two slots for the installation of the TSGs with two independent chambers and fluidics (Fig 3-4).

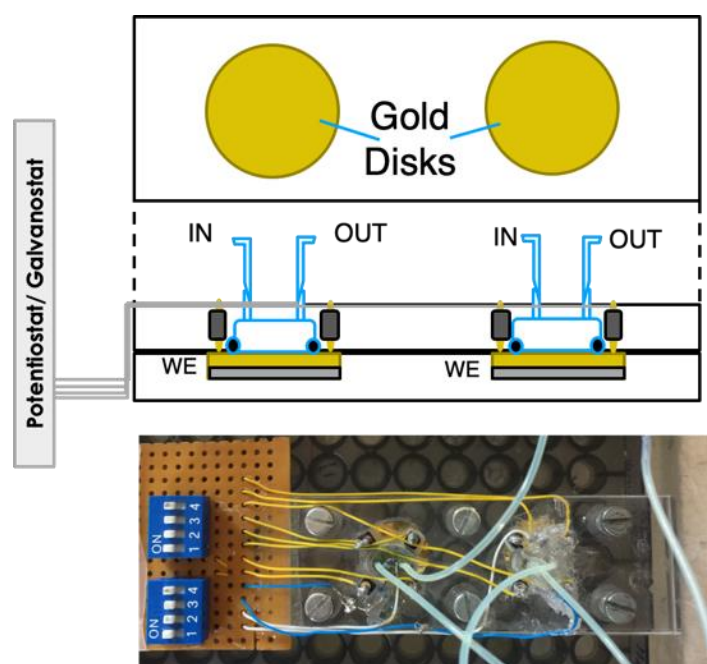


Fig 3-4. Scheme and picture of the electrochemical cell used during the work. Gold disks are TSG produced in the lab, used as working electrodes (WE). Inlet and Outlet tubing were PTF tubing (diameter). Copper wires were used to connect the cell electrodes to the Potentiostat.

The fluidics was made using PTFE Tubing, ID 0.5 mm, OD 1 mm. Solution were flowed in the cell using a Syringe Pump (Multi-Syringe Infusion/Withdrawal Pump, World precision instruments). The area where measurement took place is enclosed in the chamber using an O-ring and was about 0.23 cm<sup>2</sup>. Each individual cell volume was 13 mm<sup>3</sup>. Working electrodes were connected to the Potentiostat thanks to copper wires and gold spring contacts. All the wires were welded on a stripboard and then connected to the Autolab Potentiostat through banana plugs, using copper wires and pin connectors.

### **3.5.1 Preparation of the and functionalization of the TSGs (electrode surfaces).**

We produced our own gold electrodes (TSG) by forming a 200 nm layer of ultrapure gold (SIGMA-ALDRICH, Merck, 99.99 % purity, diam 0.20 mm) through evaporation in vacuum onto freshly cleaved muscovite mica. The mica was previously degassed overnight at 280°C in a vacuum of about 10<sup>-6</sup> Torr. The process was performed using an Edwards high-vacuum evaporator with a resistively heated specimen stage and resistive heating of the metal for the evaporation. After the evaporation, when the system is at room temperature, round glasses cover slips (12 mm in diameter) were glued on the evaporated gold layer with glue EpoTek 377 (Epoxy Technology Inc., Billerica, MA, U.S.A.). Then, the chips were heated for 2h at 150°C and cooled down to room temperature. They can be stored for later use. Before use, we removed the glass cover slide with the glued gold layer from the mica. This would be an ultra-flat and ultra-clean gold surface. The gold surfaces were sonicated 1 min in EtOH and a 1 min ultrapure water, to remove eventual organic compounds still on the surface or small residues of mica. The gold surfaces were then subjected 1min to air plasma treatment (1 min, 100% power) to further remove organic material and Argon plasma to get a reduced gold surface. A cleaner surface can be obtained performing an electrochemical pre-cleaning in H<sub>2</sub>SO<sub>4</sub> 0.5 M, using cyclic voltammetry. We performed 20 scans, series of oxidation and reduction cycles of the gold, between -0.4 V and + 1.6 V until the voltammogram was stable and reproducible. The cathodic peak, corresponding to the gold reduction, was monitored as index of the cleanness of the gold surface. The gold surface was then treated for the immobilization of the DNA probe. The proper concentration of the DNA probe was prepared in immobilization buffer (Tris-HCl 20 mM, NaCl 0.5 M, pH 7.4) and 40 µL of this solution were dropped on the gold surface. The incubation was performed overnight at room temperature in humid environment to avoid the evaporation of the solution. After the immobilization of the probe, we rinsed the surface with 2 mL of immobilization buffer and 2 mL of ultrapure water, and then passivated with 6-mercaptohexanol (MCH) 1 mM, for 30 min. The electrode was then rinsed with 2 mL of ultrapure water and dried with gentle N<sub>2</sub> flow.

### 3.5.2 Electrochemical measurements

Cyclic voltammetry and electrochemical impedance spectroscopy were used to monitor the cleanness and the functionalization of the electrodes. Cyclic voltammetry was performed in general scanning between -0.25 V and 0.5 V vs reference electrode, with potential step 0.1 V, in a solution containing 10 mM  $K_3FeCN/K_4FeCN$ , 0.1 M KCl in Tris 10 mM pH 7.4. Electrochemical impedance spectroscopy was performed in the same solution 10 mM  $K_3FeCN/K_4FeCN$ , 0.1 M KCl in Tris 10 mM pH 7.4, vs OCP (open circuit potential) potential with amplitude 0.01 V, scanning in a range of 50 frequencies between 1 Hz and 100kHz. We used NOVA software to perform all the measurements (Metrohm Autolab B.V., Utrecht, The Netherlands). DNA detection was performed using Hoechst 33258. We flowed 200  $\mu$ L of 100  $\mu$ M Hoechst solution in buffer NaCl 0.1 M  $NaH_2PO_4$  10 mM pH 7.0 in the chamber at 50  $\mu$ L/min and incubated for 1 min. The chamber was then flushed with 200  $\mu$ L of buffer NaCl 0.1 M  $NaH_2PO_4$  10 mM pH 7.0 at 50  $\mu$ L/min and the electrochemical measure was performed. Oxidation of the Hoechst was monitored in the same buffer using Linear Sweep Voltammetry (LSV), scanning between + 0.4 V and +0.7 V vs reference electrode. The oxidation of Hoechst on surface returned a peak at about 0.5-0.6 V. Hexaammineruthenium(III) chloride (RuHex) was also used to monitor probe immobilization on the surface of the electrode. 100  $\mu$ L solution of 300  $\mu$ M RuHex in KCl 0.1 M solution was flowed and the detection was performed through differential pulse voltammetry (DPV) registering the peak at about - 0.2 V characteristic of RuHex reduction.

### 3.5.3 Electrochemical detection of microRNA sequences through direct HCR

The detection of the microRNA sequence was performed out of the chamber. For the detection, 50  $\mu$ L of solution containing the desired concentration of miRNA DNA sequence in HCR buffer (NaCl 0.5 M,  $NaH_2PO_4$  50 mM pH 6.8) were dropped on the electrode and incubated 1h at room temperature. The electrode was then rinsed with 1 mL HCR buffer and dried with nitrogen flow before dropping 50  $\mu$ L of the mixture of hairpins H1 and H2 at 1  $\mu$ M each. The reaction was incubated 1h at room temperature to let the self-assembling reaction proceed. The electrodes were then rinsed with 2 mL of HCR buffer and kept in HCR buffer until the measurement in the electrochemical cell.

### 3.5.4 Electrochemical detection of microRNA sequences through triple helix-controlled HCR

Once the electrode was functionalized with the probe and passivated with MCH, 50  $\mu$ L of 3  $\mu$ M THB strand in HCR pH 5.0 buffer containing 2.5 mM  $MgCl_2$  were dropped on the surface and incubated at 37 °C for 1h before proceeding with the detection. We then rinsed the electrodes

with 2 mL of HCR buffer pH 5.0 and dropped the mixture of target with the four hairpins TH1, TH2, CH1 and CH2 at the desired concentration in the same buffer. The mixture was incubated on the electrode surface for at least 1h. We then rinsed the electrodes with 2 mL of HCR buffer pH 5.0 and kept in HCR buffer until the measurements in the electrochemical cell.

### 3.5.5 Analysis of data obtained in electrochemistry

CV data were analyzed by measuring the height of the oxidation and reduction peaks. The bare distance between the two peaks was evaluated to investigate the electrode cleanliness. Data obtained in Electrochemical Impedance Spectroscopy were evaluated by simply fitting over a semi-circle in a Nyquist plot using a R(RQ) equivalent circuit or, more exhaustively, fitting over a Nyquist plot using a  $Re(Rt[RtZw])$  circuit model (NOVA).

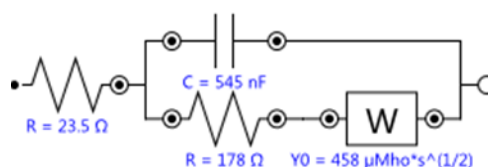


Fig 3-5. Equivalent circuit used to fit EIS data.

LSV data were analyzed after baseline correction and measuring the height of the oxidation current peak on the baseline for each samples. The height of the peak was considered proportional to the amount of DNA absorbed at the surface. The data were normalized over the responses obtained on electrodes where just the MCH passivation was performed in the same measurement session. In experiments performed using RuHex, the height of the reduction peak in DPV was evaluated.

## 3.6 LSPR

The LSPR setup used during this work was kindly provided by the group of Professor Fritzsche, of the Department of Nanobiophotonics at the Institute of Photonic Technology (IPHT) in Jena (Germany). The overall setup consists in an Halogen light source ( HL-2000 by Ocean Optics, Dunedin, USA) with a filter  $<400$  nm, a spectrophotometer (Cypher II by B&W Tek Inc., Newark, USA), a peristaltic pump for the fluidics (Ismatec Reglo ICC by Cole-Parmer GmbH, Wertheim, Germany), two optical large-core fibers and an LSPR custom-made fluidic cell. Fig 3-6 show a simplified scheme of the setup.

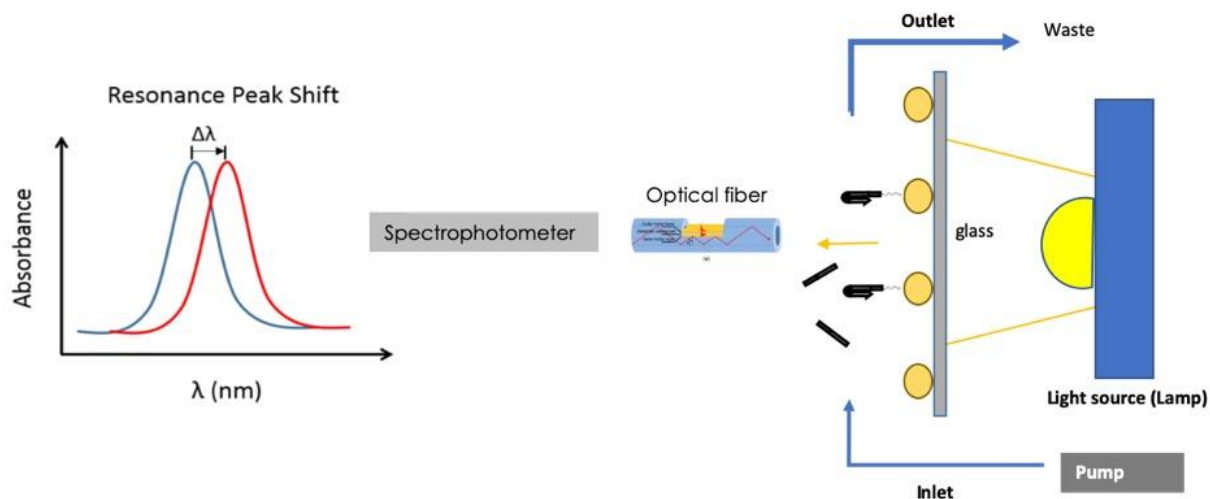


Fig 3-6. Scheme of the setup employed for LSPR based detection.

The fluidic is organized to have four inlets and two outlets. This is arranged to have always a main flow reaching the sensing area, while the subsequent solution is pre-flowed at lower rate and flashed in the waste. This is all possible thanks to two valves at the waste outlet, and a splitter at the inlet allowing the separation of the four channels. All the buffers were prepared in ultrapure water and filtered with 0.2  $\mu\text{M}$  filter before use.

### 3.6.1 Preparation of the LSPR Chips

The glass slides used were obtained from common microscope glass slides. The slides were carefully cleaned with a rinsing agent (soap) then subjected to multiple sonication in different organic solvents and water: 10 min in Acetone, 10 min in Rotisol (denatured alcohol), 10 min in ethanol and 10 min in ultrapure water. The glass slides are then dried with  $\text{N}_2$  flow. The glasses were etched by oxygen plasma for 60 min, 380 W and 1.6 mbar to removes organic residues and activate them for the silanization (Oxygen plasma etcher 200G Plasma System by TePla GmbH, Wettenberg, Germany). The affinity of the gold nanoparticles for the glass surfaces was enhanced functionalizing the glass surfaces with amine groups. The affinity of the glass surface to the gold nanoparticles is increased with aminosilanes. A solution of 1 % APTES in 1 mM acetic acid is prepared and let hydrolyze for 10 min. The cleaned slides were soaked with the APTES solution for 10 min. The slides were then washed in ultrapure water and gently dried with nitrogen. A solution of citrate capped 80 nm gold nanoparticles was centrifuged 8 min at 3220 X g (Centrifuge, UniCen 15DR by Herolab GmbH, Wiesloch, Germany) and 1800 mL of supernatant discarded to get 10-fold concentrated solution of gold nanoparticles. We dropped 20  $\mu\text{L}$  of the concentrated gold nanoparticles solution in the center of the amino-functionalized glass slides and left adsorbing 60 min. The glass was then gently rinsed with ultrapure water and dried with nitrogen flow. At the end of the procedure, a red spot should be visible in the center of the glass. We

assessed the density of the gold nanoparticles using Atomic Force Microscopy and dark field microscopy.

### **3.6.2 Functionalization of the LSPR chips**

The glass slides with the spot of gold nanoparticles were rinsed with 2 mL of ultrapure water, 2 mL of EtOH and 2 mL of ultrapure water again. The thiolated probe was reduced using TCEP 0.5 M. We added to the probe solution in ultrapure water a volume of TCEP 0.5 M to get 20 mM in the final solution and we incubated the mixture at room temperature for at least 1 h. The probe was then diluted to 2  $\mu$ M in citrate buffer 0.5 M, pH 6.0. The immobilization was performed by layering on the chip 50  $\mu$ L of this solution and incubating for about 18 hours at room temperature in closed petri dish to avoid evaporation. After the overnight incubation, the glass slides were rinsed with 2 mL of citrate buffer, 2 mL of ultrapure water and stored in the HCR buffer.

### **3.6.3 LSPR measurements and detection**

Valves, spectrophotometer, pump and the online detection were controlled using a custom-built Python program (Python 3.6). The chip with the immobilized gold nanoparticles was mounted in the chamber and fixed between the lamp and the optical fiber. The chip was inserted in the fluidic chamber in presence of buffer, in contact with a PDMS O-ring, with the spot of nanoparticles in the direction of the light source and the glass facing the optical fiber (see Fig 3-6 ). The chamber is then closed tight with four screws at the edges. The lamp spectrum is taken, making sure that no over or under exposure occurs. The chamber is then fixed between the lamp and the optical fiber as close as possible to the fiber, pointed at the center of the spot. The distance between the glass and the optical fiber was usually about 1-2 mm. This was kept constant for all the measurements. All the measurements are done in flow conditions and a spectrum is recorded every 2 s. In order to reduce the noise affecting the position of the LSPR peak during the measurement, the centroid of the LSPR peak is calculated at each point. The position of the plasmonic peak is tracked in real-time.

Steps	flowrate_1	flowrate_2	flowrate_3	flowrate_4	Time (s)	Step
1	20			10	300	HCR buffer
2	5			20	300	MCH
3	20			10	400	HCR buffer
4	5			20	300	Fish
5	20		10		400	HCR buffer
6	2		5		600	target 1 $\mu$ M
7	20	10			600	HCR buffer
8	2	5			1000	HCR
9	20			10	600	HCR buffer
10	2			30	800	Regeneration
11	20		10		400	HCR buffer

Fig 3-7. Typical experimental plan describing each step, with flow rate in  $\mu$ L/min, time in seconds and the composition of each sample flowed in the chamber in the corresponding step.

We used HCR buffer for the detection. During buffer steps, running buffer was injected at 20  $\mu$ L/min while the reagents at 5  $\mu$ L/min. During the reagents flow ( flowrate\_2, 3, 4 in Fig 3-7), buffer was injected at 3  $\mu$ L/min as preflow and reagents at 10  $\mu$ L/min. Usually buffer is flowed until the signal is stable then we injected MCH 1 mM in the same buffer for 300 s. After MCH, we flowed fish sperm DNA at a concentration of 1 mg/mL in running buffer to passivate the glass surface. After the passivation step, we were able to proceed to the detection. The desired concentration of target in running buffer was injected for 600 s in the chamber. After the injection of the target, running buffer was flowed for 300 s. To test the hybridization chain reaction, volumes of 1  $\mu$ M concentration in running buffer of each species of hairpins were mixed to get a mixture 0.5  $\mu$ M and flowed in the chamber for at least 30 min at 5  $\mu$ L/min. The regeneration of the sensor was obtained with 20 mM solution of HCl, injected for 600s at 30  $\mu$ L/min. After regeneration, we were able to repeat the experiment. All the experiments were repeated at least 3 times on the same chip after regeneration. Target and hairpins were heated up to 95  $^{\circ}$ C for 5 min and then let cool down at room temperature before usage.

#### 3.6.4 Analysis of the LSPR data

We did the analysis using Python scripts able to return graphically the data obtained during the LSPR experiments, as position in nm of the LSPR peak over time. The scripts allow us to access to all the raw data collected and calculate the mean values of centroid position in selected intervals. The basic analysis consisted in calculating the differences in the centroid position at each step. Normalization was done over the change in the position of the LSPR peak observed with 1  $\mu$ M target concentration, chosen as indicator of the amount of probe immobilized on the nanoparticles.

### 3.7 DNA templated mixed platinum-silver nanoclusters: synthesis and characterization

The DNA-Ag/Pt NCs have been prepared following a protocol based on the method described by Zheng et.al (Zheng et al., 2014a). The Annealing of the oligonucleotides was performed heating the mixture to 90 °C for 5 min then cooling down to 20 °C for 1 hour in thermocycler. The experiment was performed in TEM Buffer (50 mM Tris, 5 mM EDTA, 20 mM MgCl<sub>2</sub>, pH 8.0) and Phosphate buffer (10.0 mM, pH 7.4) to check the annealing also in the reaction conditions. The oligonucleotides were diluted to 4 μM in the buffer. 15 μL of unmethylated or methylated sequence were mixed to 15 μL of complementary strand to get 2 μM. We performed polyacrylamide gel electrophoresis to evaluate the annealing. The electrophoresis was carried in 1 × TAE Mg<sup>2+</sup> (40 mM tris-acetate, 12,5 mM magnesium acetate, 1 mM EDTA pH 8.0) at 40 V constant voltages for 3 h at room temperature. The mixed AgPt nanoclusters were formed on these templates. Briefly, 50 μL of a 150 μM AgNO<sub>3</sub> solution, 120 μL of 125 μM K<sub>2</sub>PtCl<sub>4</sub> solution were mixed to the template double stranded DNA (300 μL, 2 μM) in phosphate buffer 10.0 mM pH 7.4. After incubation for 30 min in the dark, we added immediately 40 μL of freshly prepared 5 mM NaBH<sub>4</sub> solution, under stirring conditions. The mixture was allowed to react at 37 °C for 3 h. The DNA-Ag/Pt NCs can be stored at 4°C for 1 month. In order to detect the peroxidase-like activity of DNA-Ag/Pt NCs, 10 μl of DNA-Ag/Pt NCs solution were diluted in acetate buffer 200 mM at pH 4.0, then mixed with 20 μl H<sub>2</sub>O<sub>2</sub> and 40 μl TMB to initiate the colorimetric reaction. The reaction was monitored by UV–vis spectroscopy at 652 nm using a common spectrophotometer. All the experiments were repeated three times to test the reproducibility. The formation of the nanoclusters was characterized in standard polyacrylamide gel electrophoresis in TBE 1X, in spectrophotometry scanning between 200 and 800 nm of wavelength, Atomic Force Microscopy and Transmission Electron Microscopy (TEM). ImageJ was used to analyze the TEM images to estimate the size of the nanoclusters.

## 4 Results and discussion

During the work described in this dissertation, we were able to evaluate different strategies and nanotechnological tools suitable for the development of new biosensing devices. In particular we focused on the detection of short sequences such as microRNAs (Fig 4-1). We focused on DNA-based biosensors, and we faced possible solutions to enhance the signal generated by such methods. This could be done by employing self-assembling reactions that can increase the response by increasing the local amount of DNA upon target detection. The reaction taken into consideration for this purpose was the Hybridization Chain Reaction (HCR). We tried to develop two methods based on this isothermal amplification, designing two alternative probes as connecting elements between the target detection and the amplification of the response. The first method, as in the classical HCR, is based on the direct interaction between the miRNA and one of the hairpin-like DNA strands, followed by the polymerization of the two species of monomers. We will refer to this method as “direct HCR” method. The second method was designed introducing a triple helix probe: the detection of the target takes place in a large loop of a DNA strand, which is closed forming a triple helix structure on a second strand. The probe looks like a DNA beacon with a triple helix stem. The recognition of the target would set both strands free, exposing previously hidden sequences. In our method, we used these free sequences as triggers of a double HCR-based response. We proposed an original design never reported in literature, taking advantage of both the triple-helix forming strands for to amplify the target detection. We will refer to this method as “triplex-triggered HCR” using a “triple helix probe”. We will present the efforts done towards the implementation of both the methods on biosensing platforms. Other strategies for signal enhancement were explored, working on the usage of other nanotechnological tools. Our idea was to eventually combine these tools with the proposed DNA-based methods. We worked on the realization and characterization of metal nanoparticles for this purpose. In particular, we synthesized and characterized different gold nanoparticles as possible signal transducers and enhancers in electrochemical, but also LSPR based detection methods. We had the chance to adapt our direct-HCR method on an original LSPR setup based on immobilized gold nanoparticles. Moreover, we had the chance to realize and characterize mixed DNA templated Ag/Pt nanoclusters (DNA-Ag/Pt NCs), theoretically able to return different kind of responses, through electrochemical but also optical transduction. We mainly focused on electrochemical and SPR-based transduction, evaluating the suitability and robustness of the proposed methods. All the data presented below are obtained using DNA sequences of the microRNAs. In Fig 4-1 we show a scheme illustrating the workflow of the overall project.

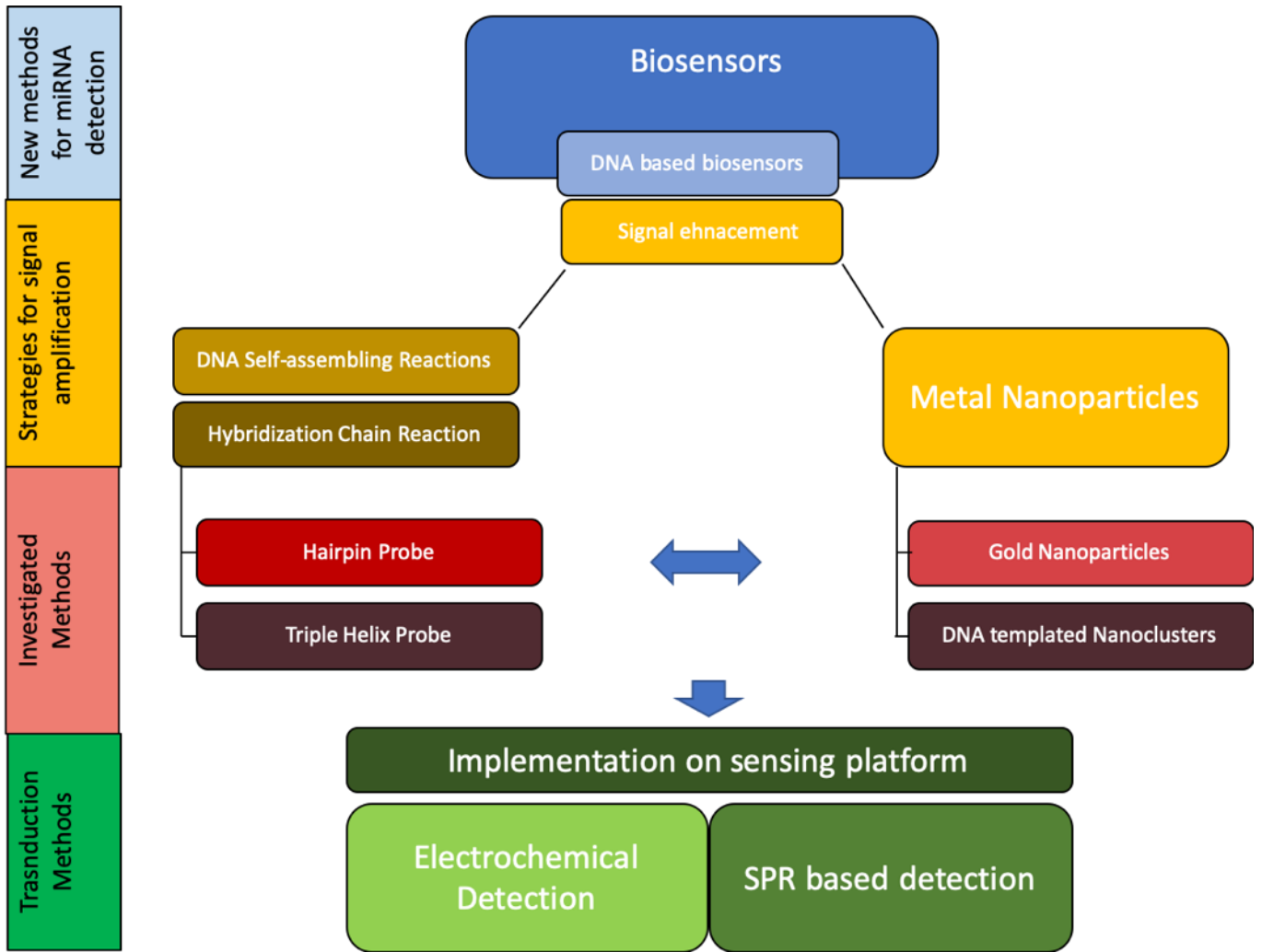


Fig 4-1. Scheme showing the summary of what we attempted to do during the project.

## 4.1 Direct Hybridization Chain Reaction

The miRNA sequences were selected out of informative miRNAs for lung cancer diagnosis, as reported in literature. A pair of hairpins was designed for each miRNA target and the self-assembling reaction was deeply characterized in solution to assess its robustness and the performances in detection. Once the reaction was characterized in solution, the subsequent step was the implementation on a biosensing platform. We were able to test the detection of a miR-17 using direct HCR on custom-build electrochemical setup, and the same was performed using LSPR setup. Results and discussion about these works are presented below.

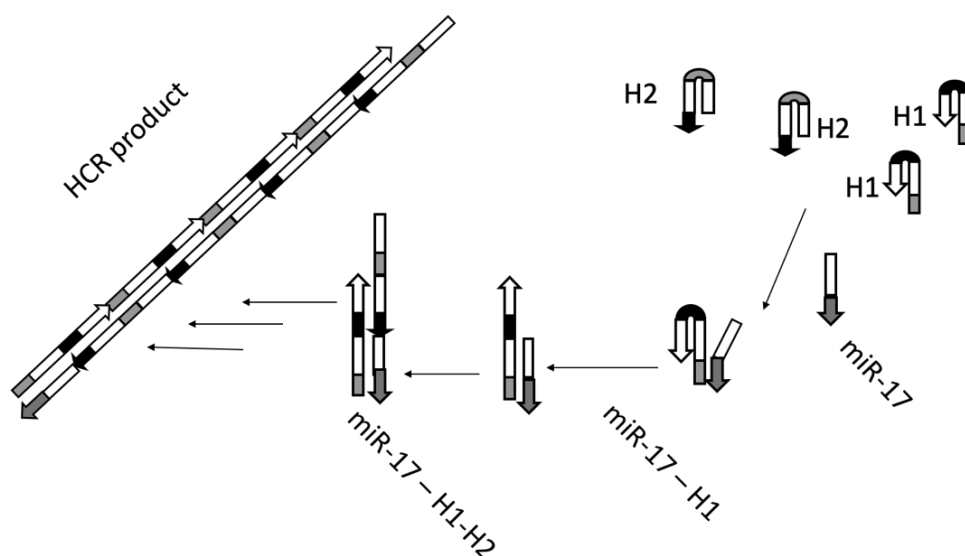


Fig 4-2. Scheme of the direct HCR method for microRNA detection.

### 4.1.1 Design of direct HCR based detection

First, attentions were directed to the selection of the miRNA targets. Bianchi and coworkers (Bianchi et al., 2011), as previously anticipated in the introduction, found signatures of circulating miRNAs related to the early diagnosis of lung cancer in plasma and serum. Boeri et al (Boeri et al., 2011) described a pool of miRNAs in common with Bianchi's study for lung cancer diagnosis. We decided to start from the common pool of miRNAs, and we chose miR-17 and miR-92a. These miRNAs were upregulated in blood in this context. In addition, we picked miR-21, known to be involved in many pathways and deregulated in a large group of tumors. In order to find possible competitors for a better evaluation of the specificity of the detection method, we used BLAST, Basic Local Alignment Search Tool (Altschul et al., 1990) to look for existing microRNAs showing similarities with the selected targets. Beside these sequences, we also selected unrelated microRNAs, also reported in the common group of miRNAs in the studies of Bianchi and Boeri.

Table 4-1. Sequences of the microRNAs took in consideration during this work. MiR-17, miR-92a and miR-21 selected as targets. miR-106b and miR-25 individuates as most similar sequences respectively to miR-17 and miR-92a; different bases are in red and '-' markers correspond to missing bases in the sequence compared to the target. The rest of miRNAs are not related to the specific targets but included in the common pool of miRNAs.

miRNA	Sequences (5' – 3')	Length (nt)
miR-17	CAAAGUGCUUACAGUGCAGGUAA	23
miR-106b	UAAAGUGCUGACAGUGCAGAU --	21
miR-92a	UAUUGCACUUGUCCCGGCCUGU	22
miR-25	CAUUGCACUUGUCUCGGUCUGA	22
miR-21	UAGCUUAUCAGACUGAUGUUGA	22
miR-30c	UGUAAACAUCCUACACUCUCAGC	23
miR-140-5p	CAGUGGUUUUACCCUAUGGUAG	22
miR-486-5p	UCCUGGUACGAGCUGCCCCGAG	22

The overall sequences of the miRNAs are collected in Table 4-1. The characterization was started for the all three targets miR-17, miR-92a and miR-21, while the other sequences were used to test the specificity. We designed hairpins for HCR amplification simply by considering the specific sequence of the microRNAs as the main constrains in the design. The stem length of the hairpins was thus dependent on the length of the target, and we kept the toeholds fixed at 6 nt, inspired by Dirks and Pierce's design (Dirks and Pierce, 2004). In the perspective of a smart design, the sequence of the first hairpin, responsible for the target detection (H1, H3, H5), was arranged to interact, through the toehold, at the 3' portion of the target. Studying the databases revealed higher differences between miRNAs in this region, thus the aim was to improve the specificity by enhancing the discrimination between similar real existing miRNAs. Moreover, the hairpin-like structure should further avoid unspecific interactions, thanks to a double-check recognition, which would involve the sequence complementarity and the thermodynamic barrier of the closed stem.

Table 4-2. Sequences of the Hairpins generated with NUPACK design and analysis. H1, H2, for HCR specific for the detection of miR-17; H3 and H4 for miR-92a; H5 and H6 for miR-21.

Name	Sequence (5' – 3')	Length (nt)
H1	CTACCTGCACTGTAAGCACTTTGAATTCGCAAAGTGCTTACAGTGC	46
H2	CAAAGTGCTTACAGTGCAGGTAGGCACTGTAAGCACTTTGCGAATT	46
H3	ACAGGCCGGGACAAGTGCAATAAATTCGTATTGCACTTGTCCCG	44
H4	TATTGCACTTGTCCCGGCCTGTCGGGACAAGTGCAATACGAATT	44
H5	TCAACATCAGTCTGATAAGCTAAATCTCTAGCTTATCAGACTGA	44
H6	TAGCTTATCAGACTGATGTTGATCAGTCTGATAAGCTAGAGATT	44

The sequences of the generated hairpins are collected in Table 4-2. We used NUPACK to design and predict the secondary structure of the hairpins. The overall structures of the hairpins corresponded in general to those specified in the design, described in the section 3.2.2 Design of the sequences for direct HCR reaction in Material and methods.

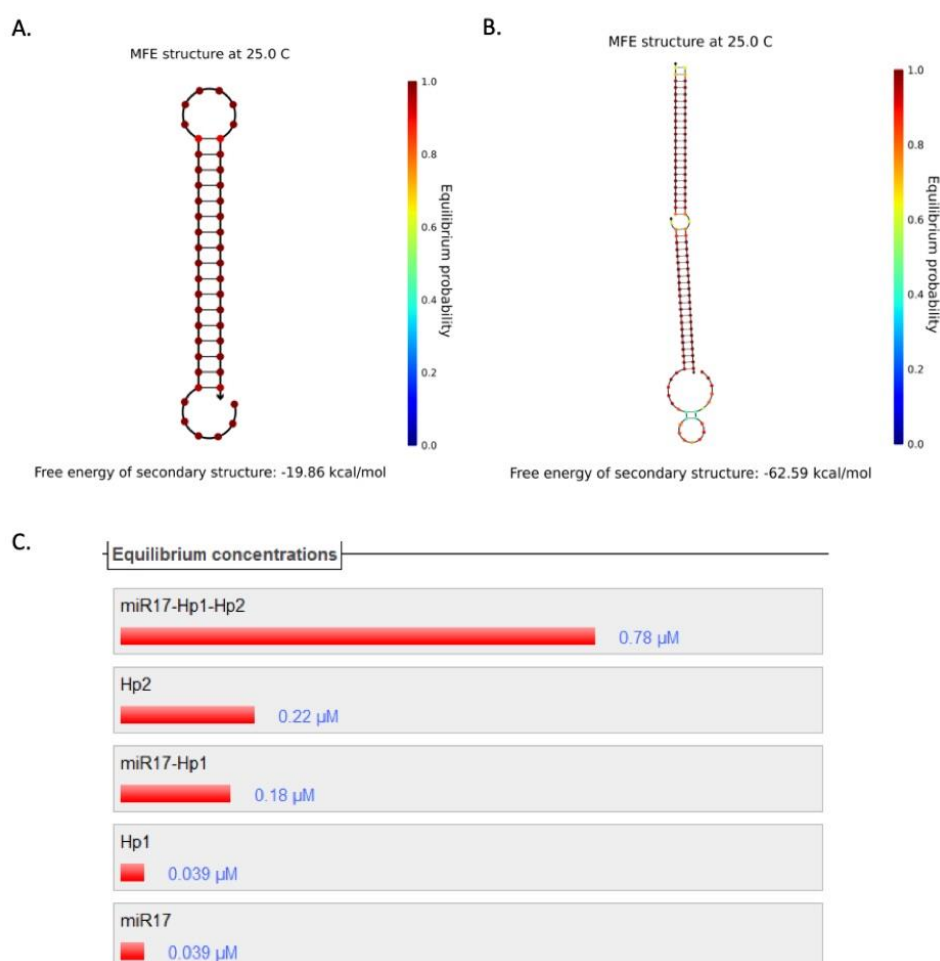


Fig 4-3. MFE (minim free energy) structures calculated by NUPACK for A). Hairpin H1 and B). the complex miR-17-H1-H2. The color scale indicates the probability of each base to occupy the depicted position. Dark red bases are more likely to be in that position, while shifting to blue the position become more uncertain. This can be considered as marker of the stability of the complex. C) Histogram showing the concentration of each species at the equilibrium, returned from the NUPACK analysis tool.

Fig 4-3 A and B show the minimum free energy structures (MFE) corresponding to H1 (A) and the complex miR17-H1-H2 (B). These are the results of the NUPACK analysis, and they give information about the stability of the proposed secondary structures by indicating the probability of finding each base in the showed position at the equilibrium. In Fig 4-3 C we can also see the predicted concentration of each complex at the equilibrium. We also investigated the theoretical formation of bigger complexes, and similar results were obtained for the detection of all the three targets (data not shown) This was used to evaluate the ability of the strands to interact and be involved in the self-assembly. Furthermore, we analyzed the interactions of the hairpins with the competitors miR-106b and miR-25 and unrelated miRNAs. The propensity of the hairpins to interact between each other without target is an important parameter to pay attention to. Since the information needed for the self-assembly is always present in solution, even if trapped in the hairpins, HCR is intrinsically subjected to “leakage”, as spontaneous spurious self-assembly due to random opening of few hairpins in solution. Thus NUPACK analysis allowed us the evaluation of the theoretical “leakage” of the reaction, as additional information about the stability of the hairpins. This was done checking the probability of formation of unspecific complexes ( with no target involved) between the hairpins. Unstable hairpins would return in NUPACK the formation of nanostructure in absence of the specific target. Once satisfied about the theoretical behavior of the generated sequences, we purchased the DNA oligonucleotides and moved to in tube experimentation.

#### **4.1.2 The product of the direct Hybridization Chain Reaction in solution**

The functionality of the hybridization chain reaction in solution was assessed mostly analyzing the final product through polyacrylamide gel electrophoresis. This technique can simply give us information about the interactions between DNA strands in final equilibrium, in the conditions of analysis. The reaction product obtained in solution was characterized through polyacrylamide gel electrophoresis.

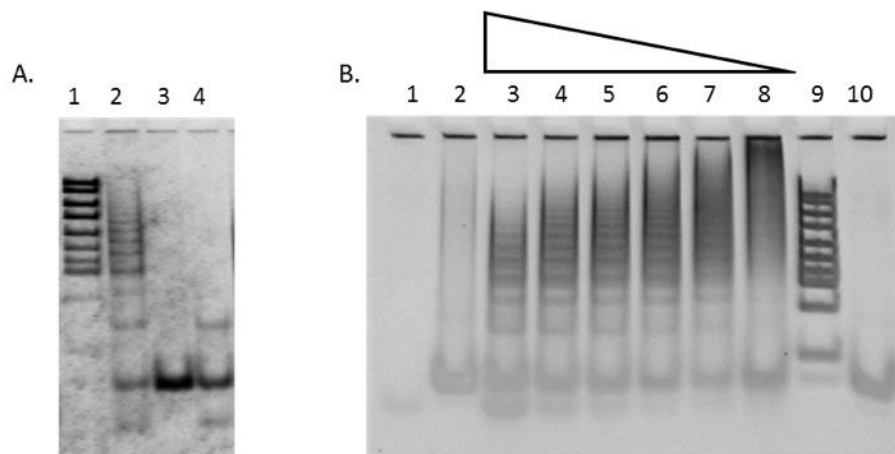


Fig 4-4. A) Section of gel electrophoresis showing HCR products (lane 2), the hairpins without target (lane 3) and H1 + miR-17 sequence (lane4). B) Section of gel electrophoresis showing the behavior of the HCR in presence of decreasing concentrations of target miR-21, 10  $\mu$ M, 3  $\mu$ M, 2  $\mu$ M, 1  $\mu$ M, 0.5  $\mu$ M, 0.1  $\mu$ M, with 1  $\mu$ M hairpins concentration.

As we can see in Fig 4-4 A electrophoresis is able to return information about the occurred self-assembling reaction. HCR product is, in general, discriminated as a group of higher molecular weight bands. In lane 2 we can see the typical product of the hybridization chain reaction in presence of 0.5  $\mu$ M target, 2:1 ratio (Hairpins: Target), in HCR buffer NaCl 0.5 M, Na<sub>2</sub>HPO<sub>4</sub> 50 mM, pH 6.8. When the target is not in the mixture (lane 3), an intense band corresponding to the hairpins is visible, with no higher molecular weight bands, suggesting that no important leakage occurred. It is very important to discriminate between the specific HCR product and the leakage of the reaction. In Fig 4-4 B, another feature of hybridization chain reaction is also visible, enlightening the mechanism of the reaction. Since the growth of the nanostructures depends on the availability of the hairpins in sustaining the polymerization, a higher concentration of target at fixed concentration of the hairpins would lead to the formation of shorter DNA nanostructures. This is due to the fact that the hairpins are more involved in the interaction with the target to form complexes containing smaller amount of monomers. A lower concentration of target triggers the formation of longer products because most of the hairpins are available to build up the nanostructure. In the gel in Fig 4-4 B, this trend is quite clear, with a higher molecular weight product at the lowest concentrations of target miR-21. Same results have been observed for the three targets, proving the efficiency of the reaction in solution and its mechanism. We further characterized the HCR product with Atomic Force Microscopy, to get information about the morphology of the double stranded linear nanostructures.

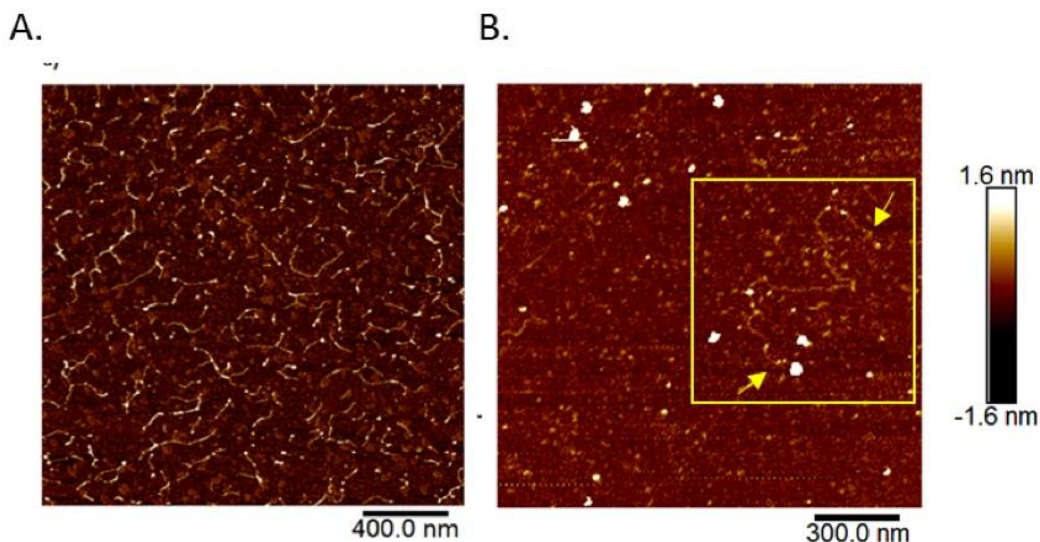


Fig 4-5. Atomic force microscopy images showing the HCR product obtained in solution.

Atomic force microscopy was used to characterize the size of the HCR product obtained. We were able to estimate the effective sizes of the HCR products and their shape. We observed structures with average of 200 nm length for reaction in 2:1 ratio (Hps:target) with linear nanostructures but also some branched structures ( Fig 4-5. A). We were also able to detect products reaching about 1  $\mu\text{m}$  in length as shown in Fig 4-5. B. Thus, hybridization chain reaction worked in the considered conditions in response to the short miRNA targets, with products coherent in morphology with the expected HCR nanostructures.

#### 4.1.3 The rate of the hybridization chain reaction

We wanted to have some rough information about the kinetics of the self-assembly. We tested the rate of the reaction simply incubating the mixture during different times and analyzing the product in gel electrophoresis.

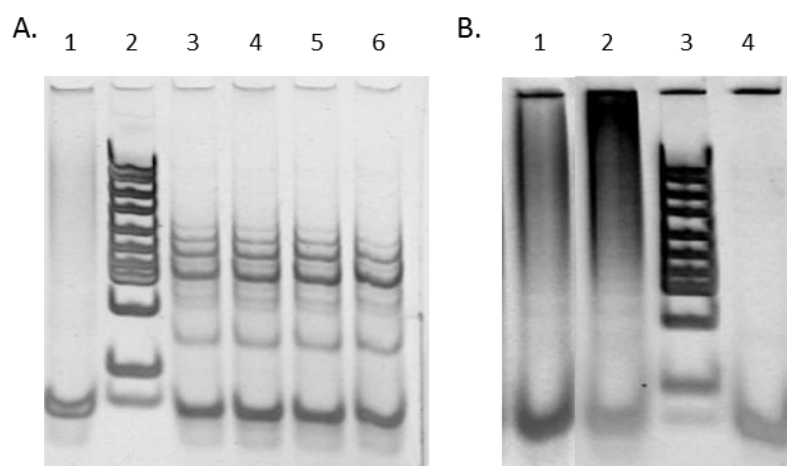


Fig 4-6.A) Section of polyacrylamide gel electrophoresis showing the product of the reaction after 120 h min (lane3) 60 min (lane 4) 30 min (lane 5) 15 min (lane 6); B) Section of gel showing product of the same reaction (10:1, Hps:target) after 2h (Lane 1) and 24 h (Lane2). Lane4: mixture of hairpins.

Assuming the separation of the reagents at the time of the analysis in electrophoresis, from Fig 4-6. A, it is clear that the HCR is very fast in producing first products. Even 15 min is enough to clearly appreciate it. No differences are evident comparing reaction incubated for 15 min and 2h. The self-assembling reaction quickly reaches a first equilibrium, however, the hairpins are not fully consumed yet. This is probably due to the achievement of a kinetically hindered status because of the reduced amount of hairpins available for the assembly and the limit of diffusion. Looking at the reaction after a longer incubation (24 h) we interestingly noted that there is probably a second slower phase, where the hairpins keep assembling on the nanostructures contributing to the growth. This is more evident for lower concentration of the target in respect to the hairpins (Fig 4-6). For our purpose, we need to focus on the first phase, thus we fixed the incubation time to 1h, at which a response would be returned towards the idea of a fast and efficient sensing application.

#### 4.1.4 The effect of temperature on the hybridization chain reaction

Since the entire process is thermodynamically driven, we tested the effect of the temperature on the reaction, to evaluate the robustness at different temperatures other than room temperature. We thus tested different conditions of incubation at 15, 25, 35 and 45°C (Fig 4-7).

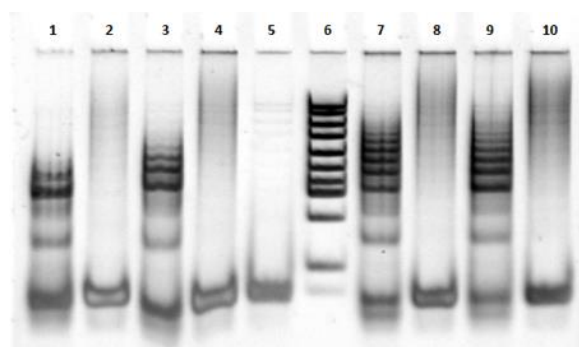


Fig 4-7. Section of polyacrylamide gel electrophoresis showing the HCR products obtained at different incubation temperatures. Lane1: HCR at 15 °C; lane 2: leakage at 15°C; lane3: HCR at 25 °C; lane 4: leakage at 25°C; lane5: H<sub>2</sub>; lane 6: molecular weight marker; lane 7: HCR at 35 °C; lane 8: leakage at 35°C; lane9: HCR at 45 °C; lane 10: leakage at 45°C.

As expected, a higher temperature correlated with a more efficient reaction but also a higher leakage of the hairpins, likely due to a decreased stability. On the contrary, at the lowest temperature of 15 °C the reaction was less effective, probably because of a consequent higher stability of stems. Despite the higher leakage at higher temperatures (35°C and 45°C), the response in presence of target is clearly different, specific and much more efficient. A different profile in electrophoresis is likely correlated to the possibility to discriminate the specific reaction from the leakage background on a biosensing platform. Moreover, the kinetic of such unspecific process is likely very different. Thus, the reaction looked robust in this condition. In addition, this

information would give us the chance to modulate the reaction conditions in order to enhance sensitivity and reduce the background. For example, it is clear that the running the reaction at 35 °C greatly enhance the formation of the HCR product with no equivalent increase in the leakage. The higher temperature could also avoid interaction with unspecific sequences by favoring instead the most specific ones, generally more stable. Moreover, the ability to detect targets at temperature closer to physiological ones is undoubtedly relevant for biosensing applications.

#### 4.1.5 The specificity of the direct HCR

The specificity of the reaction in solution have been tested over the competitors miR-106b and miR-25 as most similar to the specific targets selected miR-17 and miR-92a respectively. In Fig 4-8 we show data obtained in electrophoresis with the different products in presence of the specific target beside the product obtained in presence of the competitor. As we can see, no significant product is observed for the unspecific sequences at 1  $\mu$ M (Fig 4-8 A, Lane 3 and 8).

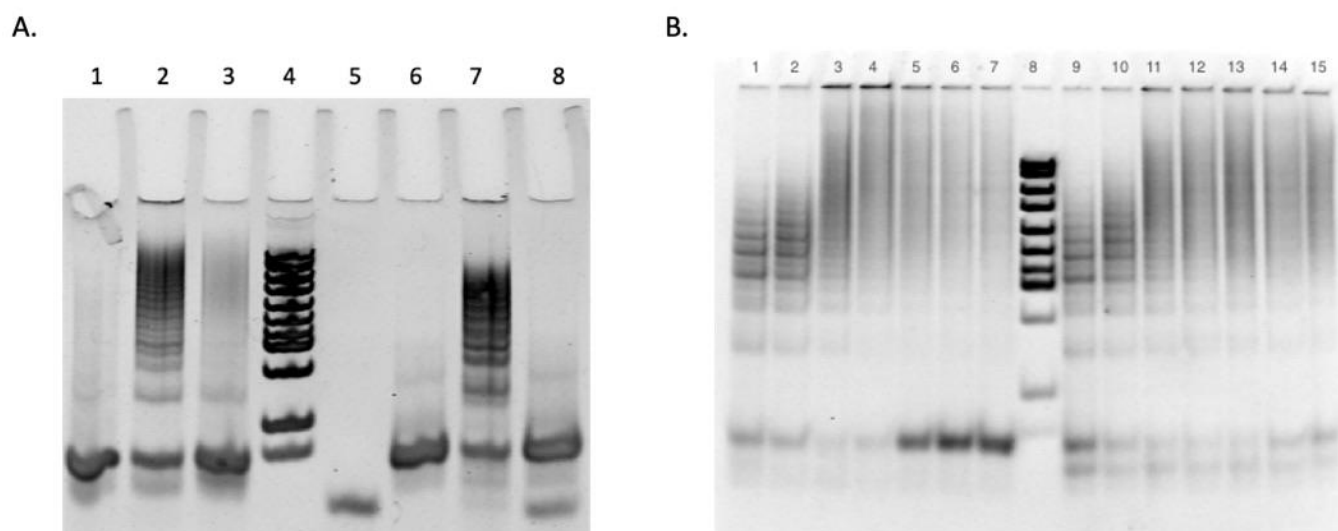


Fig 4-8. A. Section of polyacrylamide gel electrophoresis with HCR product obtained with specific and similar unspecific sequences. Lane1: H3 + H4; lane2: HCR miR-92a; lane 3: HCR miR-25; lane 5: miR-17; lane 6: H1 + H2; lane 7: HCR miR-17; lane 8: HCR miR-106b. B. HCR for miR-92a; Lanes 1-7, HCR with target concentrations 1, 0.5, 0.2, 0.1, 0.05, 0.02, 0.01  $\mu$ M; Lanes 9-15: same concentrations of miR-92a, in presence of fixed concentration of competitor miR-25.

It is to note that a slight interaction between miR-25 and the hairpins occurred, visible as a smear reaching higher molecular weight (Fig 4-8 A, lane 3). This is possibly due to an intrinsic instability of the hairpins specific for miR-92a or the partial interaction of miR-25 with the first hairpin H3 causing the weak trigger of the self-assembling reaction. Despite this interaction, the profile is very different from the one related to the specific one. As mentioned before, the unspecific response is probably slower and, likely, carefully handling the incubation time and the concentrations of the reagents, the differences in the responses can be certainly increased.

Moreover, testing the HCR in presence of miR-92a and miR-25, we can clearly see that the HCR product triggered by miR-92a is the dominant one ( Fig 4-8. B). In the experiment we compared the HCR product at different concentrations of the specific target miR-92a at different concentrations with the same product in presence of a fixed concentration of miR-25. We can argue that the effect of the competitor starts when miR-92a is about at 0.05  $\mu$ M, 10 times less concentrated. This would confirm the differences in the responses, since miR-92a is undoubtedly more effective than its competitor in triggering the assembly. These observations gave additional evidences about the ability of discriminating the unspecific response in the opportune conditions. The effect of completely unrelated sequences of microRNAs was also tested by incubating the mixture of hairpins in presence of other sequences such as miR-30c, miR-145-5p and miR-486-5p. The result is shown in Fig 4-9 for HCR specific for miR-17.

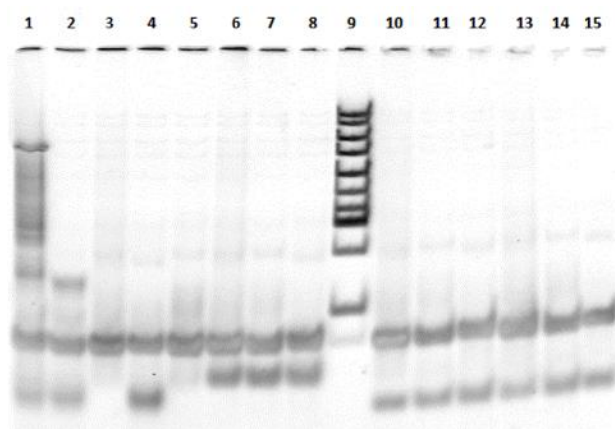


Fig 4-9. Section of polyacrylamide electrophoresis gel. Lane 1: Hp1 + Hp2 + miR-17; lane 2: Hp1 + 17; lane 3 :Hp1 + Hp2; lane 4, Hp2 + miR-17; lane 5: Hp1; lane 6: Hp1 + Hp2 + miR-30c; lane 7: Hp1 + miR-30c; lane 8: Hp2 + miR-30c; lane 9: marker; lane 10: Hp1 + Hp2 + miR-140-5p; lane 11: Hp1 + miR-140-5p; lane 12: Hp2 + miR-140-5p; lane 13: Hp1 + Hp2 + miR-486-5p; lane 14: Hp1 + miR-486-5p; lane 15: Hp2 miR-486-5p. Incubation 3h and 30 min a 25°C.

Apparently, there is no observable interaction between hairpins and the other unrelated sequences of microRNAs, as we expected. Experiments performed in presence of all the sequences in the mixtures further confirmed these observations (data not shown).

#### 4.1.6 Effect of BSA on direct HCR in solution

For sensing performances towards the detection in blood samples or other complex biological media, the specific self-assembly needs to work in media more complex than the buffer used in the test in tube.

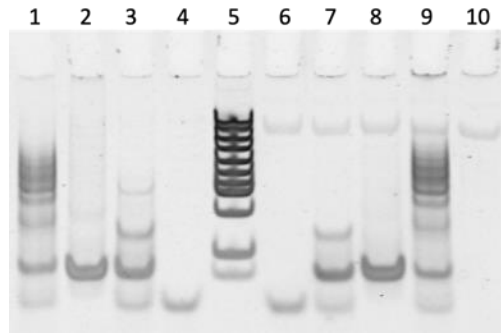


Fig 4-10. Section of polyacrylamide gel electrophoresis comparing the effect of 12.5 % BSA. Lane1: HCR in buffer; lane 2: H1+H2 in buffer; lane 3: H1 + miR-17 in buffer; lane 4: miR-17 in buffer; lane 5: miR-17 in BSA; lane 7: H1 + miR-17 in BSA; lane 8: H1 + H2 in BSA; lane 9: HCR in BSA; lane 10: BSA in buffer.

As preliminary test of the stability of the detection method and suitability in more complex media, we tested the self-assembling reaction in presence of 12.5 % of BSA in the HCR buffer (Fig 4-10). As we can notice comparing lane 1, corresponding to normal HCR buffer, with lane 9, related to the reaction in HCR buffer containing 12.5 % BSA, no significant effect due to the presence of BSA is detectable. We assumed thus that a more complex medium would not affect the performance of the hybridization chain reaction. This was expected from many examples in literature concerning the exploitation of such self-assembling reaction in cells and biological samples (see the introduction, 1.7.1 HCR in biosensing).

#### 4.1.7 Sensitivity

We tested the sensitivity in solution by incubating different concentration of target miRNA to the mixture of hairpins as explained in Material and methods in section 3.3. The lowest concentration tested was 10 nM (Fig 4-11).

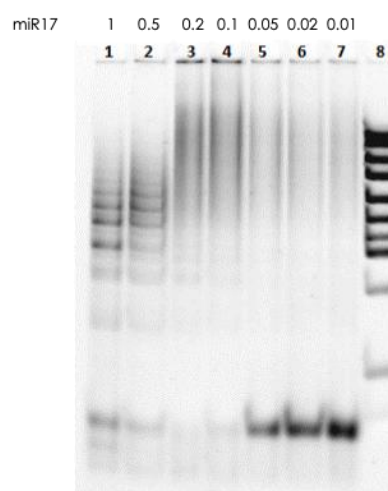


Fig 4-11. Section of polyacrylamide gel electrophoresis showing the HCR products at decreasing concentration of miR-17 in a range from 1 to 0.01  $\mu$ M.

Down to the range of tens nanomolar the reaction was able to return a visible product. That was observed for all the three targets miR-17, miR-92a and miR-21.

#### **4.1.8 Conclusions and observations**

The characterization in solution proved the robustness and the suitability of the amplification method based on direct HCR for the detection of the selected short sequences corresponding to microRNAs. HCR is demonstrated to be very versatile in these conditions, since similar results have been obtained for the three selected targets, miR-17, miR-92a and miR-21. In this design the first hairpin interacts directly with the target, acting as a probe. Our hairpin-like probe, is able to discriminate sequence of miRNAs with high homology thanks to the thermodynamical barrier of the stem and the careful selection of the toehold sequence performed. The reaction was effective at different temperatures, in different buffers and in more complex media, confirming the promising application in sensing. Even if far from the application in real samples, according to these results, we assumed the strategy effective and robust enough, also taking into account the large number of examples reported in literature about applications in real samples. The reaction is undoubtedly adaptable to sensing strategies and we moved thus towards the implementation in biosensing, for the development of an enhanced DNA based biosensors.

## **4.2 Implementation of the direct HCR on electrochemical detection**

The electrochemical method was designed simply modifying the hairpin directly involved in target detection. We chose HCR specific for miR-17 to test the implementation in electrochemical detection. We ordered a thiol modified H1 including a T4 spacer to reduce the steric hindrance on the surface and to enhance the hybridization, hence the sensitivity. The detection would take place with the same mechanism, through nucleation of the target on the toehold of the hairpin, in this case closer to the surface. For the development of the electrochemical method, first we started characterizing our custom-build electrochemical setup. We produced self-assembled monolayers and checked the electrochemical responses of the system by monitoring the charge transfer at the surface of the electrode.

### **4.2.1 Characterization and functionalization of the electrodes**

Gold surfaces were electrochemically evaluated through cyclic voltammetry (CV) and electrochemical impedance spectroscopy (EIS). Both the techniques return information about the efficiency of the charge transfer between the surface and the solution, depending on eventual adsorbed molecules on surface. Furthermore, these techniques can be used to evaluate the performances of the overall setup. Self-assembled monolayers were formed on the gold electrode using MCH or octadecyl mercaptan (C18), to assess the capability of the system to return meaningful responses. The TSGs were incubated in MCH 1 mM diluted in water or C18 in EtOH for 30 min, before rinsing and measuring in the electrochemical cell.

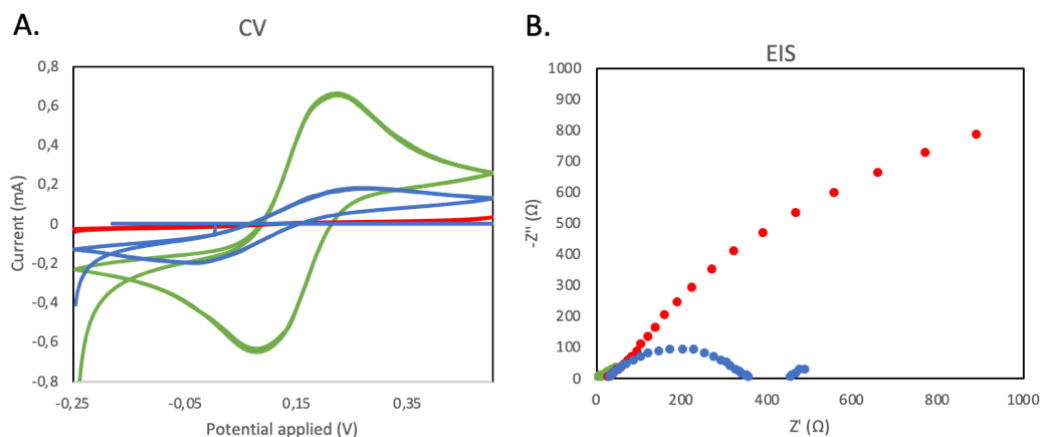


Fig 4-12. A) CV voltammogram showing obtained performing measurements on the same TSG. Green line corresponds to the measurement on clean TSG. Red line corresponds to the TSG passivated with C18, 1 mM in EtOH for 30 min. Blue line is the same TSG after 20 cycles of CV in  $\text{H}_2\text{SO}_4$  0.5 M; B) Electrochemical impedance spectroscopy measurement on the same surfaces (same color coding).

In Fig 4-12 we can see examples of the measurement on the same TSGs to monitor the adsorbed C18 on gold. The clean TSG shows quite high reduction and oxidation peak in cyclic voltammetry (Fig 4-12 A green line), corresponding to a very low impedance (green points in Fig 4-12 B). The passivation with C18 dramatically reduced the charge transfer, evident from the red voltammogram, barely distinguishable from the zero, while the EIS spectrum shows a high impedance. C18 molecules are long alkanethiols, and they induce a great hindrance to charge transfer on the surface of the electrodes. When the amount of C18 adsorbed is decreased, this is visible in the electrochemical measurements, since more current flows through the surface, as observed in CV (Fig 4-12. A, line blue) and in EIS spectroscopy (Fig 4-12. B, blue points). We were thus able to get information about the status of the gold surface and coherently with different techniques. The same method can be adopted to test the immobilization of the thiolated DNA.

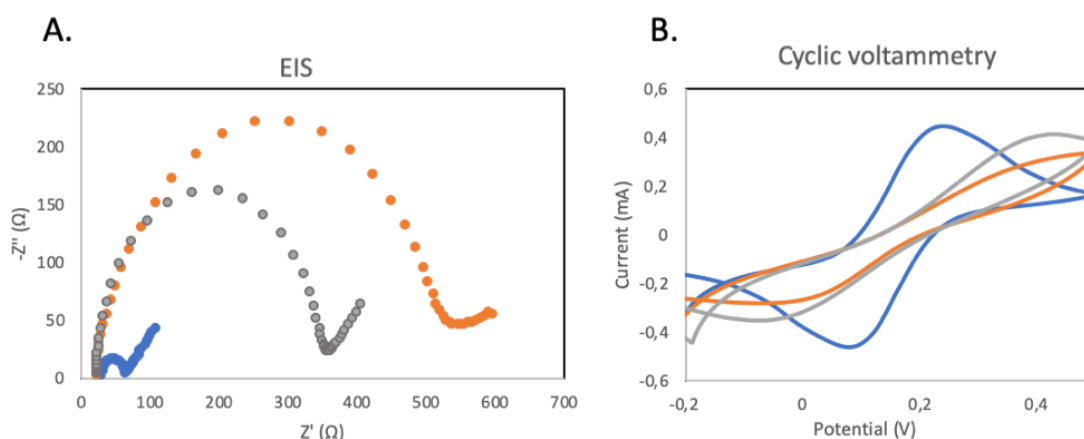


Fig 4-13. A) EIS data obtained on clean TSGs (blue) and functionalized with thiolated DNA probes (grey and orange). B) CV voltammogram obtained on clean TSG (blue) and functionalized with thiolated DNA (grey and orange).

In Fig 4-13 A. data obtained on clean and functionalized TSGs are shown. We can clearly detect the immobilized probe in both EIS (A) and CV (B). As mentioned before, the probe in use was

simply a 5' thiolated H1, with a T4 spacer. The thiol group was directly attached to the toehold of the hairpin.

SH(CH)<sub>6</sub>-TTTTCTACCTGCACTGTAAGCACTTTGAATTCGCAAAGTGCTTACAGTGC

The stem region is underlined in the sequence. The immobilization of the probe on the electrode was performed overnight, dropping 40  $\mu$ L of probe solution in Tris 20 mM, NaCl 0.5 M pH 7.4 on a freshly exposed TSG. The proper concentration was evaluated in response of the HCR efficiency on surface as we will see in the following section.

#### **4.2.2 Detection of miRNA and direct Hybridization Chain Reaction on surface**

The detection and the hybridization chain reaction were mainly evaluated labeling the DNA using Hoechst 33258, an electroactive intercalator of DNA that can be oxidized on the electrode scanning the potential between 0.4 and 0.6 V. The experiments were performed by incubating the target and the hairpins on the TSGs out of the electrochemical cells, and the incubation with Hoechst was done in the cell, by flowing the solution at 50  $\mu$ L/min using a syringe pump. The whole procedure is described in the section about the Electrochemical detection of microRNA sequences through direct HCR. After washing the Hoechst with buffer, we performed the LSV measurement. The resulting peaks were analyzed to evaluate the height on the baseline. The data were normalized on the measurement performed on TSG only passivated with MCH (Fig 4-14).

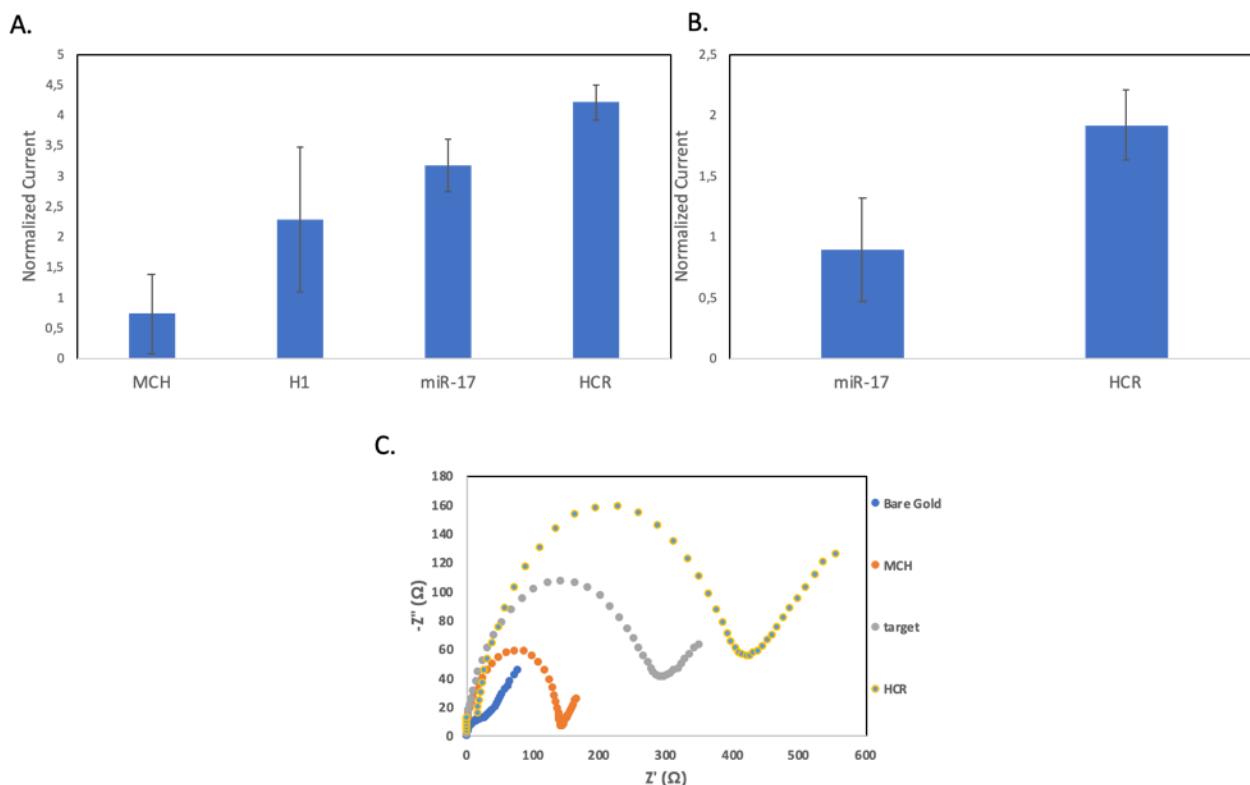


Fig 4-14. Mean values and standard deviations (N = 3) relative to the height of the oxidation peak of Hoechst. The data are normalized on the average MCH peak height. A) Normalized data for each sample; B) Normalized values relative to target detection and HCR after subtraction of the contribution of MCH and H1. C) EIS data showing the increase of faradaic resistance at each step.

We can see that the peak height is coherent with the increase of the amount of DNA on the surface. Focusing on the contribution of target and hybridization chain reaction, we can see a 2-fold amplification after hybridization chain reaction compared to the bare target detection. Each step was also evaluated in Electrochemical Impedance Spectroscopy, and data were coherent with an effective increase of material on the surface, correlated to the increase in the faradaic resistance. Probe was used at 0.2  $\mu\text{M}$ , incubated overnight at room temperature. This concentration was selected after a certain number of trials trying to evaluate the effectiveness of the reaction on surface at different concentrations of the probe. Some of the experiments are resumed in Fig 4-15.

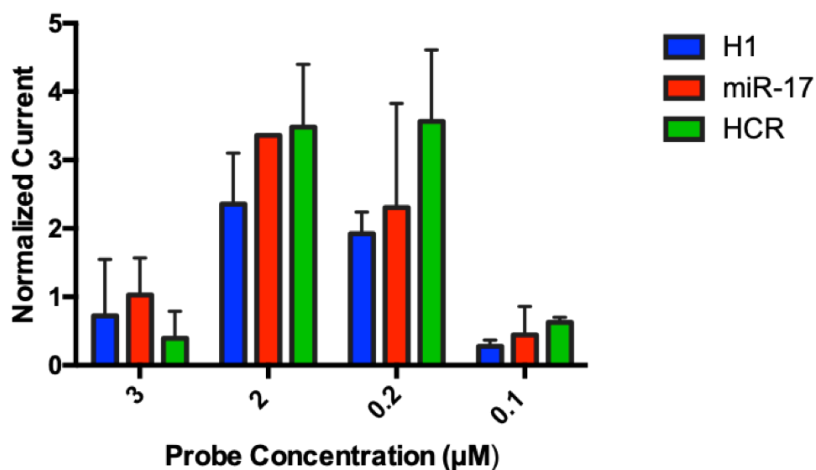


Fig 4-15. Bar plot showing the height of the Hoechst oxidation peak at different concentration of probe for probe only (blue), after target incubation (red) and after HCR (green). Bars correspond to the standard deviation calculated from the variance on several experiments.

At higher concentration, such as 3 µM, the overall trend of the data shows ineffective target recognition and ineffective HCR. Reducing the probe concentration there was a more discriminable difference. This is probably due to the different probe density affecting the overall detection method. Thus, we decided to work with concentrations of probe in the range 0.1-0.5 µM. We have to note that measurements using Hoechst were in general affected by high variability. This could be related to intrinsic defect in the electrochemical setup, requiring further optimization. Indeed, this affected the sensitivity and the reliability of results in some degree. Although we had to face the limitations in the electrochemical detection, we wanted anyway to test the hybridization chain reaction. The detection of different concentration of miRNAs was evaluated without amplification and in presence of the HCR amplification. Fig 4-16 we show the results of these experiments. In general, the target itself was barely detectable in these conditions, made more difficult by the variability of the measurements (Fig 4-16 blue spots). In general, the target only was detectable at high concentration, about 1 µM. This is probably due to the adopted electrochemical method based on Hoechst. Since our probe is a hairpin with a consistent stem, the overall contribution of the target binding is low. Hoechst binds preferentially to double stranded DNA, and the closed hairpin has a 17 base pairs in the stem. After target detection, the double stranded portion of the complex would be 23 base pairs, probably not enough to return a clear detectable response at low concentration of target.

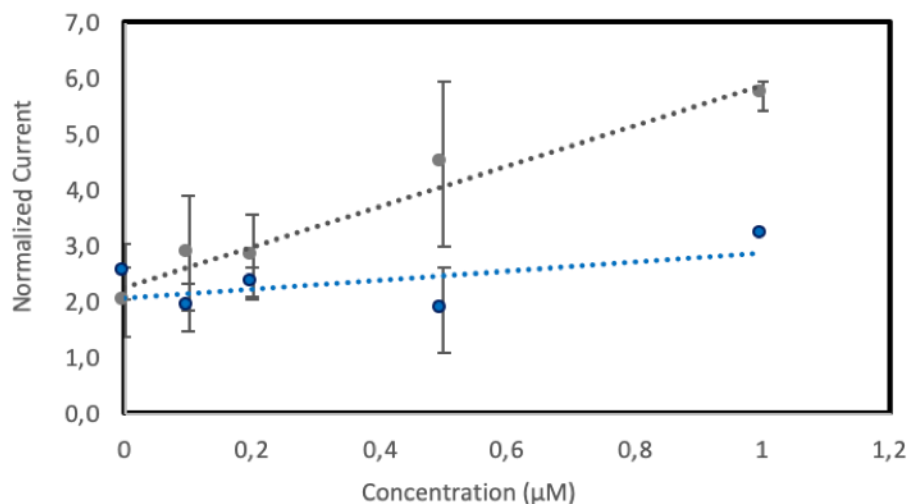


Fig 4-16. Detection of miR-17. Detection of target without amplification (blue spots and line). Detection using hybridization chain reaction (grey spots and line) Bars for standard deviation (N = 3).

Even if the variability was important, we tried to evaluate the effect of the amplification based on hybridization chain reaction. As we can see in Fig 4-16 (grey spots), the system showed a better correlation to the concentration of the target. Trying to evaluate the improvement obtained in the detection, we roughly estimated the limit of detection in the adopted conditions. Taking into account the signal of the blank sample and its standard deviation, we calculated the LOD as  $S_b + 3 \cdot \sigma$ , where  $S_b$  is the blank response and we obtained the corresponding concentration from the data fitting. No correlation is evident for the target detection with no amplification, while the estimation returned about 400 nM when the target was detected with HCR. That is obviously not a satisfying result, but it confirms an effect of the amplification, leading to an improvement starting from the absence of a meaningful detection detection.

#### 4.2.3 Conclusions and observations

More efforts need to be done to improve the electrochemical setup and reduce the variability of the measurements. The HCR mechanism could be more complex than expected and Hoechst labeling could not be the optimal strategy for this method. The label detection may be affected by the molecular crowding on the surface, limiting the amount of intercalator truly oxidized on surface. Even trials performing the target detection through EIS and CV did not show enough sensitivity in the detection. In principle, we showed that the HCR takes place on the electrode and leads to the enhancement of the response with bare target detection, assessing the working principle and the detection. This supports the application of the proposed method, but more efforts are required to obtain reliable data with this approach. First, an overall revision of the electrochemical setup would be required, then other electrochemical techniques could be tested towards the improvement of the detection. We looked thus for alternative techniques, able to return more stable responses and conceptually promising for HCR based detection.

### 4.3 LSPR based detection

Since HCR amplification could lead to an increase of the local amount of DNA, techniques sensitive to a change of the surrounding properties at the surface affected by the accumulation of DNA can be used for the detection of such process. As we have seen in the introduction at section 1.4, Surface Plasmon Resonance, techniques based on SPR are sensitive to changes in refractive index at the interface between a metal layer and the solution. The absorption of molecules on the surface can be detected thanks to this principle and correlated to the concentration in the sample. These are label-free techniques, allowing a further reduction of the complexity of the methods, thanks to the reduction in the number of steps required for a measurement.

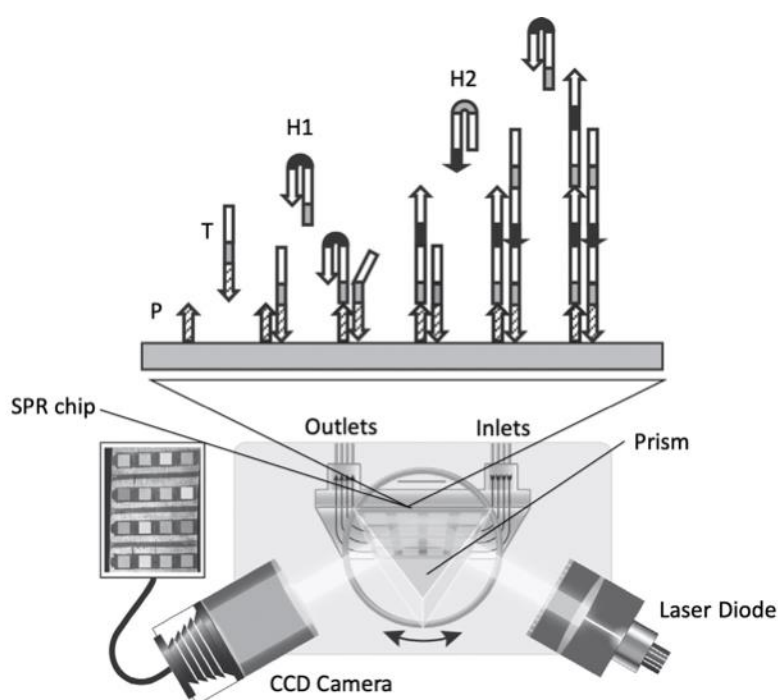


Fig 4-17 Scheme of the HCR based detection in the SPR setup. Readapted from Spiga et al (Spiga et al., 2014). Image licensed by Elsevier and Copyright Clearance Center (License number 4698291110587).

In the past, people in our lab worked on the implementation of HCR in SPR sensing for the detection of pathogens, potentially reaching a limit of detection lower than 1 pM (Fig 4-17), (Spiga et al., 2014). Part of the goal of the work presented in this thesis was to explore the employment of metal nanoparticles as transducers and signal enhancers. As we have seen in the introduction in section 1.5.2 (Localized Surface Plasmon Resonance (LSPR)) it is possible to take advantage of the plasmonic properties of metal nanoparticles to develop a strategy suitable in biosensing. LSPR is based on the same principles of SPR, but with some more advantages, such as enhancement of the sensitivity, the easier miniaturization and production thanks to the employment of metal nanoparticles instead of metal layers. The suitability of HCR for methods

based on SPR is proved, thus, in principle, LSPR based transduction could be adapted to strategies involving HCR as amplification. There are many strategies involving gold nanoparticles in solution able to show a shift in their resonance LSPR peak (change in the absorbance of the solution) upon target detection. Recently, methods based on solid-state LSPR have been proposed, taking advantage of the immobilization and proper spacing of metal nanostructures on surface to enhance the sensitivity and the overall performance of sensing methods. As reported in the Introduction (section 1.5.2), Joshi et al proposed the first method for the detection of specific microRNAs based on solid-state LSPR with immobilized nanoprisms on glass substrates, suitable for regeneration after detection (Joshi et al., 2014, Joshi et al., 2015). The detection takes place by incubating the chip in the sample, and so all the steps of washing and regeneration. The plasmonic peak was measured in a common spectrophotometer after the target detection. They claim a LOD of about 35 fM for miR-21 and in a range from 100 nM to 50 fM for miR-10 in different media. Despite the low limit of detection in complex media obtained in this approach, the proposed method does not allow the real time measurement of the target detection, and the protocol looks still complex in batch configuration, requiring long incubation times. More recently a few works have been proposed employing nanostructures surfaces for LSPR based detection of miRNAs, with good results but still involving complex preparation of the chips, long incubation and enzymes to amplify the signal (Ki et al., 2019, Na et al., 2018). Ki's work also employed HCR as part of the amplification, in combination with enzyme-assisted target recycling, with no dramatic enhancement of the signal. During the work described in this thesis, we had the chance to collaborate with the group of professor Wolfgang Fritzsche, head of the Department of Nanobiophotonics at the Institute of Photonic Technology (IPHT) of Jena (Germany). During a period spent under the supervision of Prof Fritzsche in Jena, we made efforts to implement our direct HCR based detection method on LSPR mediated sensing using an original and simple setup for LSPR measurements. The advantage of this LSPR setup compared to what is reported in literature, would be the suitability for real-time measurements in a compact format, ease of the working procedures and the employment of spherical gold nanoparticles, either provided commercially or easy to synthesize with lab facilities. We used the same thiolated H1 probe employed for the electrochemical detection (section 4.2.2 Probe immobilization and Hybridization Chain Reaction on surface) here immobilized on 80 nm gold nanoparticles for LSPR detection of miR-17 (Fig 4-18).

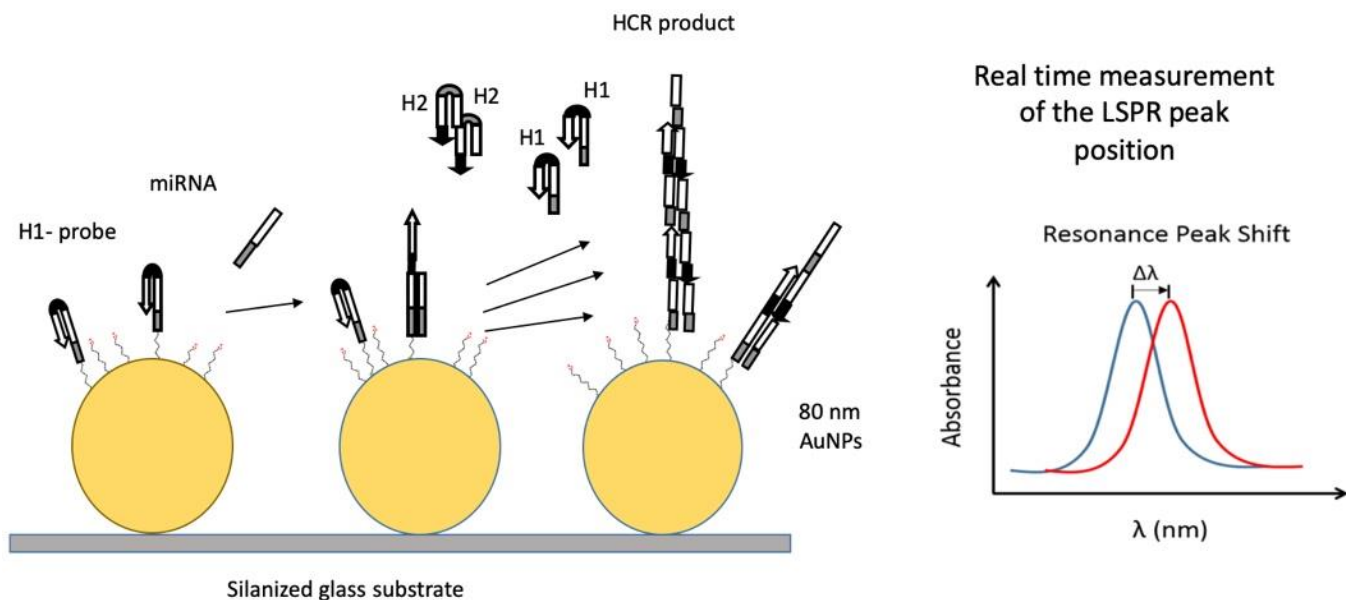


Fig 4-18. Scheme of the LSPR-based detection of microRNAs with Hybridization Chain Reaction amplification on immobilized gold nanoparticles. While the hybridization and the self-assembly take place, we can monitor the LSPR peak position over time.

### 4.3.1 Characterization of the chips

One of the advantages of the adopted LSPR approach is the ease in the production of the sensitive chips (protocol reported in section 3.6.1 Preparation of the LSPR Chips ). We were able to produce tens of chips in one day and store them for later use. The density of the gold nanoparticles on the chip should be carefully handled in order to get the proper plasmonic effect, but also in order to keep as low as possible the variability between different chips. This step is very important, since the main drawback of the employed setup was the possible variability between chips, however standardization of the procedures allowed the improvement of this aspect. Normalization is anyway required to be safely able to compare data collected on different chips. We can check the density of gold nanoparticles by Dark field microscopy or, with Atomic Force Microscopy.

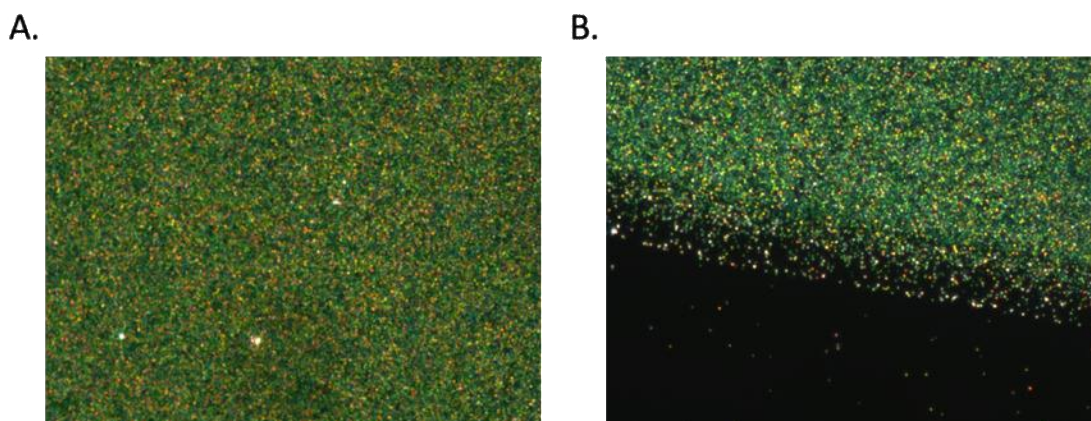


Fig 4-19. Image in Dark field microscopy of the immobilized 80 nm gold nanoparticles on the glass substrate in different areas.

Because of the strong light scattering due to the surface plasmon resonance, gold nanoparticles can be visualized as bright points under a dark field microscope (Fig 4-19). The displayed color is determined by the SPR peak wavelength. Spherical gold nanoparticles appear green due to their SPR peak and scattering in the 500 nm. A greenish color in scattering is thus expected for properly spaced 80 nm gold nanoparticles while reddish color in scattering is expected for aggregated gold nanoparticles on surface. This gives the chance to easily evaluate the general status of the chip before proceeding with the measurements.

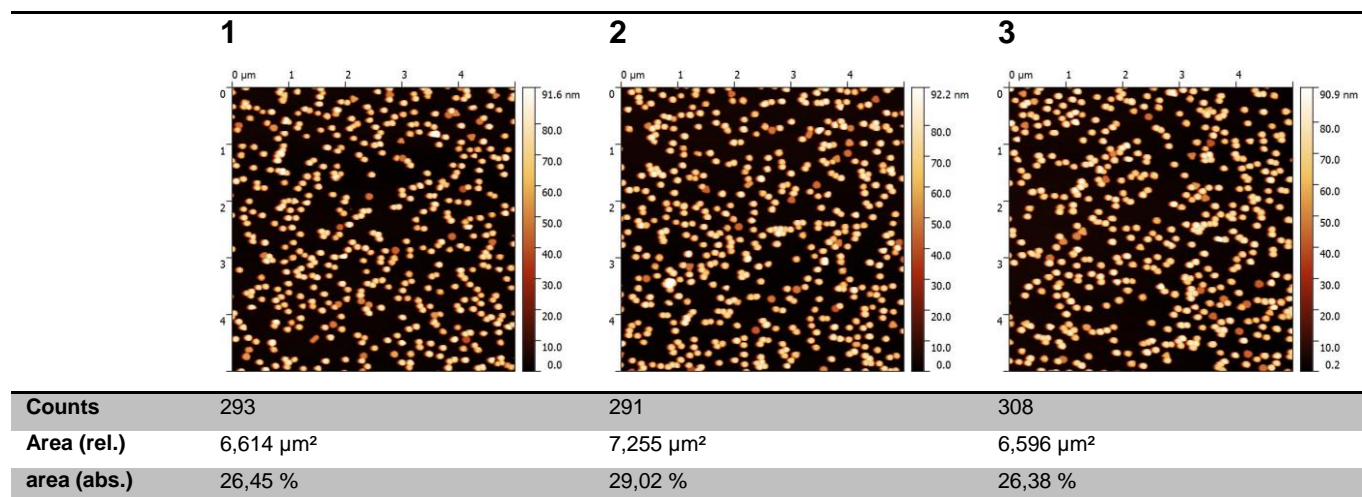


Fig 4-20. AFM images, showing the immobilized gold nanoparticles on glass for LSPR detection on three different chips. Table below report the density and the number of gold nanoparticles on the area analyzed, and the percentage of occupied area.

A deeper characterization is offered by the usage of Atomic Force Microscopy. In Fig 4-20, AFM images of the immobilized gold nanoparticles are shown. In the table below we report the number of nanoparticles and the covered area. So, a density about 300 particles/ $5 \mu\text{m}^2$ , that is 60 particles/ $\mu\text{m}^2$ , was considered an appropriate density on the base of empirical observations, such as the presence of a sharp plasmonic peak in transmittance, considered marker of a well functional chip. The acquisition of the plasmonic peak in transmittance was the last test able to confirm the good shape of the chip. Once the chip was enclosed in the microfluidic chamber, we were able to immediately detect the “absorbance” peak through the spectrophotometer included in the setup. We were then ready to start the measurement.

#### 4.3.2 Detection of miR-17

Once we made sure the goodness of the layer of gold nanoparticles, we followed the protocol illustrated in section *LSPR measurements and detection*, maintaining the same parameters. For the specific detection of miR-17, we decided to use H1-sh probe at 2  $\mu\text{M}$  for the overnight incubation. The overall setup let us follow the portion of the LSPR over time, allowing the real time monitoring of the detection. All the measurements were repeated at least three times on the same chip. Data were normalized over the shift in the position of the LSPR peak obtained with

1  $\mu\text{M}$  of the specific target miR-17, considered correlated to the amount of probe immobilized on the gold nanoparticles and the sensitivity of the chip. Since this method gives the chance to monitor in real time the interaction between the target and the probe, we can literally observe how the detection is proceeding over time. Beside information about the entity of the shift in the centroid position, we can also evaluate the kinetics of the phenomena. The detection of target was evaluated by flowing 1  $\mu\text{M}$  solution of miR-17 in running buffer after the passivation of the gold nanoparticles and the glass substrate.

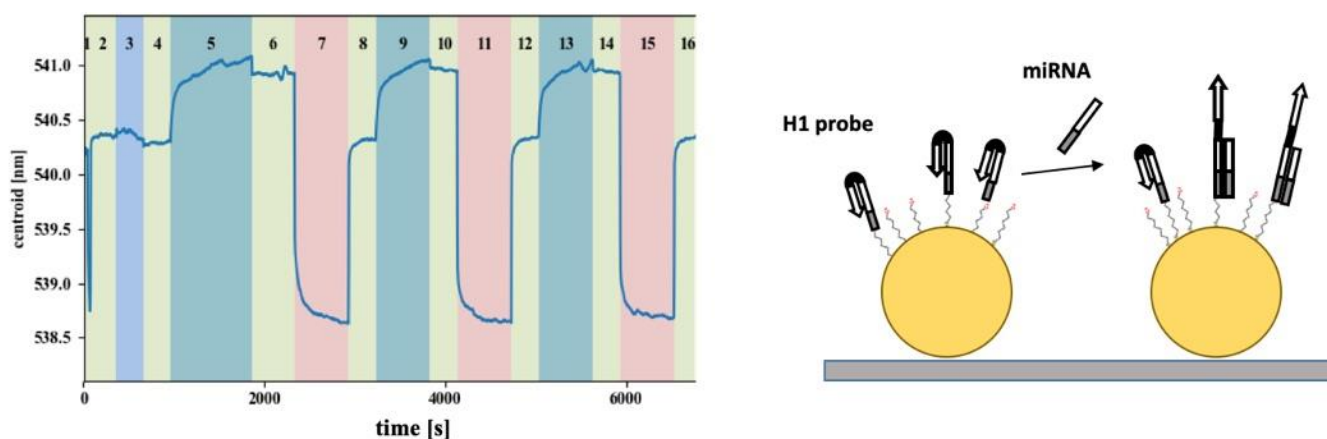


Fig 4-21. Example of result obtain for an LSPR measurement session. The graph plots the position of the LSPR peak (centroid position) over time. During steps 5, 9 and 13 (dark green) the target was flowed. Blue step corresponds to MCH, light green corresponds to running buffer while red steps correspond to regeneration through HCl 20 mM. On the right, scheme of the target detection.

In Fig 4-21 we can see the result of an experimental session in which we repeated 3 times the detection of the target, alternated by regeneration using HCl 20 mM. Upon target injection, we witnessed a fast change in the refractive index observed as a change in position of the centroid (see blue line in Fig 4-21). We can see that, injecting buffer again, the centroid position is not brought back to the previous value, meaning that the binding of the target is stable in this time scale. Instead, the regeneration step is effective in taking the centroid position back to the starting point. HCl breaks the base pairs between probe and target and prepare the sensor for the subsequent detection.

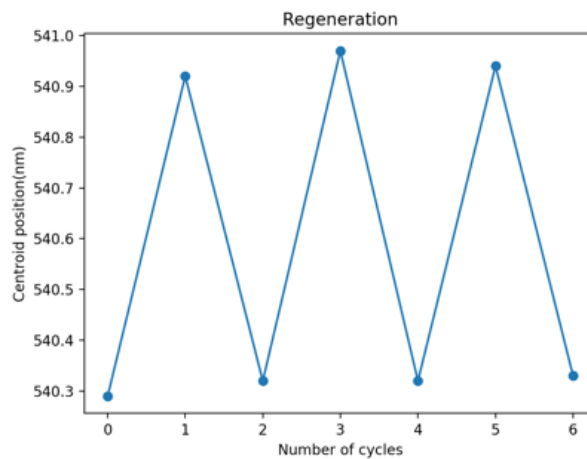


Fig 4-22. Regeneration of the sensor with HCl 20 mM.

The regeneration was also evaluated, and we observed that the probe was restored at the unhybridized form at each cycle (Fig 4-22). In general, we obtained a shift between 0.5 and 1 nm for target binding at 1  $\mu$ M of the specific target. The volume of target solution injected was 50  $\mu$ L (5  $\mu$ L/min for 600 s). This measurement was repeated at every experiment as standard to normalize the whole data obtained on the same chip.

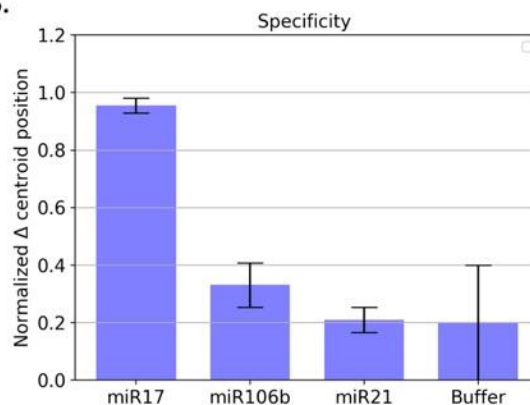
#### 4.3.3 Specificity for the detection of miR-17 in the LSPR setup

Once the detection of the target was proved and once we verified the effective regeneration of the sensors, we moved to the evaluation of the specificity, the ability to discriminate between miRNAs. Since we tested the LSPR based detection on the detection of miR-17 sequence, we tested the specificity over miR-106b, the most similar sequence found in the databases, in addition to miR-21, a completely unrelated sequence also significant for diagnosis (see sequences in Table 4-1). As explained in section 4.1.1, the specificity should be guaranteed by the H1 hairpin, adopted as probe, because of the base pairing specificity, the secondary structure and the toehold, directed to the more variable 3' portion of the target. MiR-106b should not be able to open the hairpin, since it also lacks two nucleotides in that position (Table 4-1). These deletions should affect the interaction at the toehold of H1, so the opening of the hairpin, as also confirmed by experiments in solution (see section 4.1.5, about the specificity of the direct HCR). After recording the response flowing 1  $\mu$ M solution of the specific target, we washed and flowed the solution containing the competitor miR-106b. It was done in a separate experiment for miR-21, always compared to the specific target.

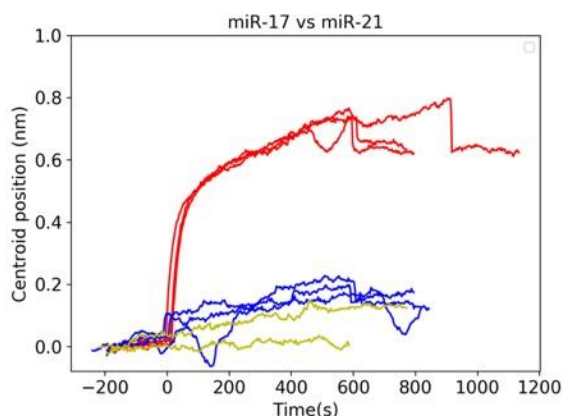
A.

miRNA	Sequences (5' – 3')	Length (nt)
miR-17	CAAAGUGCUUACAGUGCAGGUA	23
miR-106b	UAAAGUGCUGACAGUGCAGAU –	21
miR-21	UAGCUUAUCAGACUGAUGUUGA	22

B.



C.



D.

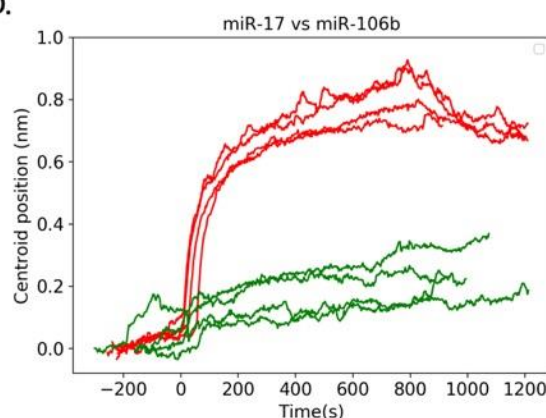


Fig 4-23. Test of the specificity of the sensor. A) Table showing the sequences of the miRNAs. B) Bar plot showing the mean values the differences in centroid position after the injection of the sequences with standard deviation (N = 3). C) Collection of the intervals corresponding to the injection of miR-17 (red lines) and miR-106b (green lines), showing centroid position (nm) over time per each interval. D) Same for miR-17 (red lines) and miR-21 (blue lines) and blank (buffer, yellow lines). Bars correspond to standard deviation N = 3.

The results are reported in Fig 4-23. Figure C and D report the centroid position over time for miR-17 (red line) and the unspecific miRNAs, respectively miR-106b (green line in D) and miR-21 (blue line in C). Fig 4-23 B summarizes these data in a bar plot, comparing the data with signal we obtained flowing just buffer. We can see that the shift in the centroid position is dramatically different for miR-106b and miR-21 compared to miR-17. The injection of the specific target induces a steep change in the centroid position with a fast kinetics, while both miR-106b and miR-21 induce an increase not so higher than the buffer alone (yellow lines in Fig 4-23 C). The slight increase of the signal compared to the background in the case of miR-106b is likely due to a leakage of H1 on surface, allowing interactions even if with low efficiency. Thus, the probe is confirmed to be specific for miR-17 in these conditions.

#### 4.3.4 Sensitivity of the LSPR-based method without HCR

Since the aim of the work was to test if HCR was able to enhance the sensitivity of biosensing strategy based on DNA, we first wanted to move to the evaluation of the sensitivity of the method without amplification. We flowed in the chamber different samples with different content of

miR-17. Every measurement was followed by a regeneration step, and then the subsequent solution was flowed.

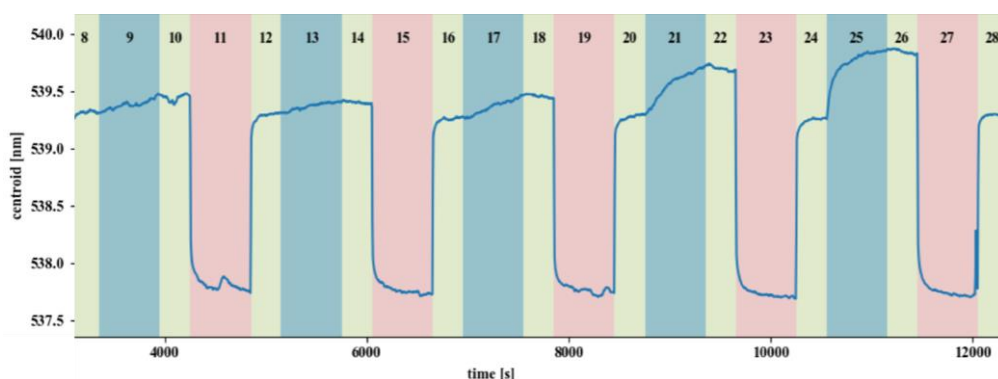


Fig 4-24. Centroid position over time during the detection of increasing amount of target: step 9, 0.0001  $\mu\text{M}$ ; step 13: 0.001  $\mu\text{M}$ ; step 17: 0.01  $\mu\text{M}$ ; step 21: 0.1  $\mu\text{M}$ ; step 25: 1  $\mu\text{M}$ .

As it can be observed in Fig 4-24, the shift in the peak position over time increased when higher concentrations of the target were flowed. The response of the sensor is thus quantitative depending on the concentration of miR-17. Further experiments have been performed to better assess the robustness of the target quantification.

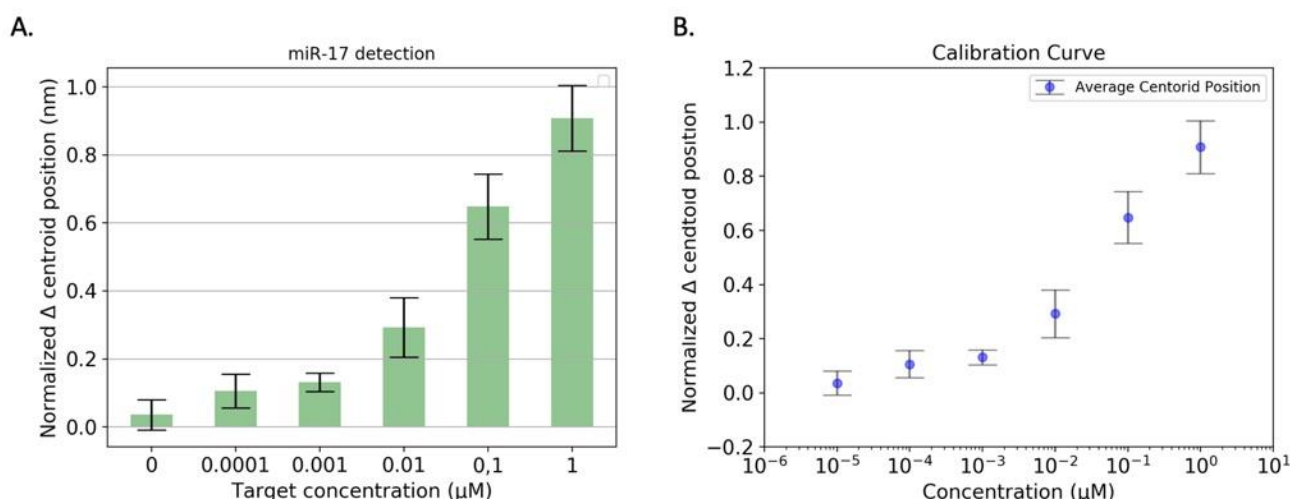


Fig 4-25 Mean values for the shift in peak position normalized for shift obtained flowing  $\mu\text{M}$  of target. A) Bar plot showing the average of the shift in the centroid position with standard deviation. B) Calibration curve in log scale. The concentration  $10^{-5}$  corresponds to the zero. Bars correspond to standard deviations calculated from the variance on several experiments.

In Fig 4-25 A and B we show the average differences in centroid position observed for different experiments. For each experiment, the detection was repeated 3 times per target concentration. Through a rough visual definition of the limit of detection, we can see a meaningful difference at about 1 nM of target compared to the blank, which consists in just running buffer. This is proved by calculating the limit of detection as  $\text{LOD} = S_b + 3\sigma$ , where  $S_b$  is the mean shift detected for the blank sample, and  $\sigma$  is the standard deviation of the blank. The LOD concentration was obtained from the data fitting. This resulted to be about 1.1 nM.

### 4.3.5 Hybridization Chain Reaction in LSPR

Once we determined the limit of detection reachable without amplification, based on the simple hairpin-like probe immobilized on the gold nanoparticles, we moved to the Hybridization Chain Reaction. First, we wanted to test the growth of the DNA nanostructure after the detection of the target.

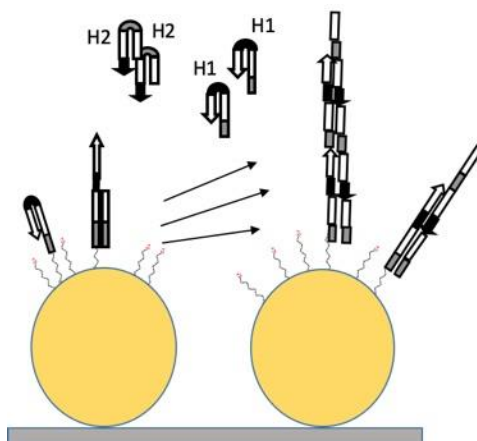


Fig 4-26. Scheme of the Hybridization chain reaction on the gold nanoparticles.

We added one by one the H1 and H2 and saw if we were able to discriminate the interaction of individual hairpins over time. In principle, SPR-based techniques such as LSPR would be able to detect every binding step until they are in the range of sensitivity. In the case of SPR, the bulk sensitivity is higher, so the technique is able to detect changes further from the surface. In LSPR, the range of sensitivity is limited by the diameter of the nanoparticles. In principle, the range is estimated to be half of the diameter of the nanoparticle, for spherical nanoparticles. It means that, for 80 nm gold nanoparticles, we expect to detect interactions on the surface until they occur within 40 nm around the nanoparticles. In the not-real case of a rigid DNA nanostructure, we would be able to see at least the interaction of 4 hairpins, taking into account the length of the individual hairpins and the probe, considering 0.34 nm the length of a base. Obviously, this is an extreme unlikely case. Likely the nanostructure would be very flexible. Moreover, the HCR product consists in a nicked double stranded structure and this surely enhance the flexibility. Thus, we expected to detect also longer HCR products. The nanostructure would more likely randomly wrap in the surrounding, affecting the refractive index around the nanoparticles.

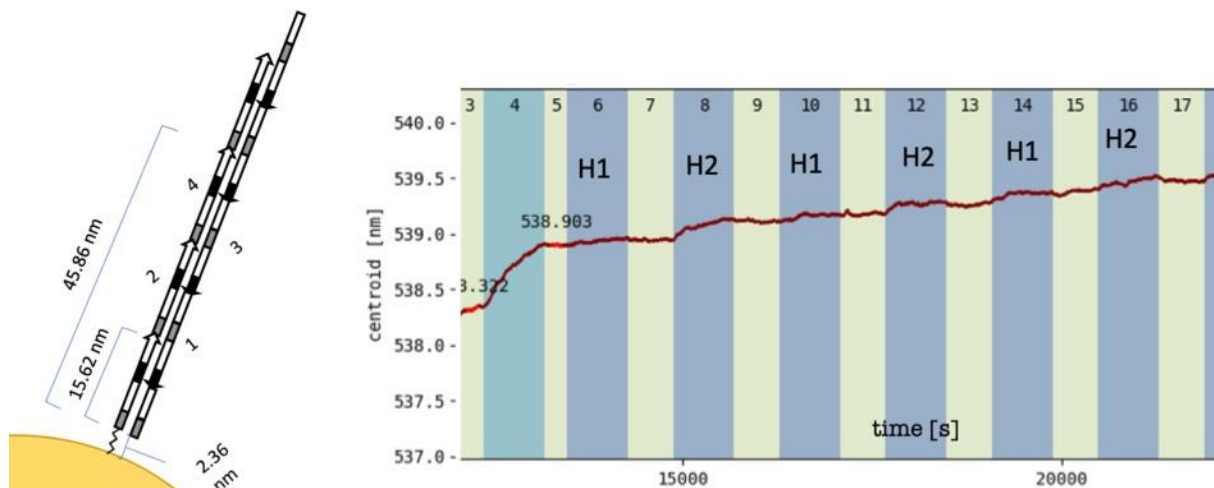


Fig 4-27. Scheme of the nanostructure on the gold nanoparticles with estimation of the length. Plot of the centroid position over time with the consecutive addition of the individual hairpins one by one. Dark green = miR-17 10 nM; Blue = Hairpin; Light green = running buffer.

However, what it is to notice is that further from the nanoparticles the interaction takes place, lower would be the contribution to the shift in the centroid position because of the decrease of the sensitivity of the evanescent field. For this reason, the contribution of the hairpin H2 was higher than the subsequent contributions. In Fig 4-27 we can appreciate what happened when single hairpins were injected after the detection of 10 nM of miR-17. Since the probe is a modified hairpin H1, no interaction is expected with H1 itself, while we can see a shift in the centroid position after the first injection of H2. Even if the subsequent contribution is not as strong as the first one, there is clearly a step-by-step process leading to an increased difference in the LSPR peak position. It is to note that, as predicted, also after the addition of the fifth hairpin the peak position is shifting, assuming the saturation of all the binding sites. We conclude that the process in principle works in the “step by step” injection proving the mechanism of the Hybridization Chain Reaction.

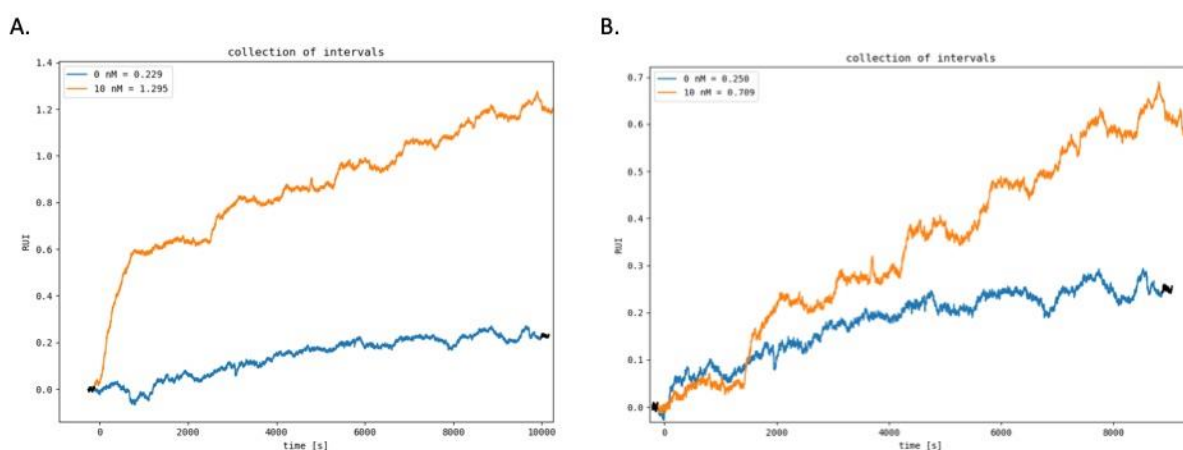


Fig 4-28. Comparison of the enhanced difference in centroid position injecting individual hairpins one by one, with 10 nM miR.17 target and 0 nM. A) The overall interval including the detection of the target. B) the contribution of the amplification upon target detection. Same data illustrated in Fig 4-27.

Fig 4-28 highlights the difference between this step-by-step process after the detection of 10 nM miR-17 target and 0 nM. In Fig 4-28 A. the intervals plotted include the detection of the target, and we can see the steep change in the centroid position in the orange line, while no change is evident in the blue line in the first 1000 s. After about 1000 s the first hairpin H1 was injected with no big effect on the peak position in both the cases. The injection of the H2 after about 2500s leads to a change in orange line while just a low change occurs in blue line corresponding to the zero. After that, we added the individual hairpins one by one and we can compare the contribution of the amplification in figure Fig 4-28 B. We are able to see the difference in the kinetics and the final peak position in presence and absence of target. In absence of the target, it is probable that some unspecific interactions occur, leading to a visible change anyway. Unspecific adsorption or leakage may be responsible of this behavior. This result clearly shows that the two phenomena had different kinetics, giving the chance to handle it by adjusting the time of the interaction. This kind of background noise can also be handled by tuning the concentration of the probe on surface and the hairpins in solution. During the work, we finally set to 0.5  $\mu\text{M}$  the concentration of the hairpins in the mixture, while the probe at 2  $\mu\text{M}$  was kept to avoid loss in the sensitivity. In these conditions it was possible to enlarge the difference between the specific signal and the background noise.

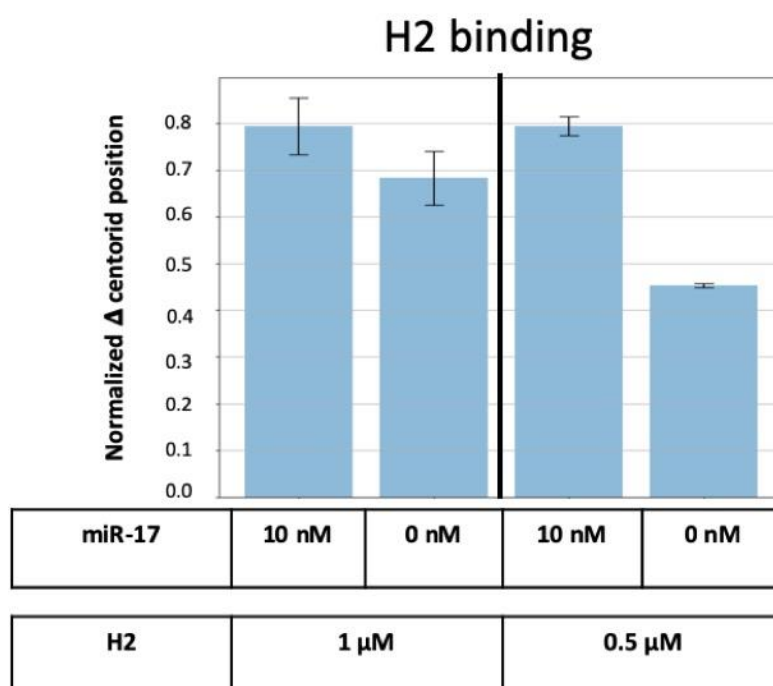


Fig 4-29. Test of the binding of H2 to evaluate the leakage of the probe on the same chip. SD is shown (N = 3).

In Fig 4-29 we showed the results of an experiment we did to evaluate the leakage of the probe, by flowing H2 hairpin and monitoring the binding in presence of the target and in absence of it. As we can see reducing the concentration of H2, expected to interact with the opened H1, was helpful to enlarge the difference between noise and specific signal. We show that to point out how

the concentration of the reagents can be optimized to further improve the method. Although the mechanism of HCR is highlighted by the previous observations, the aim was to have a triggered reaction with the mixture of hairpins in solution, consisting in the real self-assembling reaction.

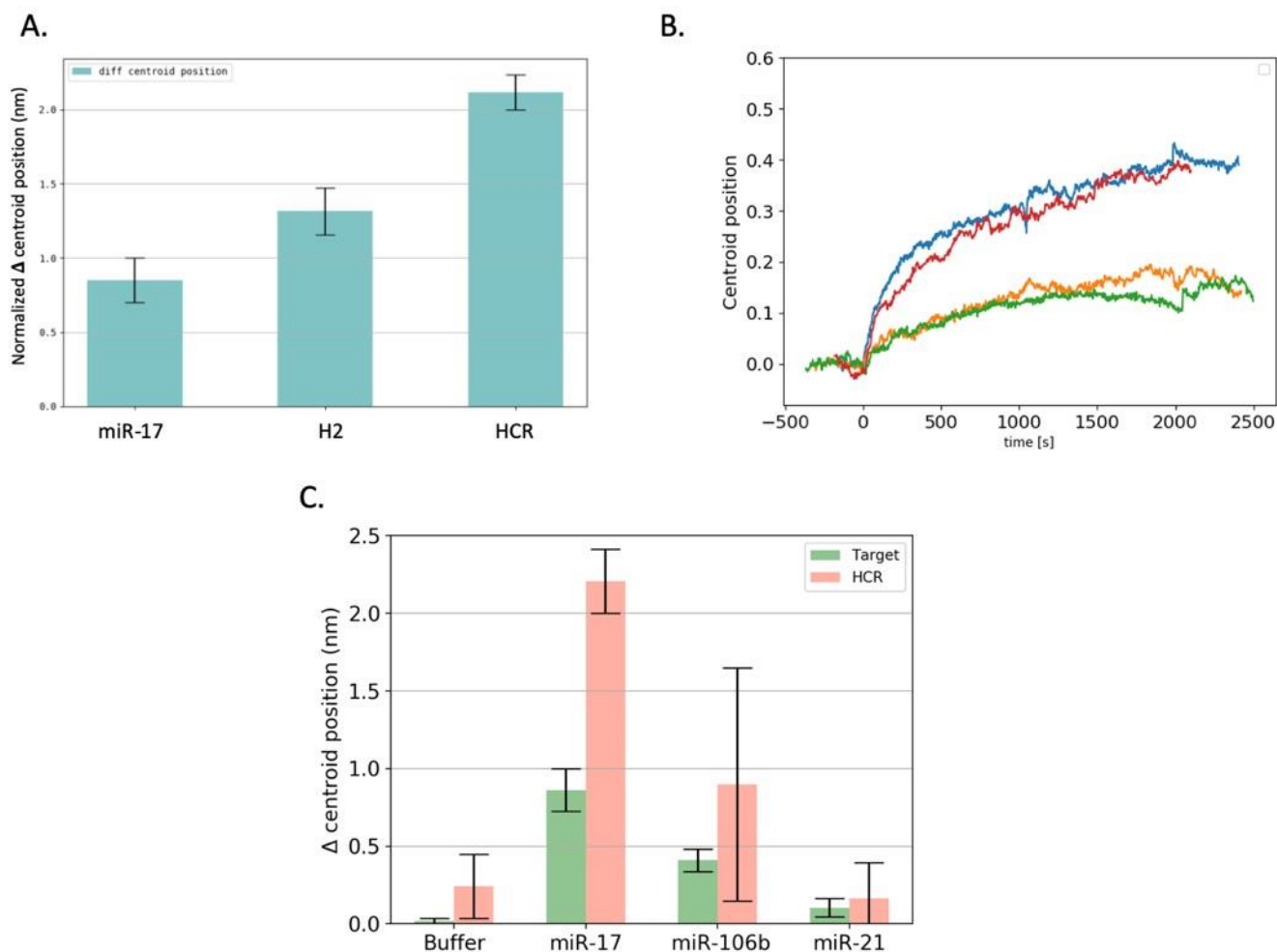


Fig 4-30. A) Peak shift with miR-17, and after H2 and HCR; B) Amplification contribution with target 1  $\mu$ M (upper curves) and 0  $\mu$ M (lower curves); C) Comparison between target step and HCR step with 0 target, 1  $\mu$ M miR-17 and 1  $\mu$ M miR-21. Bars correspond to standard deviation (N =3)

Fig 4-30 shows the data collected testing the effect of the mixture of hairpins on the amplification after target detection. In Fig 4-30 A. we compare the effect of the injection of H2 and the overall effect of the amplification with the mixture of hairpins flown at 5  $\mu$ L/min for 30 min. The effect of hairpin H2 is significative, as we have also observed in the previous data. The hybridization chain reaction lead to a further enhancement of the shift in centroid position leading to more than a 2-fold amplification after 1  $\mu$ M target detection. The hairpins were mixed right before the injection to get final concentration of 0.5  $\mu$ M each and flowed at 5  $\mu$ L/min. In Fig 4-30 B. we observe in details the interval during which the amplification occurred, highlighting the difference in the kinetics and final centroid position. We observed a shift in the LSPR peak with HCR also with the zero sample (green and orange lines), but it was clearly a lower response. While in presence of the target the kinetic was very different (red and blue lines in Fig 4-30 B), leading to a bigger shift

in the same interval of time. These experiments showed us that a significative amplification occurred also flowing the mixture of the hairpins after target detection. We wanted to test also the specific response in presence of HCR, further confirming the specificity of the process. In Fig 4-30 C we compare the signal enhancement of blank experiment, in presence of 1  $\mu\text{M}$  miR-17 and in presence of unspecific sequences. Green bars show the signal obtained with no amplification, while the red bars correspond the LSPR peak shift after flowing the mixture of hairpins. MiR-106b induces a lower shift once flowed on the chip, and the subsequent HCR response was clearly different, not stable as the response obtained with miR-17. The shift in presence of miR-21 was not significant.

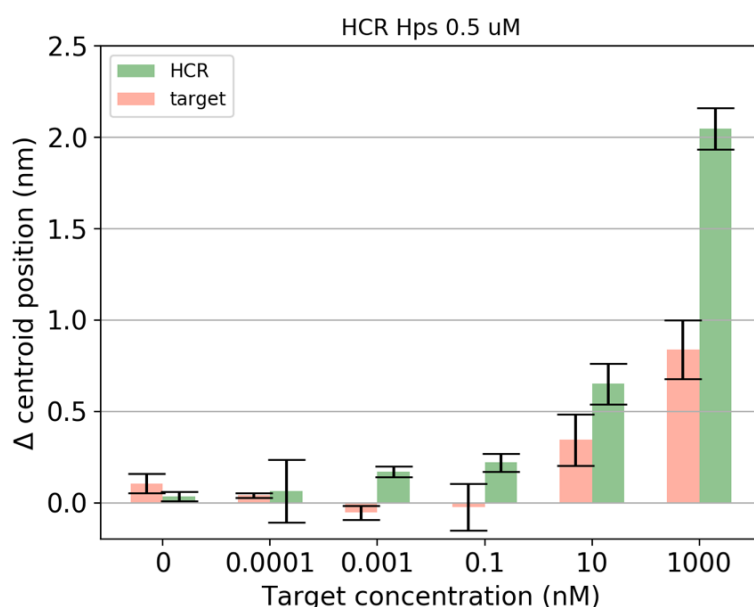


Fig 4-31. Bar plot showing in comparison the shift in centroid position obtained in presence of different concentration of the target with the improvement obtained flowing the mixture of hairpins ( $N = 3$ ). Red bars correspond to the average shift in centroid position obtained with the only target, while green bars correspond to the total enhancement after hybridization chain reaction in flow conditions.

Once defined the conditions for the HCR to take place, we tried to evaluate the sensitivity in presence of hybridization chain reaction. We flowed different concentration of the specific target miR-17, followed by injection of the mixture of hairpins at 0.5  $\mu\text{M}$ . As we can see in Fig 4-31, the limit of detection was improved performing hybridization chain reaction after the detection of the target. The target (red bars) is no more detectable at 0.1 nM, since lower than the limit of detection without amplification. Estimating the LOD as before, in presence of HCR (green bars), we obtained a LOD of about 4 pM. It means that we were able to improve the detection of about 3 order of magnitude compared to the bare target detection without amplification.

#### 4.3.6 Conclusions and observations

We implemented our direct HCR-based method for the detection of microRNAs on an original LSPR setup. The employment of a solid-state setup for such applications guarantees the development of more efficient and straightforward sensing strategies, allowing the regeneration of the sensor for further uses and the enhancement of the sensitivity. Joshi's method is the first solid-state LSPR setup proposed for the detection of microRNA, and it shows the mentioned advantages (Joshi et al., 2014). They demonstrated the high sensitivity of the strategy in complex media, thanks to the usage of peculiar sensitive gold nanoprisms for the detection. In the other hand, the proposed protocol involved overnight incubation for the hybridization, and the overall proceeding required constant manipulation of the samples and the chips, likely affecting the reproducibility and robustness of the method. Furthermore, we have to note that no data are presented about the effective discrimination between similar correlated sequences, leaving not completely solved the assessment of the specificity of their method. Another interesting approach for the detection of miRNAs is the one presented by Na et al (Na et al., 2018), proposing an LSPR method based on nanostructured surfaces and the precipitation of insoluble product upon the target detection. This method reached low LODs (in the femtomolar range) but the preparation of the chips is very complex and overnight incubations of the samples are always required for the detection, increasing the time of analysis. A recent work published by Ki et al (Ki et al., 2019) employed also HCR on LSPR based sensing, in combination with enzyme-assisted target recycling, with limit of detection of 2.45 pM. This strategy is also complex, since several steps are required, and it is able to return a limit of detection not far from what we obtained with our much simpler method. We propose a simple setup, which is easier to handle and allowed the real-time specific detection of miRNAs, improvable with HCR amplification. Spherical gold nanoparticles are commercially available, or easy to synthesize compared to nanoprisms and nanostructured metal surfaces. The real time detection is possible thanks to the adopted microfluidics, allowing the detection in flow, instead of dropping and incubating the sample on the chip. This avoids any manipulation of the chip, since, once inserted in the microfluidic chamber, wash steps and detection can be easily performed several times. Our system reached a good LOD in the detection of miR-17 without any amplification, in just 10 min (600 s). So, in principle, this could be the time needed for an analysis after the calibration of the sensor. The volume flowed in the chamber during target detection was theoretically 50  $\mu$ L. This could be reduced through the optimization of the microfluidics. In addition, this could lead to improvements of the time of analysis and limit of detection. The hairpin-like structure of our H1 probe acts as a barrier for unspecific binding, that gives advantages for the specificity, as we demonstrated. In the other hand, it could influence the sensitivity in some degree. This is related to the usage of a hairpin-like probe, but the optimization

of hybridization conditions could lead to improvements in this aspect, by tuning the stringency of the binding and the stability of the hairpin. Once we characterized the mere detection of the target, we tested the mechanism of the hybridization chain reaction upon target detection. A slight background noise was always present, as a shift in the position of the LSPR peak while flowing hairpins with no target detected. This is likely due to the leakage of the H1 probe. For the reasons explained in the introduction and during the discussion, hairpins are intrinsically affected by this phenomenon, due to the metastability of their structure. This is not affecting significantly the simple detection of the target, but, in the other hand, it cannot be ignored in the amplification through HCR. In general, the behavior of the hybridization chain reaction in the working conditions showed up to be more complex than expected. In addition to the leakage, when all the hairpins are present it is possible that they are involved in the growth of nanostructures that are not necessarily in the sensing area pointed by the optical fiber. This senses an area of about 2 mm in diameter on a spot of more or less 8 mm in diameter. This aspect could be also discussed about the detection of the target, since the reduction of the overall functionalized area, could in principle increase the efficiency of overall detection in the smaller sensing area, by reducing the loss of sample on the non-sensing area (Fig 4-32).

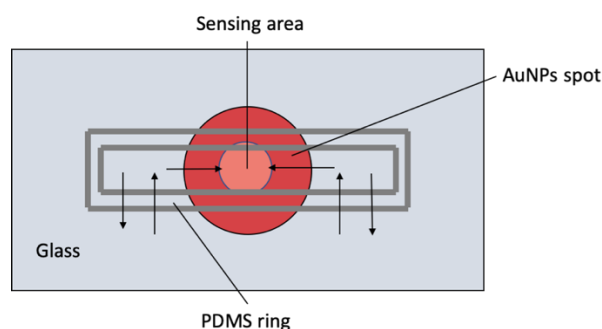


Fig 4-32. Scheme of the Chip with immobilized gold nanoparticles. The light red area corresponds to the sensitive area, that is the one directly detected by the spectrophotometer through the optical fiber. The arrows show direction of the sample while flowing in the chamber.

Nevertheless, we were able to amplify the detection of miR-17 of about 2-fold at 1  $\mu$ M. The amplification seemed to work differently for lower detection of target, likely due to steric hindrance induced by target detection. We were able to decrease the limit of detection of about 3 orders of magnitude with this method, proving the suitability of HCR for this kind of sensors based on a simple setup. Including HCR, the overall detection took 40 min. We are confident that optimization of some of the aspects that we listed, and further understanding, would lead to an improvement of the method, already demonstrated as suitable for such applications. In addition, trials in complex media would help the validation of the detection strategy towards the final development of a compact device for point of care applications and real time detection of biomarkers in biological samples.

## 4.4 Triplex-triggered HCR

The triple helix-based strategy was designed in order to explore an alternative detection method with enhanced sensitivity and selectivity, as reported for this kind of probes in literature. This was done in parallel with the implementation of the direct HCR method in response to some drawbacks eventually occurring with this approach. It may not always be convenient to design directly HCR self-assembly on the specific sequence of the target. As mentioned in the section 4.1.1, the hairpins in this approach need to be designed directly on the specific sequence of the target. It means that the most part of the hairpins would be affected by these constraints, in their stability and propensity to spontaneously assemble. In the introduction, in section 1.7 about Hybridization Chain Reaction, we mentioned the guidelines proposed by Ang and Yung, proposed to design monomers for efficient HCRs (Ang and Yung, 2016). These guidelines could not be applied to a direct HCR method, since there would not be any freedom in tuning the properties of the monomers, determined by the sequence of the specific target. An alternative strategy could involve the separation of the detection of the target from the amplification mediated by HCR. Looking in literature, we thought that a probe consisting in a triple helix of DNA would maybe represent a good tool for this purpose. There are many examples of the employment of triple helix probes in biosensing. These methods in general involve the interaction of the target, any analyte, with a large loop, setting free a second strand, which is suitable for signal amplification or transduction (Fig 4-33).

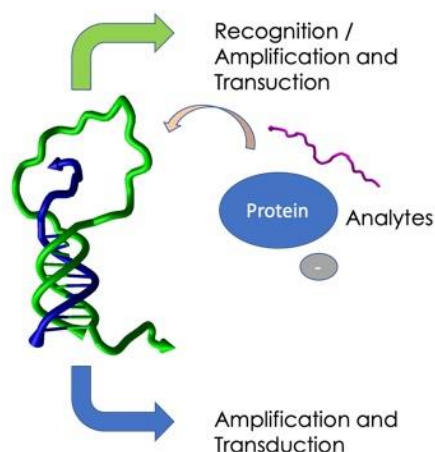


Fig 4-33. Scheme of the Triple helix-based strategies

The general structure and mechanism of such probes is similar to the one depicted in Fig 4-33. An amplification or transduction mechanism can be designed to be triggered by the free blue strand in the figure, not involved in the interaction with the target. The results presented for these strategies are good and promising but one of the strands is unfortunately discarded in solution as waste. We wanted to go further, and we presented a new strategy where both the

triple-helix-forming strands would be used to generate a response. In principle, we think that a biosensing strategy including such mechanism would be greatly improved, since this could enhance the amplification either help in the combination of different amplification/transduction strategies on the same probe. The two independent strands previously trapped in the triple helix would be free, introducing in the system more information, suitable for other purposes. Since we have expertise in Hybridization Chain Reaction, we thought to test the suitability of the strategy by designing two independent HCRs triggered by the triplex forming sequences upon target detection. To investigate such mechanism, we also thought to design the hairpins in order to build up “sticky” HCR products, able to interact once built, returning an even higher molecular weight product. We did so by introducing self-complementary short tails at the edge of the hairpins. These tails would be exposed once the nanostructure is formed, and they would lead to the interaction between the two DNA nanostructures (Fig 4-34).

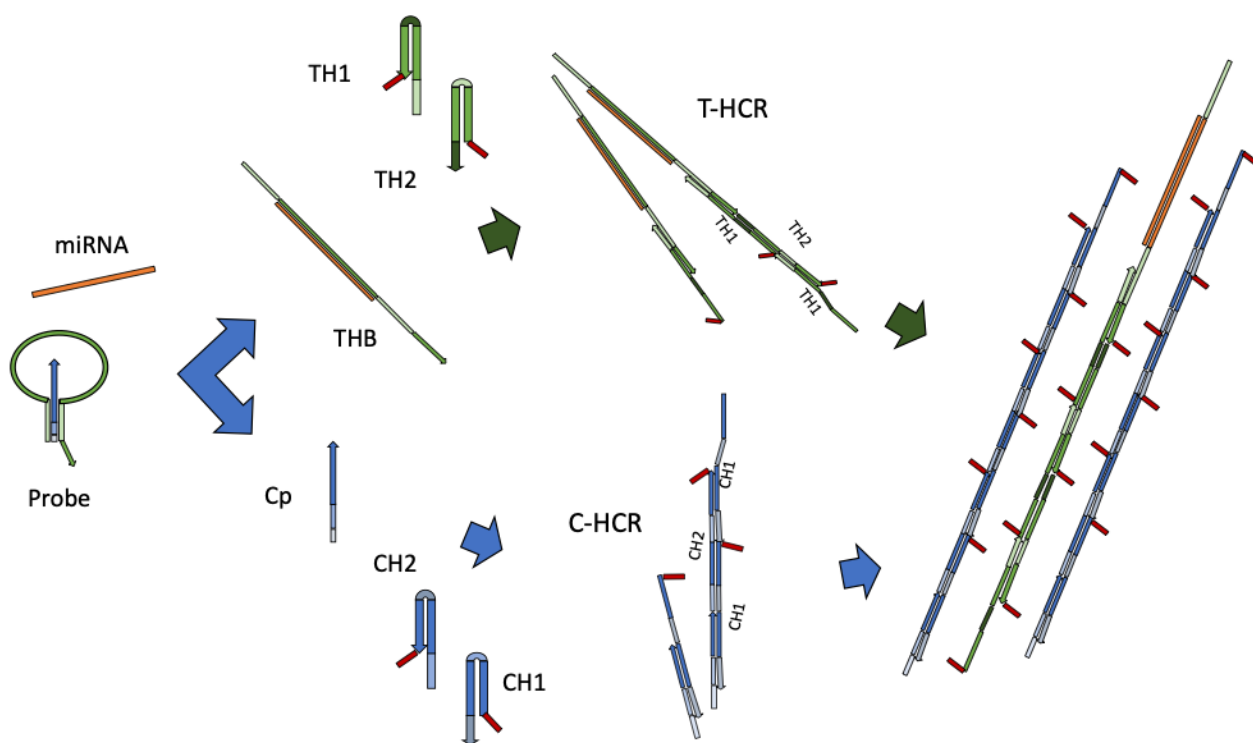


Fig 4-34. Scheme of our detection method based on Triple Helix Probe. Once the target interacted in the loop of the Triplex, the beacon should be open and released, as CP, set free after the target recognition. In presence of the hairpins, independent hybridization chain reactions are triggered both at the 3' of CP and THB. The “sticky products” interact and lead to a higher order assembly of the nanostructure.

The strategy based on triplex-HCR was designed in two main steps. First, the triple helix probe was designed based on both findings in literature and the requirements of strategy adopted. The second step had to be the design of the monomers for Hybridization Chain Reaction triggered by the strands involved in the formation of the triple helix. It is to note, that NUPACK can be used combining both the designs, reaching the optimization of both the sequences of the probe and the sequences of the hairpins for the self-assembling reaction. The experimental plan followed

quite the same logic. First experiments were directed to characterize the probe, testing the formation in solution and confirming its structure. Further experiments were instead dedicated to test the amplification and the target detection. We also tried to implement this detection method on electrochemical detection following same general procedures illustrated above for direct HCR.

#### **4.4.1 Design of the sequences of the triplex-triggered HCR**

The triple helix selected for this method was parallel triple helix (Y-RY). We based the design of the triple helix stem on previous observations performed by people in our involving a triple helix probe and on findings in literature, and we chose the sequence “CCTTCTCTTT”. Since in our design this would be involved in the interaction with the hairpins, we took into account the CG content and the position of the individual Cytosines to ensure a productive interaction with the toehold. The use of a parallel triple helix gave us the chance to evaluate the formation of the probe by changing the pH conditions, thus planning control experiments at higher pH. Based on Brucale et al, this kind of sequence should show a transition at around pH 7.0 (Brucale et al., 2005). The sequence in the cited work was 17 nt long with 47 % CG content. We shortened the sequence based on findings in literature where triple helix for sensing purpose have been used in general keeping a stem length between 6 and 10 nt. The CG content was 40%, to ensure a similar behavior. During the design, we generated a Triple Helix Beacon strand (THB) with both the polypyrimidine sequences at the edges and a large loop complementary to the sequence of the miRNA target. The 3' region of THB is designed to form a double helix with a portion of CP strand (Capture Probe), leaving a free toehold at the 3'. The 5' region of THB is completely involved in the formation of the triple helix on the CP probe, making up a beacon-like structure with a wide loop of about 23 nts and a stem of 10 base pairs. CP has thus the 5' portion completely involved in the triple helix formation, while a longer portion at the 3' is free, in proximity of to the loop. In addition, we designed a control sequence able to form a double strand with CP but not able to form the triplex: the 5' polypyrimidine region was replaced with a random sequence not involved in any interaction. We generated also shorter CP sequences, in order to assess the optimal length of the triplex stem. Concerning this, THB was designed with a variable protruding region, able to bind completely to the entire CP sequence (10 bases involved in the triple helix) but overhanging in the shorter sequences (Table 4-3). As we can see in the table, the 3' region of the THB is the one responsible for the hybridization chain reaction, while in the CP the total sequence is involved in the interaction with the first hairpin. In our design, the target would theoretically stay attached to THB, without affecting the 3' region.

Table 4-3. Sequences for the formation of the triple helix generated for the miR-17 target. The underlined sequences are involved in the formation of the triple helix. The red sequences are responsible for the trigger of the independent hybridization chain reactions. The green sequence is the random generated portion not able to form the triple helix.

Strand	Sequence	Length
THB	<u>CCTTCTCTTTCTACCTGCACTGTAAGCACTTTG</u> <u>TTTCTCTTCCAACGCACG</u>	51
cTHB	<u>ATACGTCAAT</u> CTACCTGCACTGTAAGCACTTTG <u>TTTCTCTTCCAACGCACG</u>	51
CP6	<u>GAGAAAGCGAGGTAGTGG</u>	18
CP8	<u>AAGAGAAAGCGAGGTAGTGG</u>	20
CP10	<u>GGAAGAGAAAGCGAGGTAGTGG</u>	22

In the design of the hairpins, we fixed at 6 nt the toehold and loop and 12 base pairs for the stem following the guidelines proposed by And and Yung (Ang and Yung, 2016). The only constrain in the design of the hairpins was the small portion of the toehold, affected by the triplex forming sequence, but tuned in CG content and position to guarantee the nucleation of the toehold. The rest of the sequences were generated letting NUPACK free to optimize the strands for the desired interactions allowing the optimization of the monomers for hybridization chain reaction (Table 4-4).

Table 4-4. Sequences of the Hairpins designed for the independent hybridization chain reaction. Underlined bases are involved in the stem. Red bases are part of the short tails for the enhanced amplification.

Strand	Sequence	Length
Ch1	<u>CTTGTATT</u> GCGAGGTAGTGGAAGTGGCCACTACCTCGCTTTCTC	44
Ch2	CCACTTCCACTACCTCGCGAGAAAGCGAGGTAGTGG <u>TATCATCT</u>	44
Th1	<u>AATACAAG</u> TTCCAACGCACGTCTCACCGTGCGTTGGAAGAGAAA	44
Th2	GTGAGACGTGCGTTGGAATTTCTCTTCCAACGCACG <u>AGATGATA</u>	44

In order to obtain “sticky” HCR products, we included short tails in the sequence of the hairpins, precisely on the opposite edge of the toehold. These were design to induce the interaction between the HCR products. We tested different lengths, 4 nt, 6 and 8 nt. In Table 4-4 the hairpins with longer tails are shown.

#### 4.4.2 Characterization of the DNA triple helix probe

Once we prepared and incubated the THB + CP mixture as described in section 3.4, the probe was characterized by assessing its correct formation in solution. We took advantage of the pH sensitivity of the parallel triple helix to set up some control experiments to point out differences in CD spectra and mobility in the gel electrophoresis. Analysis in electrophoresis were performed

using Tris buffer for pH 9.0 and Acetate buffers for pH 5.0 buffer as running buffers, to confirm the formation of a pH dependent complex such as the triple helix ( see section 3.3.1). We checked different length of the capture probe CP to evaluate the influence of the stem length on the stability of the structure. It was clear that  $Mg^{2+}$  was necessary in the running buffer to visualize the complex in the gel electrophoresis.

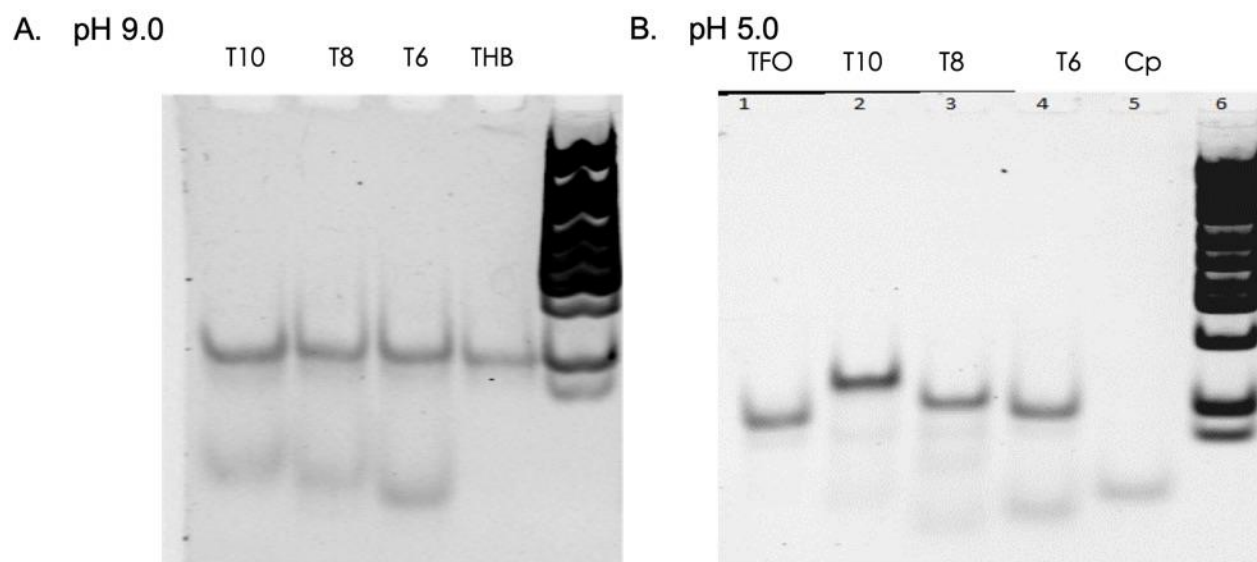


Fig 4-35. Section of polyacrylamide gel electrophoresis, showing the profiles of the mixtures THB + CP as T. T10, T8 and T6 correspond to mixtures with CP6, CP9 and CP10 respectively. Two different conditions, at pH 9.0 (A) and pH 5.0 (B).

In Fig 4-35 we have two sections of polyacrylamide electrophoresis gel run in Tris buffer pH 9.0 (A) and Acetate buffer pH 5.0 (B) in presence of 2.5  $MgCl_2$ . As we can see, at pH 9.0 there is no change in the gel migration compared to THB alone and the bands corresponding to the CP sequences are clearly visible, suggesting the missed formation of a complex in these conditions. On the contrary, at pH 5 (Fig 4-35, B) we clearly observe a shift in the position of the band, that is more evident for CP\_10 sequence. This difference could be interpreted as an increased compactness due to the formation of the complex. The triple helix conformation would give a contribution in keeping the strand THB and CP together. It is possible that at pH 8.0 the formation of a complex takes place in presence of magnesium, but the interaction is not strong enough and no difference is evident compared to the individual THB. To investigate more in deep the formation of the complex, we also performed the same experiments using a control sequence cTHB, not able to form a triple helix, but only a duplex (Fig 4-36).

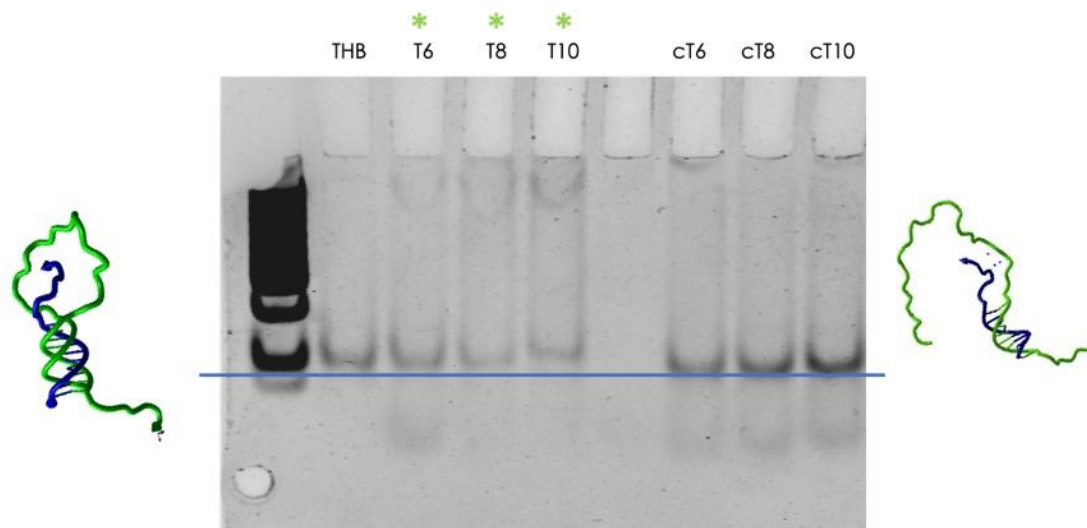


Fig 4-36. Section of polyacrylamide electrophoresis gel, run in Acetate buffer pH 5.0, MgCl<sub>2</sub> 2.5 mM. T6, T8 and T10 correspond to the mixture with THB, while cT6, cT8, cT10 correspond to mixtures with control sequence cTHB.

Fig 4-36 shows the results of the analysis of the triplex mixture with THB and cTHB control sequence. As we can see, a shift is especially visible in T10 (THB + CP10), while this is not visible with cT10. In the following experiments, we kept CP10 to form the triple helix probe, since its formation was more evident and subsequent experiments proved a better stability (data not shown). The band shift is thus visible in presence of THB, designed to form the triple helix structure, but not visible with the control sequence cTHB, identical except for the 5' polypyrimidine strand. What we can conclude from these observations is that a complex is actually forming at pH 5.0 for T samples where the formation of the triple helix is expected, but this is not visible at pH 9.0. The control sequence does not show a band shift neither at pH 5.0 nor at pH 9.0, suggesting the missed formation of a productive interaction between cTHB and CP.

Table 4-5. Table showing the composition of the samples analyzed in circular dichroism.

Sample in Acetate Buffer pH 5.0/ Tris Buffer pH 9.0			
	CP10	THB	cTHB
T	+	+	-
THB	-	+	-
CP	+	-	-
cT	+	-	+
cTHB	-	-	+

To further assess the identity of the complex formed in solution, we decided to investigate the mixtures THB + CP using circular dichroism spectroscopy. We recorded the spectra relative to samples containing THB and samples with the control sequence cTHB at pH 5.0 and pH 9.0. The samples analyzed in the experiments performed are described in Table 4-5.

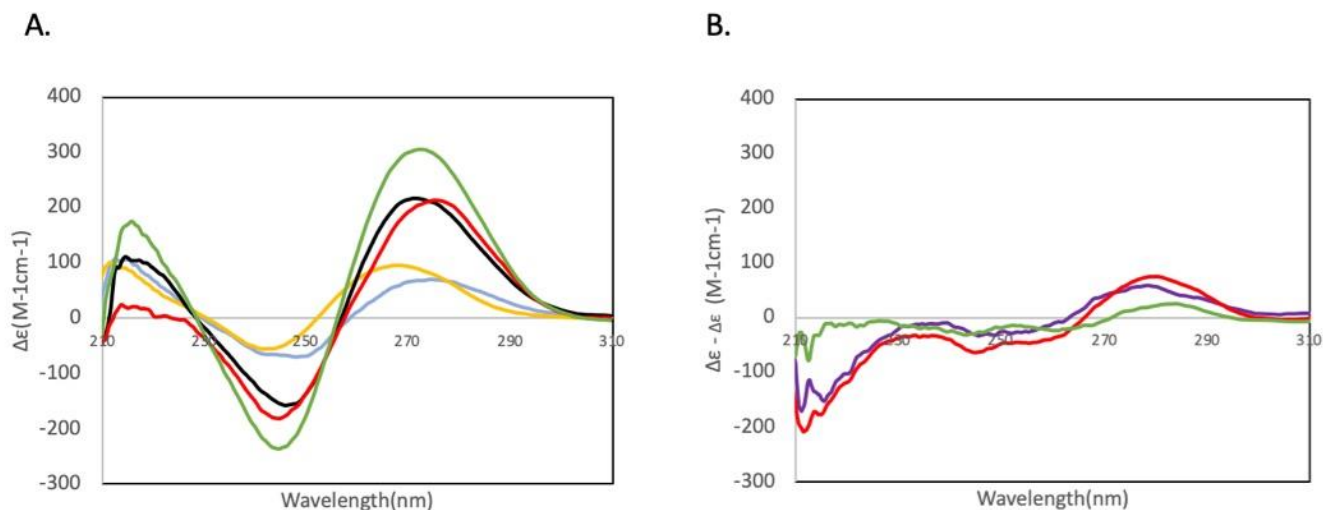


Fig 4-37. CD spectra obtained from mixtures in buffer Acetate 20 mM, NaCl 50 mM, MgCl<sub>2</sub> 20 mM pH 5.0. A. Raw data, blue line: THB; yellow line: CP10; black line: cTHB; red line: T; green line: cT. B. Difference spectra, T-(THB+CP10). Red: subtraction of the spectra of individual strands THB and CP to T spectrum. Green: same operation for cT control sample. Purple: the difference between these two spectra have been executed: T - (THB + CP10) - cT-(cTHB+CP10).

Fig 4-37 shows the raw spectra between 210 and 310 nm corresponding to samples in acetate buffer pH 5.0. The appearance of the T and cT spectra seems generally coherent with the B-DNA spectrum (Kypr et al., 2009) except for some differences. Typical B DNA shows a spectrum with a positive band at about 270-275 nm and a negative one at 242 nm, equally displaced from the crossover at 255 nm. Typical are also a maximum at 217 nm, and a minimum at about 212 nm (at the edge of the spectrum). Control cT spectrum (black line in Fig 4-37 A) shows in general these features, while, observing T raw spectrum (red line in Fig 4-37 A), a less positive peak is visible in this region, 210-220 nm. This is considered characteristic of the CD spectrum for the triple helix of DNA (Manzini et al., 1990, Xodo et al., 1990, Hashem et al., 1999, Hung et al., 1994). A red shift of the positive ellipticity peak at 275-280 nm is also visible, followed by a slight shift in the isoellipticity point to 260 nm, reported in literature for parallel triple helix (Y-RY) with analogous composition (Liu et al., 1993, Bernal-Mendez and Leumann, 2002, Sugimoto et al., 2001, Manzini et al., 1990, Gondeau et al., 1998). According to the design, just a small portion of the DNA sequences would be involved in the formation of the triple helix, thus its contribution to the spectrum could be partially hidden. The spectral features can be highlighted subtracting the CD spectra of individual THB and CP to the spectrum of T (T - THB - Cp) (Fig 4-37 B). The ellipticity arising from the triple helix DNA is isolated from the contributions of the single stranded DNA. The difference spectra in Fig 4-37 B. show clearly a strong decrease in 212-215 nm region

and an increase in peak at 280 nm for T sample (Red line) and not for cT (Green line), coherent with findings in literature as mentioned before. The lower slight changes that are observable in cT spectrum could be related to the double helix formation between cTHB and CP10. If the difference spectrum (cT-cTHB-CP10) related to cT is subtracted to T difference spectrum (T-THB-CP10), the spectral contribution due to the formation of the double helix would be deleted and the difference between T and cT profiles further highlighted (purple line). This confirms the observed features in addition to a visible more negative peak at 245 nm, also reported in literature (Gondeau et al., 1998). Once we determined the differences between T and cT samples at pH 5.0, we investigated the spectra in pH 9.0 buffer, to assess the effect of pH on the spectra.

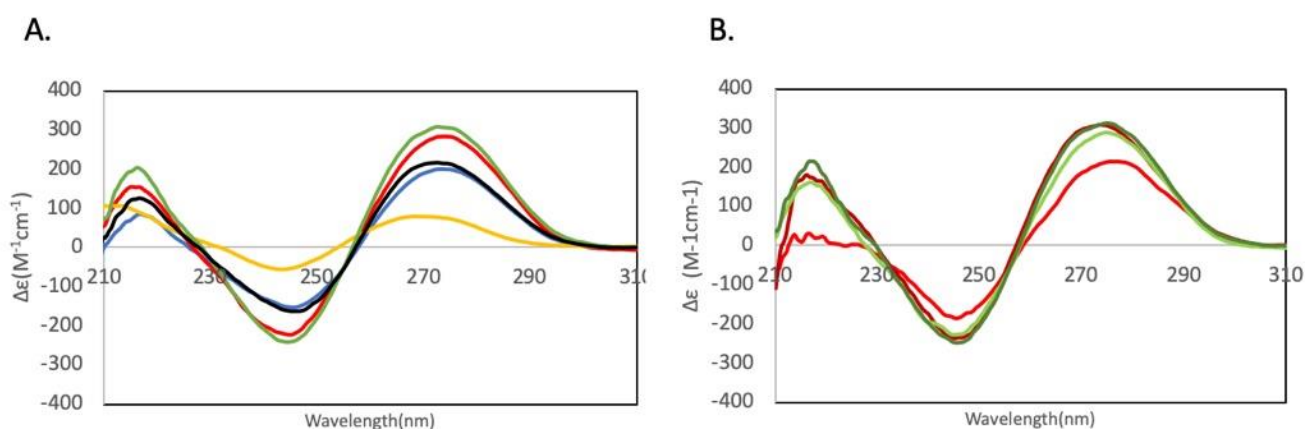


Fig 4-38. A) CD spectra corresponding to samples prepared in Tris buffer 20 mM, NaCl 50 mM, MgCl<sub>2</sub> 20 mM pH 9.0. Blue line: THB; red line: T; yellow line: CP10; green line: cT; black line: cTHB. Same data plotted with the spectra relative to T mixture at pH 5.0, B), Spectra of T and cT at different pH. Bright red line: T pH 5.0; dark red line: T pH 9.0; green line: cT pH 5.0; dark green line: cT pH 9.0.

In Fig 4-38 A, CD we plotted the spectra corresponding to samples prepared in Tris buffer at pH 9.0. It is noteworthy that the decrease in 210-220 nm region is no more visible in spectra recorded for sample T (red line) and all the spectra show a similar profile. We compared the spectra of cT and T at the different pH in Fig 4-38 B, to enlighten the differences of T pH 5.0 (red line) vs. T pH 9.0 (dark red line). T at pH 5.0 (red line) is again clearly different from the controls and pH 9.0 conditions, showing almost identical spectra. Differences between spectra have been calculated again to put in evidence the differences masked by the overall spectrum of the mixture (Fig 4-39).

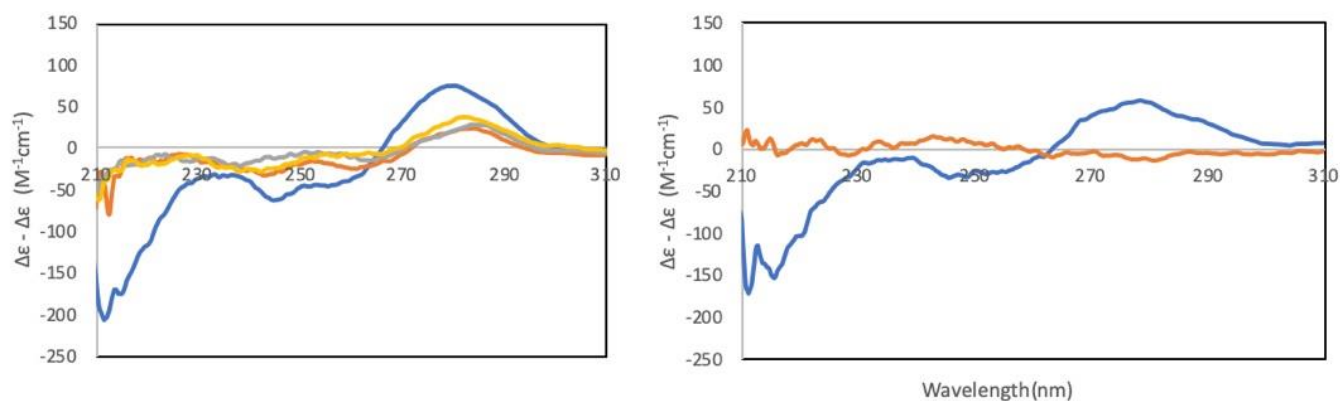


Fig 4-39. A) Difference spectra, T - (THB+CP10). Blue line: T pH 5.0; Orange line: cT pH 5.0; Grey line: T pH 9.0; Yellow: cT pH 9.0. B) Differences T – cT at pH 5,0 and pH 9.0. Blue line: T- cT pH 5.0; orange line: T-cT pH 9.0.

No strong differences are evident comparing T at pH 9.0 and control cT both at pH 9.0 and 5.0. (Fig 4-39 A, grey, yellow and orange lines respectively). This suggests that the changes previously observed at pH 5.0 do not occur at pH 9.0. The fact that the spectrum of T sample is different from the sum of individual THB and CP10 spectra but also from the cT sample suggests the presence of an additional structure beside the double helix, involving only THB and not cTHB in the interaction with CP10. In summary, the CD spectra of our T sample show traits consistent with reported data in literature for triple helix DNA structures related to Hoogsteen base pairs. Our observation is also consistent with the known dependency on pH of the parallel triple helix DNA structures (Y:R-Y), proving the design of the triple helix probe.

#### 4.4.3 “Sticky” Hybridization Chain Reactions

The self-assembling reaction was first tested separately, not taking into account the triple helix, to assess the correct ongoing of the independent hybridization chain reactions and the interaction between the built products.

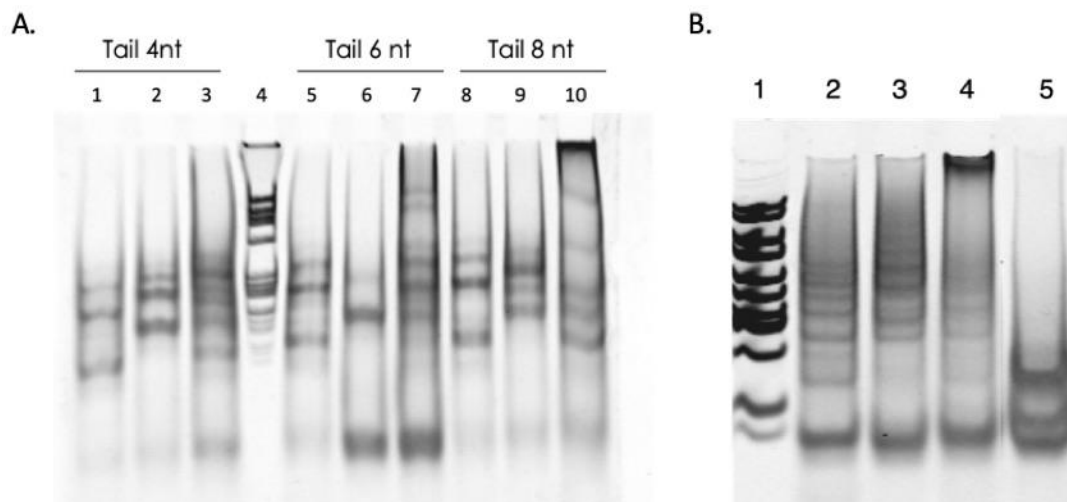


Fig 4-40. A) Section of polyacrylamide gel electrophoresis showing HCR product of single and double amplification and different tail length. Hairpins and trigger sequences THB and CP were at 2:1 ratio. Tail = 4 nt Lane 1-3: C-HCR, T-HCR, D-HCR; Tail = 6 nt Lane 5-7: C-HCR, T-HCR, D-HCR; Tails = 8 nt Lane 8-10: C-HCR, T-HCR, D-HCR. B) Section of polyacrylamide gel electrophoresis comparing single T-HCR and C-HCR (lane 2 and 3) and mixed HCR, where the HCR products have been mixed after 2 h of incubation at room temperature. Lane 5 show the mixture of the 4 hairpins in solution incubated in the same conditions.

In Fig 4-40 A. we can see the product of the single self-assembling reactions and combination of both in solution for three sets of hairpins with different length of the tails. We call C-HCR, T-HCR and D-HCR, the HCR triggered in presence of respectively CP, THB and both of them. This experiment was done to evaluate the potential of the self-assembling reaction with the three sets of hairpins. These hairpins have the same sequences, with the only difference in the length of the tail. The experiment was performed using a 2:1 ratio of the reagents Hps:target in HCR buffer, and all the reagents for T-HCR and C-HCR self-assembly were mixed to obtain the combined HCR product D-HCR, assuming not enough time neither the proper conditions for the formation of the triple helix. The gel was run in presence of  $Mg^{2+}$  to keep the nanostructures stable during the electrophoresis. It is to note how, as expected, longer tailed hairpins led to a higher molecular weight product when in combination to form the “sticky” HCR products. This is visible as an intense band in proximity of the well in lane 10 in Fig 4-40 A. Something also can be seen in lane 3 and 7 of the same figure, with hairpins with shorter tails, 4 nt and 6 nt respectively. There is clearly an interaction between the HCR products, visible comparing the electrophoresis profile to the profile of the individual HCR products C-HCR and T-HCR. Hairpins with 8 nt tails were chosen for the following experiments. In Fig 4-40 B. we show the result of a control experiment, where the two HCR products were mixed after 2h of incubation at room temperature, to get a false-DHCR. The mixture was then kept 2h at room temperature before electrophoresis analysis. We can see how in general a similar profile is visible. In this case the ratio was 4:1, with hairpins  $1 \mu M$  while THB and CP at  $0.25 \mu M$ . We can see the higher molecular weight product in lane 2 and 3 compared to lane 8 and 9 in Fig 4-40A., due to the different ratio adopted. Fig 4-40 B. also gives information about the mixture of hairpins in solution with no triggering sequences, so about

the leakage. We can see how a slight interaction between the hairpins is present, surely due to the 8 nt tails but without leakage. The hairpins are likely involved in some soft interactions due to the self-complementary tails, but this does not seem to affect the dual self-assembling reaction. We tried to characterize the product using Atomic Force Microscopy and we found long nanostructures interacting together in different manners. In Fig 4-41 A and B we have respectively T-HCR product and C-HCR product, with long linear nanostructures. For D-HCR, we did not expect great homogeneity, since the interaction between the nanostructures could take place in random fashion, depending on the conditions in solution and on random contacts between the tails in the nanostructures, leading to wrapped nanostructures either interactions in precise domains.

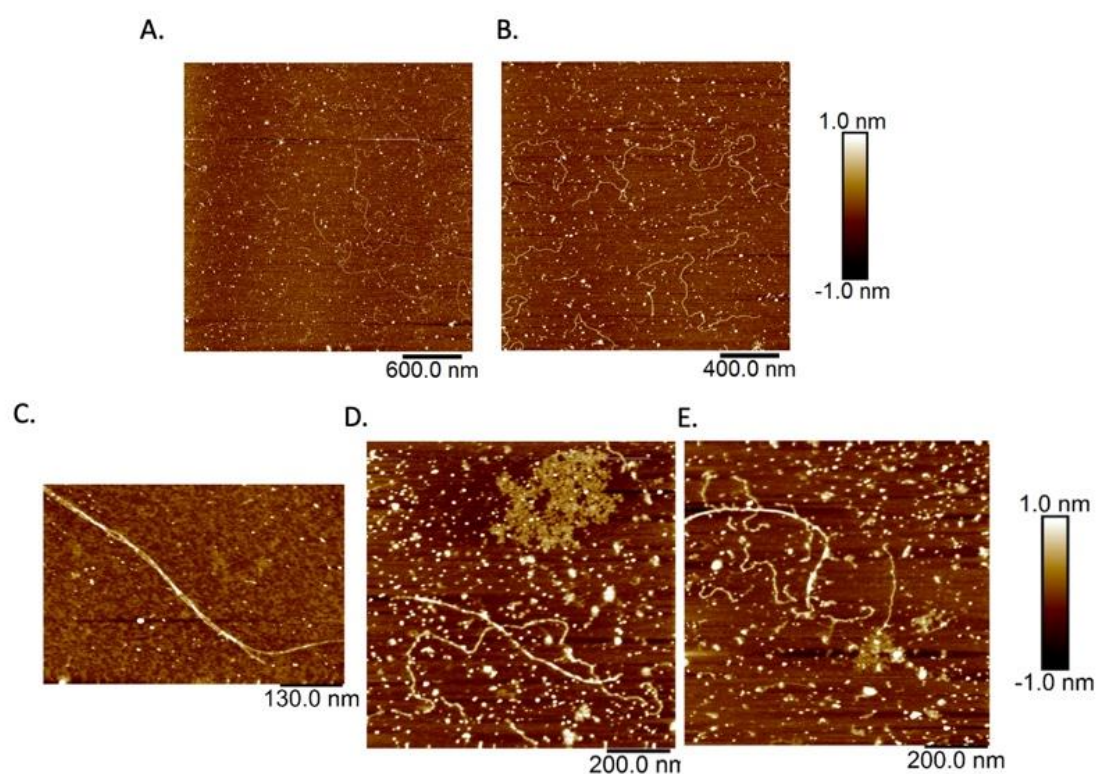


Fig 4-41. AFM imaging of the double HCR products on mica. A. T-HCR product; B. C-HCR product; C, D and E, double HCR samples, the three pictures show different nanostructures found in the same sample.

In Fig 4-41 C, D and E we can see the AFM images of the D-HCR product with heterogeneity in the morphology. Compared to the single HCR products C-HCR and T-HCR, the nanostructures showed higher complexity and branched and interacting long double stranded DNA nanostructure were visible. These structures are not be able to easily migrate in the gel during the electrophoresis, returning the profile enlighten in Fig 4-40. We were thus able to make the two independent HCR products interact together to form a bigger nanostructure, clearly visible in gel electrophoresis and with differences detected in AFM. In principle, the two independent HCR products, triggered by the triplex forming strands, are able to produce a nanostructure with a higher order of complexity. This phenomenon should be a response to the interaction between

the target miR-17 and the triple helix probe, theoretically able to open the complex and separate the two triggers.

#### 4.4.4 miRNA detection

The detection of the miR-17 in solution was first evaluated in gel electrophoresis. We started testing the ability of the target as trigger of the two independent hybridization chain reactions T-HCR and C-HCR through the interaction with the triple helix.

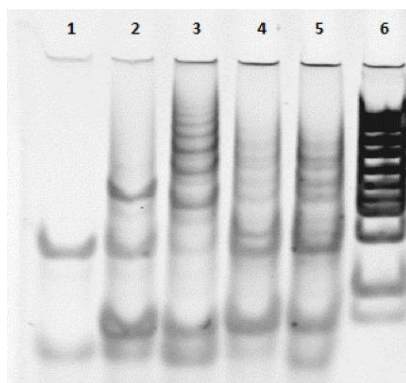


Fig 4-42. Section of polyacrylamide gel electrophoresis in TBE 1X. Lane1: triple helix probe; lane2: T-HCR sequences without target; lane3: T-HCR product in presence of the target; lane4: C-HCR without target; lane 5: C-HCR in presence of the target.

In Fig 4-42 we show the results of a PAGE analysis of samples in which all the reagents were at 0.5  $\mu$ M. The gel was run in TBE 1X. As mentioned before in these conditions (in absence of magnesium) it was not possible to see the complex of the triple helix, as we can note in lane 1, while the HCR product is always visible. In these experiments we focused on the final HCR product in presence and in absence of the target, not investigating the triplex complex. The aim was to understand if at the endpoint there was or not the specific HCR product. The triple helix here was formed in HCR buffer (NaCl 0.5 M, Na<sub>2</sub>HPO<sub>4</sub> 50 mM) at pH 5.0 and so the HCR took place in the same buffer. We can see, comparing lane 2 with lane 3, that there is an effect of the target miR-17. In lane 3 an HCR product is evident, with high molecular weight bands, while, in lane 2, we discriminate the band corresponding to THB, and maybe a spurious interaction between THB and Th1, but no more bands are visible in the higher molecular weight range. Similar behavior is visible in lane 4 and 5: higher molecular weight products are visible in lane 5, while in lane 4 this is not as evident, even if in this case some unspecific polymerization occurred. This is probably due to the hardness in tuning the stoichiometry of the triple helix complex in solution, since it is not easy to prevent the presence of non-complexed strands. Nevertheless, we clearly see a difference in the product of the reaction as effect of the presence of the target.

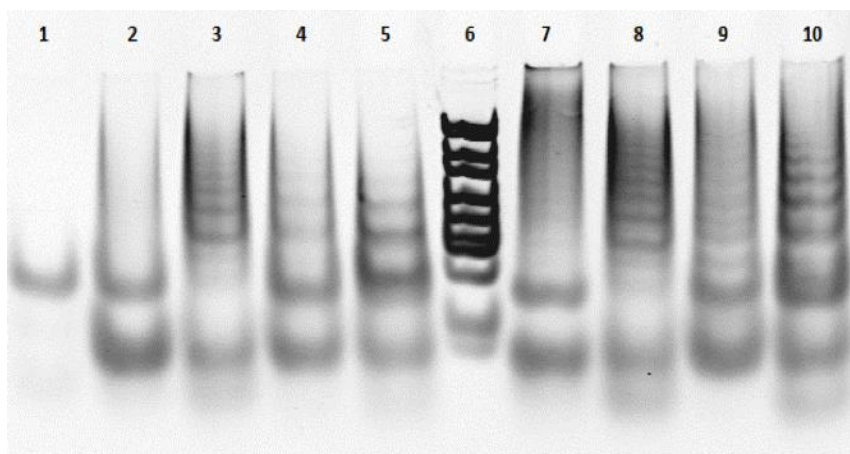


Fig 4-43. Section of polyacrylamide gel electrophoresis showing the detection of the target with independent HCR product at pH 5.0, lane 2-5, and pH 8.0, lane 7-10. Gel run in presence of magnesium. Lane 1: triple helix probe; lane 2: T-HCR, no target, pH 5.0; lane 3: T-HCR, target, pH 5.0; lane 4 and lane 5, C-HCR with no target and with target at pH 5.0. In lane 7 and 8, T-HCR without and with target at pH 8.0; lanes 9 and 10, C-HCR without and with target at pH 8.0.

As control experiment, we performed the same experiment also at pH 8.0. To do so we simply formed the triple helix in HCR buffer ( NaCl 0.5 M, Na<sub>2</sub>HPO<sub>4</sub> 50 mM) at pH 5.0 and at pH 8.0 and performed the detection in the same buffers (Fig 4-43). All the reagents were at 0.5  $\mu$ M. This experiment proved that the process was dependent on pH of the process, thus likely controlled by the stability of the triple helix probe. Since the triple helix probe is the mediator between the target detection and the amplification, when its stability is compromised (at higher pH) we expect a loss of control on the HCR. In Fig 4-43 we show the products obtained in the different conditions of the independent HCRs. The profile in lanes 2-5 is analogous to what we have seen in Fig 4-42: the target clearly triggered the T-HCR and C-HCR responses at pH 5.0. In lanes 7-10, we can see the effect of the higher pH on the stability of the system: lane 7 and lane 9, supposed to be the blanks, show higher molecular weight products, even if slightly different from the product in presence of the specific target. We proved thus the dependency of the amplification on the target but also that the stability of the triple helix probe, proving the working principle of the designed strategy. In the following steps, we wanted to prove that the assembly is well controlled by the presence of the target also in the mixed conditions, with both C-HCR and T-HCR monomers, and that the process is able to return a quantitative information. The experiment was performed in HCR buffer (NaCl 0.5 M, Na<sub>2</sub>HPO<sub>4</sub> 50 mM) pH 5.0, using the same buffer for formation of the triple helix probe and during the detection, as done before. We incubated different concentrations of target miR-17 with the mixtures including the hairpins TH1, TH2, CH1, CH2 and the triple helix probe.

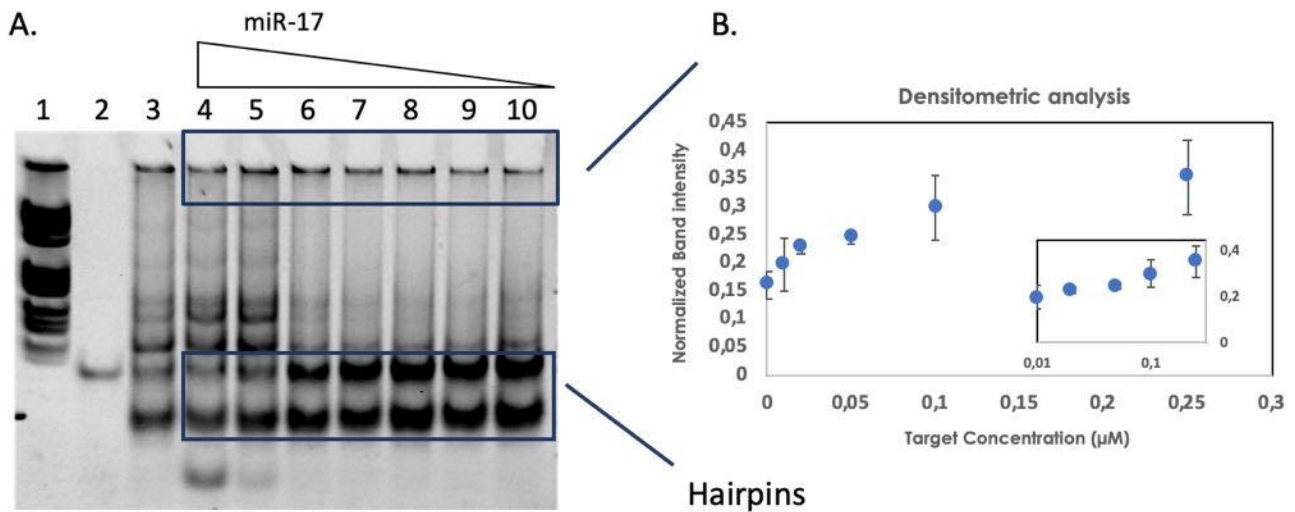


Fig 4-44. Detection of different concentration of target miR-17 using the triple helix probe mediated double HCR amplification. A. Section of polyacrylamide gel electrophoresis showing the products of the amplification at different concentration of the target in range 0.5 – 0  $\mu\text{M}$  (Lanes 3-10 respectively); Lane 2, triple helix probe. Gel run in TBE 1X 12 mM MgCl<sub>2</sub>. B. Plot showing the intensity of the high molecular weight bands detected in the gel over the concentration of the target).

In Fig 4-44 the results are shown. The experiment was performed with hairpins at 0.5  $\mu\text{M}$  and triple helix probe at 0.25  $\mu\text{M}$ . As expected, and suggested by the previous observations in section 4.4.3, in Fig 4-40, the higher molecular weight product is in proximity of the wells of the gel. We can see the effect of the target concentration: Lanes 3-10 show the product obtained with decreasing concentration of target, from 0.5  $\mu\text{M}$  (in excess compared to the probe) to 0  $\mu\text{M}$ . We can see a gradual decrease of the consumption of the bands of the hairpins. These are more intense at decreasing concentration of target. If we focus on the higher molecular weight band in proximity of the wells, we can appreciate a slight increase of the intensity of the band increasing the concentration of the target. In Fig 4-44 B. the results of the densitometric analysis on the higher molecular weight bands are showed: there is clearly an effect of the target concentration, and it is possible to correlate the intensity of this band and the intensity of the band of the hairpins to the target concentration. It means that the amplification, as we proved before, is dependent on the presence of the target and that this is also dependent on its concentration, confirming the possible applications in the quantitative detection.

#### 4.4.5 Electrochemical detection using the triple helix probe

To perform trials towards the electrochemical detection using the triple helix probe and the combined double HCR products, we ordered a modified CP probe, with a thiol at the 5' edge and a T spacer.

SH-CP      SH – TTTTGGAAGAGAAAGCGAGGTAGTGG

The electrochemical detection was tested following the same protocol illustrated in section 3.5.4, using Hoechst as electroactive label. First, we tested the amplification on surface on TSGs, where CP was immobilized and passivated with MCH. The normalization of the data was done over the response on TSG passivated with MCH, without probe. First, we tested the possibility to detect an amplification on the single immobilized CP, thus the C-HCR on surface. We can see in Fig 4-45, how HCR leads to more than 2-fold the signal obtained with CP alone.

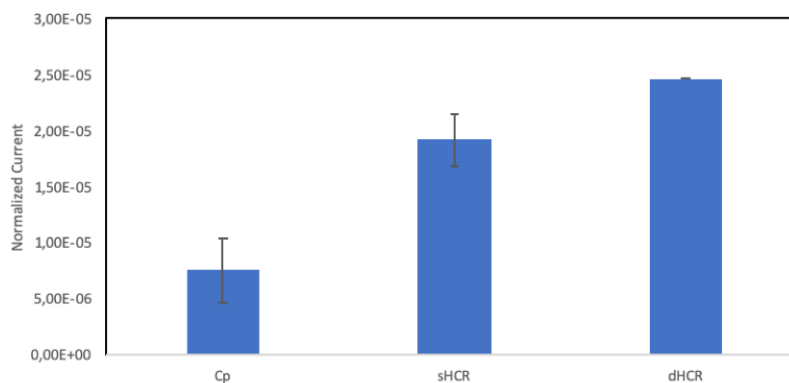


Fig 4-45. Test of the amplification on CP, immobilized on TSG electrodes. Average height of the oxidation peak of Hoechst with SD (N = 3).

We tested the principle of the DHCR. We suppose that T-HCR would be able to stay attached to the immobilized C-HCR product upon detection of the target, thanks to the short tails of the hairpins. We appreciate an increase of the response when the T-HCR product is incubated even if not dramatic. This means that the amount of DNA is probably increased on the surface. No relevant response was observed with hairpin mixtures incubated on MCH passivated TSG without probe. The low effect of the DHCR on surface in electrochemical detection could be related to a diffusion limitation to the Hoechst labeling or a related inefficient charge transfer at the surface due to a sort of hindrance caused by the amount of DNA on surface. As for the electrochemical detection in direct HCR, this technique is probably not the ideal to perform such measurements, and the electrochemical setup has to be optimized to allow more meaningful measurements, for example in impedance. In principle, also in this triplex-HCR method, the increased amount of DNA on surface should be detectable through electrochemical impedance spectroscopy as increased resistance to faradaic currents. Efforts should be done for the optimization and amelioration of the electrochemical setup to perform such measurements or the usage of alternative labels. Anyway, we tried to get some preliminary data of the detection of miR-17 in these conditions. The probe was incubated at the concentration of 0.5  $\mu$ M on TSG overnight. Despite the variability, we tried to investigate the correlation of the electrochemical response and the concentration of the target.

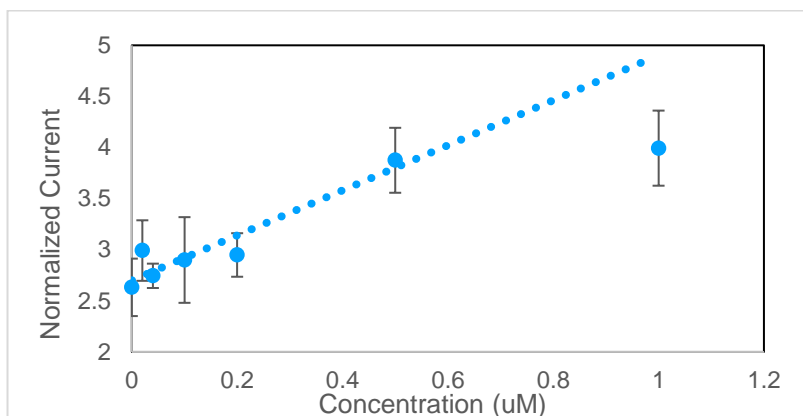


Fig 4-46. Detection of miR-17. Concentrations in the range 0 - 1  $\mu$ M.

In Fig 4-46, we show the results obtained trying to detect different concentrations of miR-17 using the triple helix probe and the DHCR on surface. We can see that a slight correlation can be observed, despite the high variability. Trying to roughly estimate the limit of detection employing the same method explained before, the limit of detection was found to be about 350 nM. This is obviously a first preliminary result, which is encouraging about the application of the method, but still needing a deep characterization. More efforts are required in the determination of the individual contribution of the single T-HCR and C-HCR and a deeper analysis of the behavior of the triple helix probe on the surface.

#### 4.4.6 Conclusions and observations

We designed an original triple helix probe, adapted to the detection of microRNAs and combined to a double hybridization chain reaction as signal amplification. Beside the challenge in the adaptation on electrochemical detection, an evaluation of the specificity of the triple helix probe need to be properly faced, ensuring the stability of the probe and the discrimination of similar target sequences. We anyway proved the possibility to combine two responses on the same triple helix probe and that these can be triggered ( thus controlled) by the presence of the target. This is a completely original strategy for the adaptation of triple helix probes in sensing. Our design would allow the combination of different amplification and transduction methods on the same probe. This would likely lead to a more reliable detection, by offering a new universal and versatile tool. Our system was able to trigger two independent self-assembling reactions to form more complex nanostructures, in principle detectable in biosensing and leading to a further amplification of the signal.

## 4.5 Metallic nanoparticles and nanoclusters as biosensing tools

As explained in the first paragraph of this Results and discussion section, the work involved the exploration of alternative ways to enhance signal in DNA biosensors. In order to amplify the signal generated by a detection method, as anticipated in section 1.5, metal nanoparticles could be employed thanks to their peculiar properties and easy production. As we have seen in LSPR based detection, optical properties of metal nanoparticles can be used as transducer in biosensing strategies. Gold nanoparticles are thus a good choice for such purposes, able to transduce but also amplify the signal in electrochemical and optical sensors. In alternative to gold nanoparticles, metal nanoclusters can also be used as labels or signal enhancer in biosensing. These small nanoparticles (up to 2 nm of diameter in general) have many optical properties and they can serve in many strategies thanks to their fluorescence, plasmonic effect, or catalytic activity. Moreover, interestingly, this kind of particles can be apparently synthesized directly in situ on specific DNA sequences. This fact attracted our attention, since DNA based sensors could logically take advantage of such transducers for signal enhancement in SPR, electrochemical and colorimetric biosensing. In particular, we noticed the application of Ag/Pt DNA templated nanoclusters, able to induce a signal enhancement in SPR but also presenting a peroxidase catalytic activity. These nanoclusters too, can be synthesized directly on specific DNA sequences, allowing the precise localization of such catalytic/plasmonic labels on the DNA. For this purpose, we started a collaboration to characterize such Ag/Pt DNA templated nanoclusters and test an eventual strategy. Thanks to the expertise of the group of Dr Morteza Hosseini, at the University of Tehran, we were able to test the selective synthesis of catalytic NCs, able to generate a readable signal, potentially in both SPR (thanks to the optical properties) and electrochemical sensing (thanks to the peroxidase-like activity). These experiments were part of a work published in collaboration with the Iranian group. The goal was to develop a method to detect the M.SssI methyltransferase (MTase) activity in biological samples. DNA methylation is a significant epigenetic process for the modulation of the gene expression. In some diseases such as infections and cancers, these mechanisms are affected and an abnormal concentration of DNA methyltransferase is analyzed an informative biomarker for the diagnosis (Robertson, 2001, Robertson, 2005). M.SssI recognizes CGCG palindromic site on DNA and is known that silver nanoclusters can be formed on C-rich DNA sequences. C-rich DNA sequences including this recognition sites have been used as template for the formation of Ag/Pt nanoclusters. It was found that the methylation of the cytosines could affect and inhibit the catalytic activity of those nanoclusters, probably preventing their formation of influencing the local environment of the nanoclusters. This let us to explore the suitability of such nanoclusters by characterizing a testing them, investigating their possible application in our aim.

#### 4.5.1 Synthesis and characterization of the DNA templated Ag/Pt nanoclusters

Ag/Pt DNA templated nanoclusters have been synthesized and characterized following the protocols described in the material and methods, section 3.7. The formation of the Pt/Ag nanoclusters was tested on purchased DNA sequences (Table 4-6).

Table 4-6. Sequences selected to test the formation the DNA templated Ag/Pt nanoclusters and their characterization.

DNA strand	Sequence	Length (nt)
S1	CGCGCCCCTAATCCCCCGCG	20
S2	GCGCGGGGATTAGGGGGCGC	20
S3	C(CH <sub>3</sub> )GC(CH <sub>3</sub> )GC(CH <sub>3</sub> )CCCTAATCCCC(CH <sub>3</sub> )GC(CH <sub>3</sub> )G-	20
S4	TCCTGGTCCGAGCTGCCCGAG	22

S1 is a c-rich sequences, including the target sequences of the enzyme CGCG, while S2 is its complementary strand. S3 is the methylated form of S1, also purchased already modified imitating the methylation of the enzyme. S4 was used a C-rich control sequence. The nanoclusters were formed on the single stranded and double stranded DNA obtained through annealing of S2 with unmethylated S1 either methylated S3. The characterization did not show any meaningful difference between nanoclusters formed on double stranded or single stranded DNA. We started the characterization by investigating the spectrum in spectrophotometry and characterizing their morphology though TEM and AFM.

#### 4.5.2 Spectroscopic analysis of the DNA-templated Ag/Pt nanoclusters

We measured the absorbance of the samples between 230 and 500 nm (Fig 4-47). In Fig 4-47 A. Beside the typical 260 nm peak of DNA, we observed a slight overall increase in absorbance involving the entire spectrum 230 – 380 nm region in DNA templated Pt/Ag NCs using S1 (orange line), when compared with the controls with just S1 in the same dilution (blue line) and with buffer (grey line). Thus, orange line and blue line spectra correspond to the same amount of DNA, but the absorbance is clearly different. The formation of platinum nanoparticles is often related in literature to a peculiar profile in spectrophotometry, with high absorbance close to 200 nm, decreasing going towards higher wavelength (Fig 4-47. C) (Watanabe et al., 2009). This is slightly visible in the S1 spectrum (orange line). In samples prepared with buffer only, there was also a slight difference compared to the blank, likely due to the formation of some nanoclusters also in absence of DNA. This sample was prepared mixing AgNO<sub>3</sub>, K<sub>2</sub>PtCl<sub>4</sub> and NaBH<sub>4</sub> following the

same protocol. Subtracting the DNA contribution (measured separately) to the absorbance, we were able to highlight the contribution of the NCs mixture (Fig 4-47 B.).

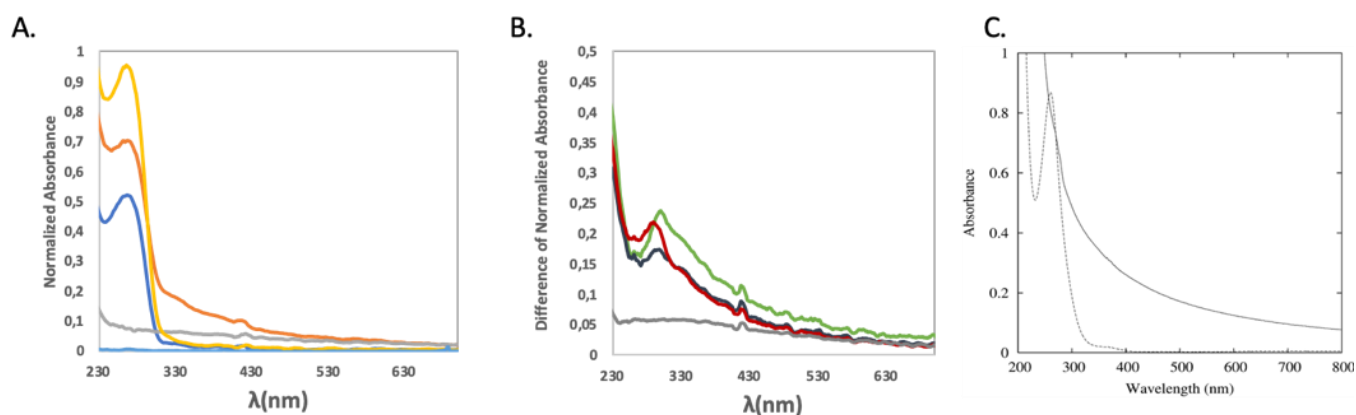


Fig 4-47. Spectra obtained in spectrophotometry of the DNA-templated Pt/Ag nanoclusters. A) yellow: starting DNA; orange: DNA templated Pt/Ag nanoclusters; blue: control DNA (same dilution no NCs); grey: buffer with NCs reagents; light blue: blank. B) Analysis of the Pt/Ag nanoclusters formed on S1 (dark blue), S3 (red), S4 (green) and buffer(grey). C) Typical spectra correlated to  $K_2PtCl_4$  (dotted line) and Pt nanoparticles (line) (Watanabe et al., 2009). Figure C was adapted from Watanabe et al, 2009, Image licensed by IOP publishing and Copyright Clearance Center (License ID 1001228-1).

We discriminated a peak close to 300 nm for different DNA sequences tested, S1 (dark blue), S3 (red), S4 (green). These features were reproducible in subsequent measurements. The absorbance profile can now be further correlated to the presence of platinum nanoparticles. It is to note that all samples with methylated and unmethylated sequences showed these aspects, suggesting that the same phenomena occurred regardless the state of methylation of the cytosines. A peak is evident between 260 and 330 nm, not visible in samples without DNA (Fig 4-47 B). grey line). It is hard to determine with no doubts its identity. As we can see in Fig 4-47 C. a sharp peak at 260 can be also related to the presence  $PtCl_6^{2-}$  in solution. But interestingly, a plasmon band at about 280 nm is also reported for Ag/Pt nanoparticles, with blue shift with increasing amount of Ag (Adekoya et al., 2014) It cannot be excluded that a contribution to this peak would be related to the amount of reduced Ag complexed in the DNA with platinum. We can argue that different height of this peak in the different samples could be related to differences in these aspects: remaining  $K_2PtCl_4$  and the content of silver in the nanoclusters. S1 and S3 samples may contain more silver in the clusters or higher presence of unreduced platinum. While S4, also a C-rich sequence, could contain less silver and a different consumption of platinum salt in solution. Absorbance of S4 is also in general higher in the overall spectrum (also at higher wavelengths) compared to the other samples, suggesting a more efficient formation of the platinum particles. There are not many examples of the spectrometric characterization of such DNA-templated nanoclusters in literature, thus, it is hard to validate our observations. Nevertheless, a spectrometric profile related to already reported for presence of platinum

nanoparticles can be observed in all the tested samples, suggesting that irrelevancy of the methylation for this process.

#### 4.5.3 Morphological characterization of the DNA templated Ag/Pt nanoclusters

Since we were not able to find a difference in the spectroscopic analysis of the samples for methylated and unmethylated DNA sequences, we proceeded to the assessment of the presence of such nanoclusters in the samples and to characterize their morphology.

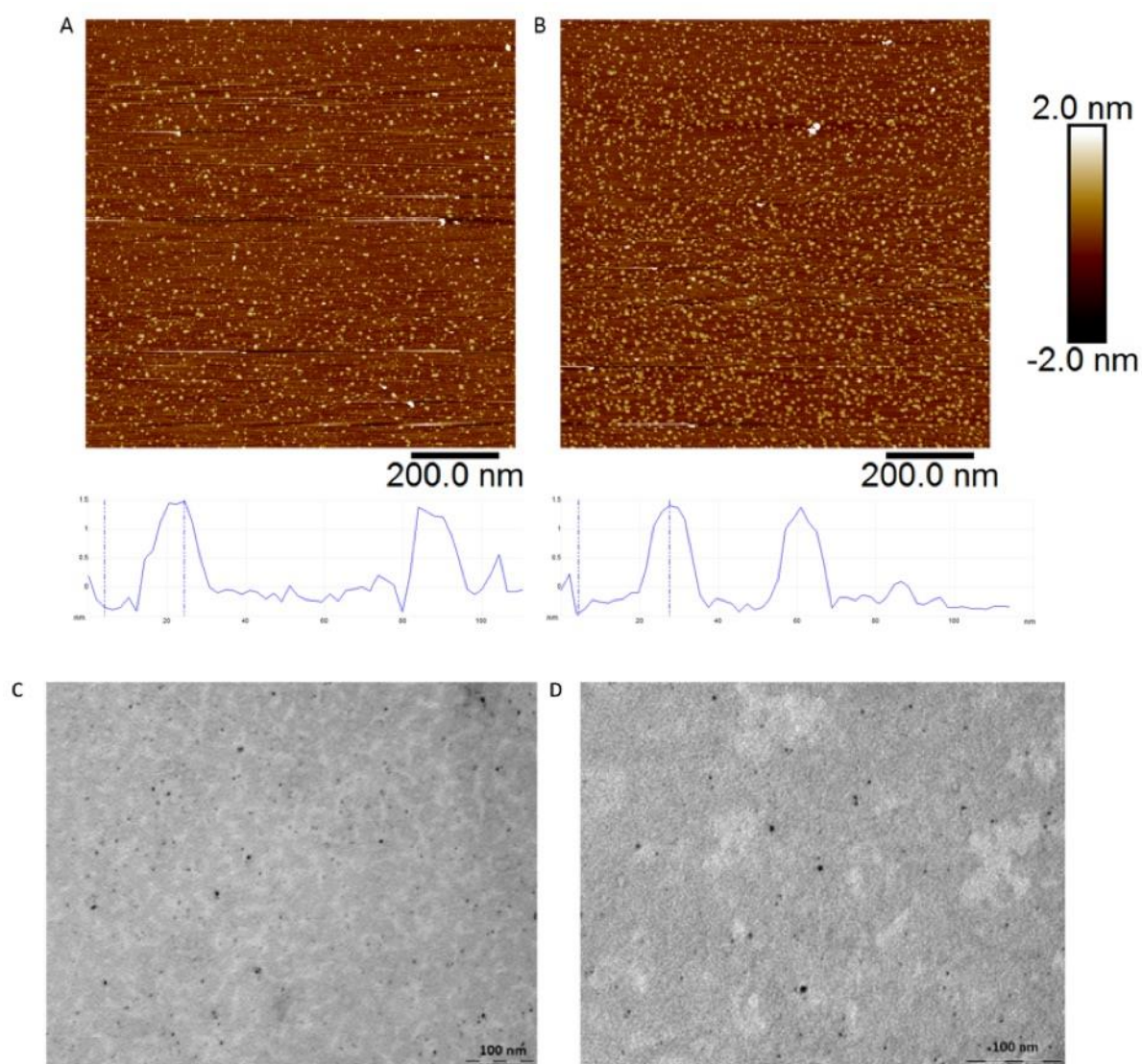


Fig 4-48. A) AFM images of unmethylated and B) methylated DNA templated Ag/Pt nanoclusters. C) TEM images of unmethylated and D) methylated DNA Ag/Pt nanoclusters.

The samples in analysis contained annealed double stranded DNA (S1-S2 for unmethylated, S3-S2 for methylated). Atomic force microscopy returned the presence of small roughly spherical particles, with average diameter of 2 nm in both the samples, with unmethylated and methylated DNA (Fig 4-48 A and B). Observations were confirmed by TEM imaging (Fig 4-48 C and D). We were not able to discriminate any significant difference in the size for methylated and unmethylated DAN templates. A slightly higher percentage of nanoclusters formed on methylated

DNA were smaller than 1.5 nm compared to those obtained on the unmethylated template, but it is not known if this could be a meaningful difference. Thus, nanoclusters formed in the same samples, with methylated and unmethylated DNA, confirming the results of the spectroscopic analysis.

#### 4.5.4 Catalytic activity of the DNA templated Ag/Pt nanoclusters

The last step had to be the characterization of the peroxidase-like activity of the nanoclusters obtained in different samples.

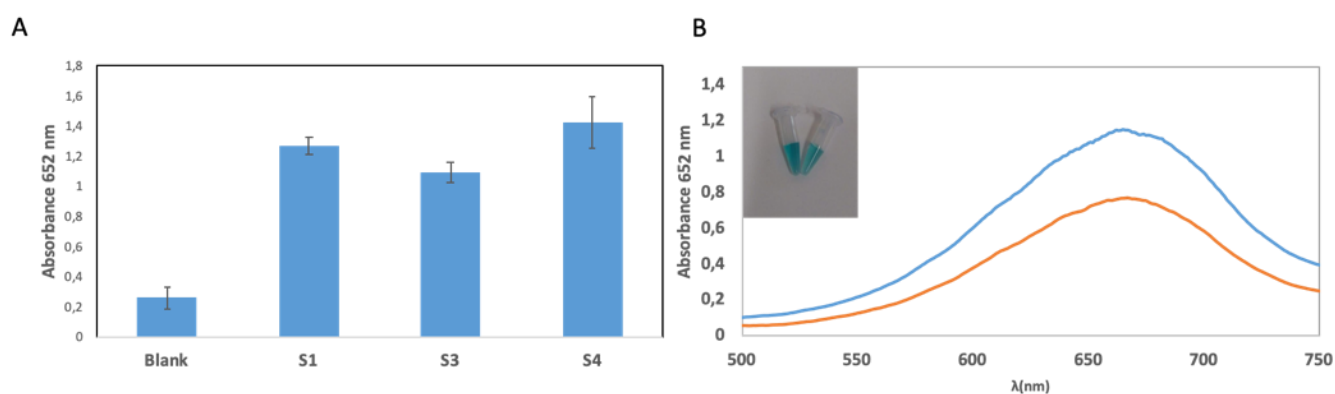


Fig 4-49. A) Bar plot showing absorbance spectrum of the DNA templated Ag/Pt NCs after the incubation with TMB and  $H_2O_2$ , and different DNA strands S1, S3, S4. SD is shown with  $N = 3$  B) Catalytic activity of the double stranded DNA-templated Ag/Pt NCs. Blue line S1/S2 double strand; Orange line: S2/S3 double strand.

In Fig 4-49 A. we show a bar plot with the results of the colorimetric reaction performed on different samples, with no DNA, with sequence S1, S3 and S4. This was done after the addition of TMB and  $H_2O_2$  and measuring the absorbance at 652 nm. As we can see a slight difference can be seen between unmethylated and methylated single stranded DNA. C-rich sequence S4 sample had the higher peroxidase-like activity. Looking at the catalytic activity of the double stranded DNA S1-S2 and S2-S3 (Fig 4-49 B.) we observed a not dramatically different behavior. The difference in the catalytic activity is not so different for methylated and unmethylated sequences, but this was likely improved moving at the biosensing application by optimizing the protocols (Kermani et al., 2018). We concluded that the difference in the catalytic activity is likely not due necessarily to the missed formation of the nanoclusters but rather to other combined phenomena. Interestingly the sequence S4 showed a reproducible higher peroxidase-like activity, and looking at the spectrum in Fig 4-47 B. the S4-templated Ag/Pt nanoclusters showed a profile consistent with the higher presence of Pt particles, responsible for the catalysis. In addition, a slight difference is visible in the peak at 260-300 nm of S1 and S3 -templated Ag/Pt nanoclusters, likely related to a difference in the activity. If the blue shift of this peak is related to the amount of silver, we can roughly argue that the content in silver is somehow related to the catalytic

activity. Indeed, as mentioned in the Introduction, section 1.5.3, the catalytic activity depends on the presence of platinum, while silver nanoclusters do not show such activity.

#### **4.5.5 Conclusions and observations**

In conclusion, in our opinion, methylation alone does not affect the formation of the DNA-Ag/Pt NCs, since spectroscopic analysis suggested the presence of such particles in both methylated and unmethylated DNA strands, later observed in AFM and TEM. The methylation could probably eventually affect, instead, the composition of the nanoclusters or the local environment, influencing the catalytic activity. In the presented biosensing applications for the detection of the catalytic activity of M.Sssl methyltransferase (Kermani et al., 2018), the different catalytic activity could be also an effect of the interaction of the enzyme on the specific DNA sequence, affecting the catalysis or the formation of the nanoclusters. A combined effect, physical enzyme interaction and methylation, could be considered. These observations do not compromise the results presented in the published work: the C-rich S1-S2 DNA used to detect the activity of the enzyme could be subjected to methylation and host the active enzyme, letting both the phenomena affect the final response. More efforts are needed to investigate this, but it was not part of the aim of the project. Our contribution helped the understanding of the formation and the morphology of these DNA-Ag/Pt NCs, not characterized in other published works. The information obtained and the experiments performed led then to the application of such nanoclusters to the development of a bioassay for the specific detection of M.Sssl methyltransferase activity in samples. The activity of the enzyme was actually able to inhibit the catalytic activity of the nanoclusters, and the limit of detection reached was 0.05 U/ml. On the other hand, taking into account some trials performed on non-C-rich DNA sequences (data not shown), we can confirm that the formation of such nanoclusters is enhanced by the presence of DNA. Likely, some C-rich sequences are more effective in this, as observed for S4, but it is not easy to undoubtedly confirm the specificity of the process. The spurious formation of PtNCs could also be taken into account. These would make other applications more complex, and higher control of the reaction is certainly required. This is a limit for our goals in using SPR or electrochemical detection, since, until now, no special advantages would be obtained by applying such nanoclusters as transducers if specificity is not sufficient. For these reasons, we suspended our efforts towards the implementation of DNA templated Ag/Pt nanoclusters for miRNA biosensing.

## 5 Conclusions

The overall work consisted of developing and testing different strategies for the amplification of the signal in DNA based biosensors, especially for the detection of short nucleic acids such as microRNAs. We took the potential of DNA nanotechnology in the design of special probes and self-assembling reaction for signal enhancement. In addition, we explored the employment of metal nanoparticles and nanoclusters as transducer and signal enhancers for this purpose. We designed a direct HCR method, based on Hybridization Chain Reaction which recognizes specific sequences of miRNA that are informative for early diagnosis of lung cancer. We paid special attention in the triggering interaction to ensure the specificity. In principle the direct Hybridization Chain Reaction that we designed was confirmed to be suitable for different transduction methods. We were able to observe the amplification of the signal due to the formation of the DNA nanostructures, previously characterized in solution. We made efforts towards the implementation of such method in biosensing platforms, exploiting two transduction methods. The first involved electrochemical detection on a custom-made electrochemical setup. Even if we proved that the amplification was occurring, the system needed optimization to return reliable results. Other strategies, such as label-free approaches involving impedance, should likely return a better signal upon optimization. However, we were able to observe an amplification of signal in the presence of HCR, returning a correlation with target concentration. This at least proved an improvement when hybridization chain reaction occurred. We wanted to move to an alternative transduction method, which does not involve any labeling during the detection. The applicability of the direct-HCR amplification resulted to be more promising in a label-free approach based on LSPR, likely thanks to a reduced complexity of the method and the optimized setup. We were able to combine our method with gold nanoparticles as transducers-enhancer in an original LSPR setup. This was done under the supervision of Prof. Wolfgang Fritzsche at the IPHT of Jena. This strategy was demonstrated to be very simple and allowed the real time specific detection of microRNA sequences with the limit of detection at about 1 nM without amplification, and we demonstrated an improvement of about 3 orders of magnitude applying HCR amplification (manuscript in preparation). Compared to previously reported methods, this method is simpler in fabrication, it allows real-time detection, and it is undoubtedly open to further improvements and optimization towards highly sensitive point of care detection. We can conclude that our Hybridization Chain Reaction was undoubtedly suitable for biosensing implementation, but that the combination with label-free LSPR detection was proved to be more effective. Since HCR on surface seemed to be more complex than expected, the application on simple label-free effective setup is surely advantageous. During the work, we also introduced an original strategy involving a triple helix of DNA as probe for miRNA detection. We proposed the employment of a triple helix probe to

combine two independent responses after target detection, something never reported in literature. We proposed the following advantages: separation of the amplification from the recognition of the target, no waste of sequence information, universality and theoretically the possibility to combine different transduction and amplification methods on the same probe (manuscript in preparation). More investigations would be required, and the adaptation on a more simple and robust detection method, similar to the label-free LSPR-based method above, would surely further enlighten the suitability of the method. We anyway proved the effectiveness of our design and the working principle of the strategy for further implementation, showing very preliminary results for electrochemical detection. During the exploration of alternatives for signal enhancement, we faced the characterization and employment of metal particles. After considering different alternatives, we concentrated on special metal nanoclusters with peroxidase-like activity. We characterized the formation and catalysis of DNA templated Ag/Pt nanoclusters in collaboration with Dr Morteza Hosseini's group from of the University of Tehran. Even though, the DNA Ag/Pt NCs were found effective in the detection of Methyltransferase activity, we considered these nanoclusters not suitable for our purposes in the signal enhancement of DNA based detection methods because of the difficulties in controlling their formation on precise DNA sequences.

## 6 References

- ABD-EL-FATTAH, A. A., SADIK, N. A., SHAKER, O. G. & ABOULFTOUH, M. L. 2013. Differential microRNAs expression in serum of patients with lung cancer, pulmonary tuberculosis, and pneumonia. *Cell Biochem Biophys*, 67, 875-84.
- ABI, A., MOHAMMADPOUR, Z., ZUO, X. L. & SAFAVI, A. 2018. Nucleic acid-based electrochemical nanobiosensors. *Biosensors & Bioelectronics*, 102, 479-489.
- ADEKOYA, J. A., DARE, E. O. & MESUBI, M. A. 2014. Tunable morphological properties of silver enriched platinum allied nanoparticles and their catalysed reduction of p-nitrophenol. *Advances in Natural Sciences-Nanoscience and Nanotechnology*, 5.
- ALTSCHUL, S. F., GISH, W., MILLER, W., MYERS, E. W. & LIPMAN, D. J. 1990. BASIC LOCAL ALIGNMENT SEARCH TOOL. *Journal of Molecular Biology*, 215, 403-410.
- ANG, Y. S. & YUNG, L. Y. L. 2016. Rational design of hybridization chain reaction monomers for robust signal amplification. *Chemical Communications*, 52, 4219-4222.
- ARROYO, J. D., CHEVILLET, J. R., KROH, E. M., RUF, I. K., PRITCHARD, C. C., GIBSON, D. F., MITCHELL, P. S., BENNETT, C. F., POGOSOVA-AGADJANYAN, E. L., STIREWALT, D. L., TAIT, J. F. & TEWARI, M. 2011. Argonaute2 complexes carry a population of circulating microRNAs independent of vesicles in human plasma. *Proceedings of the National Academy of Sciences of the United States of America*, 108, 5003-5008.
- AUGSPURGER, E. E., RANA, M. & YIGIT, M. V. 2018. Chemical and Biological Sensing Using Hybridization Chain Reaction. *Acs Sensors*, 3, 878-902.
- AUSHEV, V. N., ZBOROVSKAYA, I. B., LAKTIONOV, K. K., GIRARD, N., CROS, M. P., HERCEG, Z. & KRUTOVSKIKH, V. 2013. Comparisons of microRNA Patterns in Plasma before and after Tumor Removal Reveal New Biomarkers of Lung Squamous Cell Carcinoma. *Plos One*, 8, 10.
- AVINO, A., FRIEDEN, M., MORALES, J. C., DE LA TORRE, B. G., GARCIA, R. G., AZORIN, F., GELPI, J. L., OROZCO, M., GONZALEZ, C. & ERITJA, R. 2002. Properties of triple helices formed by parallel-stranded hairpins containing 8-aminopurines. *Nucleic Acids Research*, 30, 2609-2619.
- BAHADIR, E. B. & SEZGINTURK, M. K. 2016. A review on impedimetric biosensors. *Artificial Cells Nanomedicine and Biotechnology*, 44, 248-262.
- BERNAL-MENDEZ, E. & LEUMANN, C. J. 2002. Stability and kinetics of nucleic acid triplexes with chimaeric DNA/RNA third strands. *Biochemistry*, 41, 12343-12349.
- BERTOK, T., LORENCOVA, L., CHOCHOLOVA, E., JANE, E., VIKARTOVSKA, A., KASAK, P. & TKAC, J. 2019. Electrochemical Impedance Spectroscopy Based Biosensors: Mechanistic

- Principles, Analytical Examples and Challenges towards Commercialization for Assays of Protein Cancer Biomarkers. *Chemelectrochem*, 6, 989-1003.
- BI, S., YUE, S. Z. & ZHANG, S. S. 2017. Hybridization chain reaction: a versatile molecular tool for biosensing, bioimaging, and biomedicine. *Chemical Society Reviews*, 46, 4281-4298.
- BIANCHI, F., NICASSIO, F., MARZI, M., BELLONI, E., DALL'OLIO, V., BERNARD, L., PELOSI, G., MAISONNEUVE, P., VERONESI, G. & DI FIORE, P. P. 2011. A serum circulating miRNA diagnostic test to identify asymptomatic high-risk individuals with early stage lung cancer. *Embo Molecular Medicine*, 3, 495-503.
- BIANCHI, F., NICASSIO, F., VERONESI, G. & DI FIORE, P. P. 2012. Circulating microRNAs: next-generation biomarkers for early lung cancer detection. *Ecancermedicalscience*, 6, 246.
- BOERI, M., VERRI, C., CONTE, D., ROZ, L., MODENA, P., FACCHINETTI, F., CALABRO, E., CROCE, C. M., PASTORINO, U. & SOZZI, G. 2011. MicroRNA signatures in tissues and plasma predict development and prognosis of computed tomography detected lung cancer. *Proceedings of the National Academy of Sciences of the United States of America*, 108, 3713-3718.
- BRUCALE, M., ZUCCHERI, G. & SAMORI, B. 2005. The dynamic properties of an intramolecular transition from DNA duplex to cytosine-thymine motif triplex. *Organic & Biomolecular Chemistry*, 3, 575-577.
- CAGNIN, S., CARABALLO, M., GUIDUCCI, C., MARTINI, P., ROSS, M., SANTAANA, M., DANLEY, D., WEST, T. & LANFRANCHI, G. 2009. Overview of Electrochemical DNA Biosensors: New Approaches to Detect the Expression of Life. *Sensors*, 9, 3122-3148.
- CAI, H., XU, C., HE, P. G. & FANG, Y. Z. 2001. Colloid Au-enhanced DNA immobilization for the electrochemical detection of sequence-specific DNA. *Journal of Electroanalytical Chemistry*, 510, 78-85.
- CAI, S., CAO, Z. J., LAU, C. W. & LU, J. Z. 2014. Label-free technology for the amplified detection of microRNA based on the allosteric hairpin DNA switch and hybridization chain reaction. *Analyst*, 139, 6022-6027.
- CALIN, G. A. & CROCE, C. M. 2006. MicroRNA signatures in human cancers. *Nature Reviews Cancer*, 6, 857-866.
- CAO, X. D., YE, Y. K. & LIU, S. Q. 2011. Gold nanoparticle-based signal amplification for biosensing. *Analytical Biochemistry*, 417, 1-16.
- CARDOSO, A. R., MOREIRA, F. T. C., FERNANDES, R. & SALES, M. G. F. 2016. Novel and simple electrochemical biosensor monitoring attomolar levels of miRNA-155 in breast cancer. *Biosensors & Bioelectronics*, 80, 621-630.

- CHAICHI, M. J. & EHSANI, M. 2016. A novel glucose sensor based on immobilization of glucose oxidase on the chitosan-coated Fe<sub>3</sub>O<sub>4</sub> nanoparticles and the luminol-H<sub>2</sub>O<sub>2</sub>-gold nanoparticle chemiluminescence detection system. *Sensors and Actuators B-Chemical*, 223, 713-722.
- CHANDRA, S., VIMAL, D., SHARMA, D., RAI, V., GUPTA, S. C. & CHOWDHURI, D. K. 2017. Role of miRNAs in development and disease: Lessons learnt from small organisms. *Life Sciences*, 185, 8-14.
- CHANG, Y. Q., ZHANG, Z., HAO, J. H., YANG, W. S. & TANG, J. L. 2016. BSA-stabilized Au clusters as peroxidase mimetic for colorimetric detection of Ag<sup>+</sup>. *Sensors and Actuators B-Chemical*, 232, 692-697.
- CHAO, J., ZHU, D., ZHANG, Y. N., WANG, L. H. & FAN, C. H. 2016. DNA nanotechnology-enabled biosensors. *Biosensors & Bioelectronics*, 76, 68-79.
- CHEN, H. J., KOU, X. S., YANG, Z., NI, W. H. & WANG, J. F. 2008a. Shape- and size-dependent refractive index sensitivity of gold nanoparticles. *Langmuir*, 24, 5233-5237.
- CHEN, Q. G., GUO, Q. Q., CHEN, Y., PANG, J., FU, F. F. & GUO, L. Q. 2015a. An enzyme-free and label-free fluorescent biosensor for small molecules by G-quadruplex based hybridization chain reaction. *Talanta*, 138, 15-19.
- CHEN, T. X., TAN, S. Z., LI, W. & ZHU, Y. Q. 2017. Amplified Fluorescent Detection of Mercuric Ions by Conjugation of the ThT-induced G-Quadruplex Based Hybridization Chain Reaction. *Analytical Sciences*, 33, 1333-1337.
- CHEN, X., BA, Y., MA, L. J., CAI, X., YIN, Y., WANG, K. H., GUO, J. G., ZHANG, Y. J., CHEN, J. N., GUO, X., LI, Q. B., LI, X. Y., WANG, W. J., ZHANG, Y., WANG, J., JIANG, X. Y., XIANG, Y., XU, C., ZHENG, P. P., ZHANG, J. B., LI, R. Q., ZHANG, H. J., SHANG, X. B., GONG, T., NING, G., ZEN, K., ZHANG, J. F. & ZHANG, C. Y. 2008b. Characterization of microRNAs in serum: a novel class of biomarkers for diagnosis of cancer and other diseases. *Cell Research*, 18, 997-1006.
- CHEN, Y., XU, J., SU, J., XIANG, Y., YUAN, R. & CHAI, Y. Q. 2012. In Situ Hybridization Chain Reaction Amplification for Universal and Highly Sensitive Electrochemiluminescent Detection of DNA. *Analytical Chemistry*, 84, 7750-7755.
- CHEN, Y. J., GROVES, B., MUSCAT, R. A. & SEELIG, G. 2015b. DNA nanotechnology from the test tube to the cell. *Nature Nanotechnology*, 10, 748-760.
- CHEN, Y. X., PHIPPS, M. L., WERNER, J. H., CHAKRABORTY, S. & MARTINEZ, J. S. 2018. DNA Templated Metal Nanoclusters: From Emergent Properties to Unique Applications. *Accounts of Chemical Research*, 51, 2756-2763.

- CHOI, H. M. T., BECK, V. A. & PIERCE, N. A. 2014. Next-Generation in Situ Hybridization Chain Reaction: Higher Gain, Lower Cost, Greater Durability. *Acs Nano*, 8, 4284-4294.
- CHOI, H. M. T., CALVERT, C. R., HUSAIN, N., HUSS, D., BARSÌ, J. C., DEVERMAN, B. E., HUNTER, R. C., KATO, M., LEE, S. M., ABELIN, A. C. T., ROSENTHAL, A. Z., AKBARI, O. S., LI, Y. W., HAY, B. A., STERNBERG, P. W., PATTERSON, P. H., DAVIDSON, E. H., MAZMANIAN, S. K., PROBER, D. A., VAN DE RIJN, M., LEADBETTER, J. R., NEWMAN, D. K., READHEAD, C., BRONNER, M. E., WOLD, B., LANSFORD, R., SAUKA-SPENGLER, T., FRASER, S. E. & PIERCE, N. A. 2016. Mapping a multiplexed zoo of mRNA expression. *Development*, 143, 3632-3637.
- CHOI, J. & MAJIMA, T. 2011. Conformational changes of non-B DNA. *Chemical Society Reviews*, 40, 5893-5909.
- CSAKI, A., STRANIK, O. & FRITZSCHE, W. 2018. Localized surface plasmon resonance based biosensing. *Expert Review of Molecular Diagnostics*, 18, 279-296.
- DANIELS, J. S. & POURMAND, N. 2007. Label-free impedance biosensors: Opportunities and challenges. *Electroanalysis*, 19, 1239-1257.
- DENG, H. M. & GAO, Z. Q. 2015. Bioanalytical applications of isothermal nucleic acid amplification techniques. *Analytica Chimica Acta*, 853, 30-45.
- DENG, R. J., ZHANG, K. X. & LI, J. H. 2017. Isothermal Amplification for MicroRNA Detection: From the Test Tube to the Cell. *Accounts of Chemical Research*, 50, 1059-1068.
- DIRKS, R. M. & PIERCE, N. A. 2004a. An algorithm for computing nucleic acid base-pairing probabilities including pseudoknots. *Journal of Computational Chemistry*, 25, 1295-1304.
- DIRKS, R. M. & PIERCE, N. A. 2004b. Triggered amplification by hybridization chain reaction. *Proceedings of the National Academy of Sciences of the United States of America*, 101, 15275-15278.
- DONG, H. F., MENG, X. D., DAI, W. H., CAO, Y., LU, H. T., ZHOU, S. F. & ZHANG, X. J. 2015. Highly Sensitive and Selective MicroRNA Detection Based on DNA-Bio-Bar-Code and Enzyme-Assisted Strand Cycle Exponential Signal Amplification. *Analytical Chemistry*, 87, 4334-4340.
- DONG, J., CUI, X., DENG, Y. & TANG, Z. 2012. Amplified detection of nucleic acid by G-quadruplex based hybridization chain reaction. *Biosens Bioelectron*, 38, 258-63.
- DU, Y. D., MAO, Y. F., HE, X. X., WANG, K. M., YAN, G. P., LIU, J. Q. & WANG, Y. H. 2014. A signal on aptamer-based electrochemical sensing platform using a triple-helix molecular switch. *Analytical Methods*, 6, 6294-6300.

- EBRAHIMI, A., RAVAN, H. & KHAJOUEI, S. 2019. DNA nanotechnology and bioassay development. *Trac-Trends in Analytical Chemistry*, 114, 126-142.
- ESTEVEZ, M. C., ALVAREZ, M. & LECHUGA, L. M. 2012. Integrated optical devices for lab-on-a-chip biosensing applications. *Laser & Photonics Reviews*, 6, 463-487.
- FARAZI, T. A., SPITZER, J. I., MOROZOV, P. & TUSCHL, T. 2011. miRNAs in human cancer. *Journal of Pathology*, 223, 102-115.
- FERAPONTOVA, E. E. 2018. DNA Electrochemistry and Electrochemical Sensors for Nucleic Acids. *Annual Review of Analytical Chemistry, Vol 11*, 11, 197-218.
- FONG, K. E. & YUNG, L. Y. L. 2013. Localized surface plasmon resonance: a unique property of plasmonic nanoparticles for nucleic acid detection. *Nanoscale*, 5, 12043-12071.
- FOUDEH, A. M., DIDAR, T. F., VERES, T. & TABRIZIAN, M. 2012. Microfluidic designs and techniques using lab-on-a-chip devices for pathogen detection for point-of-care diagnostics. *Lab on a Chip*, 12, 3249-3266.
- GANDINI, A., BARTOLINI, M., TEDESCO, D., MARTINEZ-GONZALEZ, L., ROCA, C., CAMPILLO, N. E., ZALDIVAR-DIEZ, J., PEREZ, C., ZUCCHERI, G., MITI, A., FEOLI, A., CASTELLANO, S., PETRALLA, S., MONTI, B., ROSSI, M., MODA, F., LEGNAME, G., MARTINEZ, A. & BOLOGNESI, M. L. 2018. Tau-Centric Multitarget Approach for Alzheimer's Disease: Development of First-in-Class Dual Glycogen Synthase Kinase 3 beta and Tau-Aggregation Inhibitors. *Journal of Medicinal Chemistry*, 61, 7640-7656.
- GAO, Z. Q., XU, M. D., HOU, L., CHEN, G. N. & TANG, D. P. 2013. Irregular-shaped platinum nanoparticles as peroxidase mimics for highly efficient colorimetric immunoassay. *Analytica Chimica Acta*, 776, 79-86.
- GE, Z. L., LIN, M. H., WANG, P., PEI, H., YAN, J., SHO, J. Y., HUANG, Q., HE, D. N., FAN, C. H. & ZUO, X. L. 2014. Hybridization Chain Reaction Amplification of MicroRNA Detection with a Tetrahedral DNA Nanostructure-Based Electrochemical Biosensor. *Analytical Chemistry*, 86, 2124-2130.
- GENG, Q., FAN, T., ZHANG, B. Y., WANG, W., XU, Y. & HU, H. 2014. Five microRNAs in plasma as novel biomarkers for screening of early-stage non-small cell lung cancer. *Respiratory Research*, 15, 9.
- GONDEAU, C., MAURIZOT, J. C. & DURAND, M. 1998. Circular dichroism and UV melting studies on formation of an intramolecular triplex containing parallel T\*A : T and G\*G : C triplets: netropsin complexation with the triplex. *Nucleic Acids Research*, 26, 4996-5003.
- GOWERS, D. M. & FOX, K. R. 1999. Towards mixed sequence recognition by triple helix formation. *Nucleic Acids Research*, 27, 1569-1577.

- GRAYBILL, R. M. & BAILEY, R. C. 2016. Emerging Biosensing Approaches for microRNA Analysis. *Analytical Chemistry*, 88, 431-450.
- GUO, X. S., LIANG, B., JIAN, J. M., ZHANG, Y. L. & YE, X. S. 2014. Glucose biosensor based on a platinum electrode modified with rhodium nanoparticles and with glucose oxidase immobilized on gold nanoparticles. *Microchimica Acta*, 181, 519-525.
- HASHEM, G. M., WEN, J. D., DO, Q. & GRAY, D. M. 1999. Evidence from CD spectra and melting temperatures for stable Hoogsteen-paired oligomer duplexes derived from DNA and hybrid triplexes. *Nucleic Acids Research*, 27, 3371-3379.
- HEEGAARD, N. H. H., SCHETTER, A. J., WELSH, J. A., YONEDA, M., BOWMAN, E. D. & HARRIS, C. C. 2012. Circulating micro-RNA expression profiles in early stage nonsmall cell lung cancer. *International Journal of Cancer*, 130, 1378-1386.
- HENNESSEY, P. T., SANFORD, T., CHOUDHARY, A., MYDLARZ, W. W., BROWN, D., ADAI, A. T., OCHS, M. F., AHRENDT, S. A., MAMBO, E. & CALIFANO, J. A. 2012. Serum microRNA Biomarkers for Detection of Non-Small Cell Lung Cancer. *Plos One*, 7, 6.
- HER, S., JAFFRAY, D. A. & ALLEN, C. 2017. Gold nanoparticles for applications in cancer radiotherapy: Mechanisms and recent advancements. *Advanced Drug Delivery Reviews*, 109, 84-101.
- HERIZCHI, R., ABBASI, E., MILANI, M. & AKBARZADEH, A. 2016. Current methods for synthesis of gold nanoparticles. *Artificial Cells Nanomedicine and Biotechnology*, 44, 596-602.
- HIGUCHI, A., SIAO, Y. D., YANG, S. T., HSIEH, P. V., FUKUSHIMA, H., CHANG, Y., RUAAN, R. C. & CHEN, W. Y. 2008. Preparation of a DNA aptamer-Pt complex and its use in the colorimetric sensing of thrombin and anti-thrombin antibodies. *Analytical Chemistry*, 80, 6580-6586.
- HOA, X. D., KIRK, A. G. & TABRIZIAN, M. 2007. Towards integrated and sensitive surface plasmon resonance biosensors: A review of recent progress. *Biosensors & Bioelectronics*, 23, 151-160.
- HU, Y. W., CECCONELLO, A., IDILI, A., RICCI, F. & WILLNER, I. 2017. Triplex DNA Nanostructures: From Basic Properties to Applications. *Angewandte Chemie-International Edition*, 56, 15210-15233.
- HUANG, J., YANG, X. H., HE, X. X., WANG, K. M., LIU, J. B., SHI, H., WANG, Q., GUO, Q. P. & HE, D. G. 2014. Design and bioanalytical applications of DNA hairpin-based fluorescent probes. *Trac-Trends in Analytical Chemistry*, 53, 11-20.
- HUNG, S. H., YU, Q., GRAY, D. M. & RATLIFF, R. L. 1994. EVIDENCE FROM CD-SPECTRA THAT D(PURINE)CENTER-DOT-R(PYRIMIDINE) AND R(PURINE)CENTER-DOT-D(PYRIMIDINE)

- HYBRIDS ARE IN DIFFERENT STRUCTURAL CLASSES. *Nucleic Acids Research*, 22, 4326-4334.
- HWANG, H. W. & MENDELL, J. T. 2006. MicroRNAs in cell proliferation, cell death, and tumorigenesis. *British Journal of Cancer*, 94, 776-780.
- IDILI, A., PORCHETTA, A., AMODIO, A., VALLEE-BELISLE, A. & RICCI, F. 2015. Controlling Hybridization Chain Reactions with pH. *Nano Letters*, 15, 5539-5544.
- JAIN, A., WANG, G. & VASQUEZ, K. M. 2008. DNA triple helices: Biological consequences and therapeutic potential. *Biochimie*, 90, 1117-1130.
- JOSHI, G. K., DEITZ-MCELYEA, S., JOHNSON, M., MALI, S., KORC, M. & SARDAR, R. 2014. Highly Specific Plasmonic Biosensors for Ultrasensitive MicroRNA Detection in Plasma from Pancreatic Cancer Patients. *Nano Letters*, 14, 6955-6963.
- JOSHI, G. K., DEITZ-MCELYEA, S., LIYANAGE, T., LAWRENCE, K., MALI, S., SARDAR, R. & KORC, M. 2015. Label-Free Nanoplasmonic-Based Short Noncoding RNA Sensing at Attomolar Concentrations Allows for Quantitative and Highly Specific Assay of MicroRNA-10b in Biological Fluids and Circulating Exosomes. *Acs Nano*, 9, 11075-11089.
- JUNG, L. S., CAMPBELL, C. T., CHINOWSKY, T. M., MAR, M. N. & YEE, S. S. 1998. Quantitative interpretation of the response of surface plasmon resonance sensors to adsorbed films. *Langmuir*, 14, 5636-5648.
- KANG, K. A., WANG, J. T., JASINSKI, J. B. & ACHILEFU, S. 2011. Fluorescence Manipulation by Gold Nanoparticles: From Complete Quenching to Extensive Enhancement. *Journal of Nanobiotechnology*, 9.
- KELLER, A., LEIDINGER, P., GISLEFOSS, R., HAUGEN, A., LANGSETH, H., STAEHLER, P., LENHOF, H.-P. & MEESE, E. 2011. Stable serum miRNA profiles as potential tool for non-invasive lung cancer diagnosis. *Rna Biology*, 8, 506-516.
- KERMANI, H. A., HOSSEINI, M., MITI, A., DADMEHR, M., ZUCCHERI, G., HOSSEINKHANI, S. & GANJALI, M. R. 2018. A colorimetric assay of DNA methyltransferase activity based on peroxidase mimicking of DNA template Ag/Pt bimetallic nanoclusters. *Analytical and Bioanalytical Chemistry*, 410, 4943-4952.
- KI, J., LEE, H. Y., SON, H. Y., HUH, Y. M. & HAAM, S. 2019. Sensitive Plasmonic Detection of miR-10b in Biological Samples Using Enzyme-Assisted Target Recycling and Developed LSPR Probe. *Acs Applied Materials & Interfaces*, 11, 18923-18929.
- KIM, D. K., YOO, S. M., PARK, T. J., YOSHIKAWA, H., TAMIYA, E., PARK, J. Y. & LEE, S. Y. 2011. Plasmonic Properties of the Multispot Copper-Capped Nanoparticle Array Chip and Its Application to Optical Biosensors for Pathogen Detection of Multiplex DNAs. *Analytical Chemistry*, 83, 6215-6222.

- KYPR, J., KEJNOVSKA, I., RENCIU, D. & VORLICKOVA, M. 2009. Circular dichroism and conformational polymorphism of DNA. *Nucleic Acids Research*, 37, 1713-1725.
- LATORRE, A., LORCA, R. & SOMOZA, A. 2013. Fluorescent DNA Stabilized Silver Nanoclusters as Biosensors. *Journal of Chemistry*.
- LEE, K. S. & EL-SAYED, M. A. 2006. Gold and silver nanoparticles in sensing and imaging: Sensitivity of plasmon response to size, shape, and metal composition. *Journal of Physical Chemistry B*, 110, 19220-19225.
- LERMUSIAUX, L. & FUNSTON, A. M. 2018. Plasmonic isomers via DNA-based self-assembly of gold nanoparticles. *Nanoscale*, 10, 19557-19567.
- LI, J. J., ZHU, J. J. & XU, K. 2014. Fluorescent metal nanoclusters: From synthesis to applications. *Trac-Trends in Analytical Chemistry*, 58, 90-98.
- LI, R. M., ZOU, L., LUO, Y. W., ZHANG, M. J. & LING, L. S. 2017. Ultrasensitive colorimetric detection of circulating tumor DNA using hybridization chain reaction and the pivot of triplex DNA. *Scientific Reports*, 7, 10.
- LI, R. S., LIU, H., CHEN, B. B., ZHANG, H. Z., HUANG, C. Z. & WANG, J. 2016. Stable gold nanoparticles as a novel peroxidase mimic for colorimetric detection of cysteine. *Analytical Methods*, 8, 2494-2501.
- LI, X. Y., YE, M. S., ZHANG, W. Y., TAN, D., JAFFREZIC-RENAULT, N., YANG, X. & GUO, Z. Z. 2019. Liquid biopsy of circulating tumor DNA and biosensor applications. *Biosensors & Bioelectronics*, 126, 596-607.
- LI, Y. Y., SCHLUESENER, H. J. & XU, S. Q. 2010. Gold nanoparticle-based biosensors. *Gold Bulletin*, 43, 29-41.
- LI, Z. B., MIAO, X. M., XING, K., ZHU, A. H. & LING, L. S. 2015. Enhanced electrochemical recognition of double-stranded DNA by using hybridization chain reaction and positively charged gold nanoparticles. *Biosensors & Bioelectronics*, 74, 687-690.
- LIANG, M. J., PAN, M., HU, J. L., WANG, F. & LIU, X. Q. 2018. Electrochemical Biosensor for MicroRNA Detection Based on Cascade Hybridization Chain Reaction. *Chemelectrochem*, 5, 1380-1386.
- LIU, K. L., MILES, H. T., FRAZIER, J. & SASISEKHARAN, V. 1993. A NOVEL DNA DUPLEX - A PARALLEL-STRANDED DNA HELIX WITH HOOGSTEEEN BASE-PAIRING. *Biochemistry*, 32, 11802-11809.
- LIU, L., LIU, J. W., WU, H., WANG, X. N., YU, R. Q. & JIANG, J. H. 2018. Branched Hybridization Chain Reaction Circuit for Ultrasensitive Localizable Imaging of mRNA in Living Cells. *Analytical Chemistry*, 90, 1502-1505.

- LIU, P., YANG, X. H., SUN, S., WANG, Q., WANG, K. M., HUANG, J., LIU, J. B. & HE, L. L. 2013a. Enzyme-Free Colorimetric Detection of DNA by Using Gold Nanoparticles and Hybridization Chain Reaction Amplification. *Analytical Chemistry*, 85, 7689-7695.
- LIU, S., LIN, Y., LIU, T., CHENG, C., WEI, W., WANG, L. & LI, F. 2014. Enzyme-free and label-free ultrasensitive electrochemical detection of DNA and adenosine triphosphate by dendritic DNA concatamer-based signal amplification. *Biosens Bioelectron*, 56, 12-8.
- LIU, S. F., FANG, L., TIAN, Y. S., WEI, W. J. & WANG, L. 2017. Label-free, non-enzymatic and ultrasensitive electrochemical nucleic acid biosensing by tandem DNA-fueled target recycling and hybridization chain reaction. *Sensors and Actuators B-Chemical*, 244, 450-457.
- LIU, S. F., WANG, Y., MING, J. J., LIN, Y., CHENG, C. B. & LI, F. 2013b. Enzyme-free and ultrasensitive electrochemical detection of nucleic acids by target catalyzed hairpin assembly followed with hybridization chain reaction. *Biosensors & Bioelectronics*, 49, 472-477.
- LU, J., WANG, J., HU, X. L., GYIMAH, E., YAKUBU, S., WANG, K., WU, X. Y. & ZHANG, Z. 2019. Electrochemical Biosensor Based on Tetrahedral DNA Nanostructures and G-Quadruplex-Hemin Conformation for the Itrasensitive Detection of MicroRNA-21 in Serum. *Analytical Chemistry*, 91, 7353-7359.
- LUPI, F. F., GIAMMARIA, T. J., MITI, A., ZUCCHERI, G., CARIGNANO, S., SPARNACCI, K., SEGUINI, G., DE LEO, N., BOARINO, L., PEREGO, M. & LAUS, M. 2018. Hierarchical Order in Dewetted Block Copolymer Thin Films on Chemically Patterned Surfaces. *Acs Nano*, 12, 7076-7085.
- MA, C. P., WANG, W. S., MULCHANDANI, A. & SHI, C. 2014. A simple colorimetric DNA detection by target-induced hybridization chain reaction for isothermal signal amplification. *Analytical Biochemistry*, 457, 19-23.
- MACHINEK, R. R. F., OULDRIDGE, T. E., HALEY, N. E. C., BATH, J. & TURBERFIELD, A. J. 2014. Programmable energy landscapes for kinetic control of DNA strand displacement. *Nature Communications*, 5.
- MALEKZAD, H., ZANGABAD, P. S., MIRSHEKARI, H., KARIMI, M. & HAMBLIN, M. R. 2017. Noble metal nanoparticles in biosensors: recent studies and applications. *Nanotechnology Reviews*, 6, 301-329.
- MALHOTRA, B. D., SINGHAL, R., CHAUBEY, A., SHARMA, S. K. & KUMAR, A. 2005. Recent trends in biosensors. *Current Applied Physics*, 5, 92-97.
- MANZINI, G., XODO, L. E., GASPAROTTO, D., QUADRIFOGLIO, F., VANDERMAREL, G. A. & VANBOOM, J. H. 1990. TRIPLE HELIX FORMATION BY OLIGOPURINE-OLIGOPYRIMIDINE

- DNA FRAGMENTS - ELECTROPHORETIC AND THERMODYNAMIC BEHAVIOR. *Journal of Molecular Biology*, 213, 833-843.
- MARIANI, S. & MINUNNI, M. 2014. Surface plasmon resonance applications in clinical analysis. *Analytical and Bioanalytical Chemistry*, 406, 2303-2323.
- MASSENZIO, F., PENA-ALTAMIRA, E., PETRALLA, S., VIRGILI, M., ZUCCHERI, G., MITI, A., POLAZZI, E., MENGONI, I., PIFFARETTI, D. & MONTI, B. 2018. Microglial overexpression of fALS-linked mutant SOD1 induces SOD1 processing impairment, activation and neurotoxicity and is counteracted by the autophagy inducer trehalose. *Biochimica Et Biophysica Acta-Molecular Basis of Disease*, 1864, 3771-3785.
- MATSUOKA, Y., ONODERA, T., KOJIMA, T., CHANG, Y., CHEN, W. Y., IMANAKA, T., FUKUSHIMA, H. & HIGUCHI, A. 2007. Novel enzymatic properties of DNA-Pt complexes. *Biomacromolecules*, 8, 2684-2688.
- MENDELL, J. T. & OLSON, E. N. 2012. MicroRNAs in Stress Signaling and Human Disease. *Cell*, 148, 1172-1187.
- MIAO, X. M., CHENG, Z. Y., LI, Z. B. & WANG, P. 2017. A novel sensing platform for sensitive cholesterol detection by using positively charged gold nanoparticles. *Biochemical Engineering Journal*, 117, 21-27.
- MITCHELL, P. S., PARKIN, R. K., KROH, E. M., FRITZ, B. R., WYMAN, S. K., POGOSOVA-AGADJANYAN, E. L., PETERSON, A., NOTEBOOM, J., O'BRIANT, K. C., ALLEN, A., LIN, D. W., URBAN, N., DRESCHER, C. W., KNUDSEN, B. S., STIREWALT, D. L., GENTLEMAN, R., VESSELLA, R. L., NELSON, P. S., MARTIN, D. B. & TEWARI, M. 2008. Circulating microRNAs as stable blood-based markers for cancer detection. *Proceedings of the National Academy of Sciences of the United States of America*, 105, 10513-10518.
- MITI, A. & ZUCCHERI, G. 2018. Hybridization Chain Reaction Design and Biosensor Implementation. In: ZUCCHERI, G. (ed.) *DNA Nanotechnology: Methods and Protocols*. New York, NY: Springer New York.
- NA, H. K., WI, J. S., SON, H. Y., OK, J. G., HUH, Y. M. & LEE, T. G. 2018. Discrimination of single nucleotide mismatches using a scalable, flexible, and transparent three-dimensional nanostructure-based plasmonic miRNA sensor with high sensitivity. *Biosensors & Bioelectronics*, 113, 39-45.
- NAVANI, N. K. & LI, Y. F. 2006. Nucleic acid aptamers and enzymes as sensors. *Current Opinion in Chemical Biology*, 10, 272-281.
- NGUYEN, H. H., PARK, J., KANG, S. & KIM, M. 2015. Surface Plasmon Resonance: A Versatile Technique for Biosensor Applications. *Sensors*, 15, 10481-10510.

- O'BRIEN, J., HAYDER, H., ZAYED, Y. & PENG, C. 2018. Overview of MicroRNA Biogenesis, Mechanisms of Actions, and Circulation. *Frontiers in Endocrinology*, 9.
- OU, J. M., TAN, H. J., CHEN, X. D. & CHEN, Z. 2018. DNA-Assisted Assembly of Gold Nanostructures and Their Induced Optical Properties. *Nanomaterials*, 8.
- PARAB, H. J., JUNG, C., LEE, J. H. & PARK, H. G. 2010. A gold nanorod-based optical DNA biosensor for the diagnosis of pathogens. *Biosensors & Bioelectronics*, 26, 667-673.
- PATEL, S., NANDA, R., SAHOO, S. & MOHAPATRA, E. 2016. Biosensors in Health Care: The Milestones Achieved in Their Development towards Lab-on-Chip-Analysis. *Biochemistry Research International*.
- PEREZ-LOPEZ, B. & MERKOCI, A. 2011. Nanomaterials based biosensors for food analysis applications. *Trends in Food Science & Technology*, 22, 625-639.
- PINGARRON, J. M., YANEZ-SEDENO, P. & GONZALEZ-CORTES, A. 2008. Gold nanoparticle-based electrochemical biosensors. *Electrochimica Acta*, 53, 5848-5866.
- QIN, X., XU, H. S., GONG, W. R. & DENG, W. B. 2015. The tumor cytosol miRNAs, fluid miRNAs, and exosome miRNAs in lung cancer. *Frontiers in Oncology*, 4, 7.
- RABINOWITS, G., GERCEL-TAYLOR, C., DAY, J. M., TAYLOR, D. D. & KLOECKER, G. H. 2009. Exosomal MicroRNA: A Diagnostic Marker for Lung Cancer. *Clinical Lung Cancer*, 10, 42-46.
- ROBERTSON, K. D. 2001. DNA methylation, methyltransferases, and cancer. *Oncogene*, 20, 3139-3155.
- ROBERTSON, K. D. 2005. DNA methylation and human disease. *Nature Reviews Genetics*, 6, 597-610.
- RONKAINEN, N. J., HALSALL, H. B. & HEINEMAN, W. R. 2010. Electrochemical biosensors. *Chemical Society Reviews*, 39, 1747-1763.
- SADOWSKI, J. P., CALVERT, C. R., ZHANG, D. Y., PIERCE, N. A. & YIN, P. 2014. Developmental self-assembly of a DNA tetrahedron. *ACS Nano*, 8, 3251-9.
- SASSOLAS, A., LECA-BOUVIER, B. D. & BLUM, L. J. 2008. DNA biosensors and microarrays. *Chemical Reviews*, 108, 109-139.
- SAYED, D. & ABDELLATIF, M. 2011. MICRORNAS IN DEVELOPMENT AND DISEASE. *Physiological Reviews*, 91, 827-887.
- SCHNEIDER, T., JAHR, N., JATSCHKA, J., CSAKI, A., STRANIK, O. & FRITZSCHE, W. 2013. Localized surface plasmon resonance (LSPR) study of DNA hybridization at single nanoparticle transducers. *Journal of Nanoparticle Research*, 15.
- SEELIG, G., SOLOVEICHIK, D., ZHANG, D. Y. & WINFREE, E. 2006. Enzyme-free nucleic acid logic circuits. *Science*, 314, 1585-1588.

- SEEMAN, N. C. 2007. An overview of structural DNA Nanotechnology. *Molecular Biotechnology*, 37, 246-257.
- SEEMAN, N. C. 2010a. Nanomaterials Based on DNA. *In*: KORNBERG, R. D., RAETZ, C. R. H., ROTHMAN, J. E. & THORNER, J. W. (eds.) *Annual Review of Biochemistry, Vol 79*. Palo Alto: Annual Reviews.
- SEEMAN, N. C. 2010b. Structural DNA Nanotechnology: Growing Along with Nano Letters. *Nano Letters*, 10, 1971-1978.
- SETHI, S., ALI, S. & SARKAR, F. H. 2014. MicroRNAs in personalized cancer therapy. *Clinical Genetics*, 86, 68-73.
- SHANG, L., DONG, S. J. & NIENHAUS, G. U. 2011. Ultra-small fluorescent metal nanoclusters: Synthesis and biological applications. *Nano Today*, 6, 401-418.
- SHIMRON, S., WANG, F., ORBACH, R. & WILLNER, I. 2012. Amplified detection of DNA through the enzyme-free autonomous assembly of hemin/G-quadruplex DNAzyme nanowires. *Anal Chem*, 84, 1042-8.
- SOARES, L., CSAKI, A., JATSCHKA, J., FRITZSCHE, W., FLORES, O., FRANCO, R. & PEREIRA, E. 2014. Localized surface plasmon resonance (LSPR) biosensing using gold nanotriangles: detection of DNA hybridization events at room temperature. *Analyst*, 139, 4964-4973.
- SONG, S. P., WANG, L. H., LI, J., ZHAO, J. L. & FAN, C. H. 2008. Aptamer-based biosensors. *Trac-Trends in Analytical Chemistry*, 27, 108-117.
- SPADAVECCHIA, J., BURRAS, A., LYSKAWA, J., WOISEL, P., LAURE, W., PRADIER, C. M., BOUKHERROUB, R. & SZUNERITS, S. 2013. Approach for Plasmonic Based DNA Sensing: Amplification of the Wavelength Shift and Simultaneous Detection of the Plasmon Modes of Gold Nanostructures. *Analytical Chemistry*, 85, 3288-3296.
- SPIGA, F. M., BONYAR, A., RING, B., ONOFRI, M., VINELLI, A., SANTHA, H., GUIDUCCI, C. & ZUCCHERI, G. 2014. Hybridization chain reaction performed on a metal surface as a means of signal amplification in SPR and electrochemical biosensors. *Biosensors & Bioelectronics*, 54, 102-108.
- SRINIVAS, N., OULDRIDGE, T. E., SULC, P., SCHAEFFER, J. M., YURKE, B., LOUIS, A. A., DOYE, J. P. K. & WINFREE, E. 2013. On the biophysics and kinetics of toehold-mediated DNA strand displacement. *Nucleic Acids Research*, 41, 10641-10658.
- STOBIECKA, M. & CHALUPA, A. 2015. Biosensors based on molecular beacons. *Chemical Papers*, 69, 62-76.
- SUFEN, W., TUZHI, P. & YANG, C. F. 2002. Electrochemical studies for the interaction of DNA with an irreversible redox compound - Hoechst 33258. *Electroanalysis*, 14, 1648-1653.

- SUGAWA, K., TAHARA, H., YAMASHITA, A., OTSUKI, J., SAGARA, T., HARUMOTO, T. & YANAGIDA, S. 2015. Refractive Index Susceptibility of the Plasmonic Palladium Nanoparticle: Potential as the Third Plasmonic Sensing Material. *Acs Nano*, 9, 1895-1904.
- SUGIMOTO, N., WU, P., HARA, H. & KAWAMOTO, Y. 2001. pH and cation effects on the properties of parallel pyrimidine motif DNA triplexes. *Biochemistry*, 40, 9396-9405.
- TANG, S. X., ZHAO, J. Q., STORHOFF, J. J., NORRIS, P. J., LITTLE, R. F., YARCHOAN, R., STRAMER, S. L., PATNO, T., DOMANUS, M., DHAR, A., MIRKIN, C. A. & HEWLETT, I. K. 2007. Nanoparticle-based biobarcode amplification assay (BCA) for sensitive and early detection of human immunodeficiency type 1 capsid (p24) antigen. *Aids-Journal of Acquired Immune Deficiency Syndromes*, 46, 231-237.
- TELES, F. R. R. & FONSECA, L. R. 2008. Trends in DNA biosensors. *Talanta*, 77, 606-623.
- TENG, Y., TATEISHI-KARIMATA, H., TSURUOKA, T. & SUGIMOTO, N. 2018. A Turn-On Detection of DNA Sequences by Means of Fluorescence of DNA-Templated Silver Nanoclusters via Unique Interactions of a Hydrated Ionic Liquid. *Molecules*, 23.
- TIAN, D., DUAN, C., WANG, W., LI, N., ZHANG, H., CUI, H. & LU, Y. 2009. Sandwich-type electrochemiluminescence immunosensor based on N-(aminobutyl)-N-ethylisoluminol labeling and gold nanoparticle amplification. *Talanta*, 78, 399-404.
- TIAN, T., WANG, J. Q. & ZHOU, X. 2015. A review: microRNA detection methods. *Organic & Biomolecular Chemistry*, 13, 2226-2238.
- TIWARI, P. M., VIG, K., DENNIS, V. A. & SINGH, S. R. 2011. Functionalized Gold Nanoparticles and Their Biomedical Applications. *Nanomaterials*, 1, 31-63.
- TRIFONOV, A., SHARON, E., TEL-VERED, R., KAHN, J. S. & WILLNER, I. 2016. Application of the Hybridization Chain Reaction on Electrodes for the Amplified and Parallel Electrochemical Analysis of DNA. *Journal of Physical Chemistry C*, 120, 15743-15752.
- TURCHINOVICH, A., WEIZ, L., LANGHEINZ, A. & BURWINKEL, B. 2011. Characterization of extracellular circulating microRNA. *Nucleic Acids Research*, 39, 7223-7233.
- TURKMEN, E., BAS, S. Z., GULCE, H. & YILDIZ, S. 2014. Glucose biosensor based on immobilization of glucose oxidase in electropolymerized poly(o-phenylenediamine) film on platinum nanoparticles-polyvinylferrocenium modified electrode. *Electrochimica Acta*, 123, 93-102.
- VIDIGAL, J. A. & VENTURA, A. 2015. The biological functions of miRNAs: lessons from in vivo studies. *Trends in Cell Biology*, 25, 137-147.
- WAN, S., ZHANG, L. Q., WANG, S., LIU, Y., WU, C. C., CUI, C., SUN, H., SHI, M. L., JIANG, Y., LI, L., QIU, L. P. & TAN, W. H. 2017. Molecular Recognition-Based DNA Nanoassemblies

- on the Surfaces of Nanosized Exosomes. *Journal of the American Chemical Society*, 139, 5289-5292.
- WANG, D., CHAI, Y. Q., YUAN, Y. L. & YUAN, R. 2019. Precise Regulation of Enzyme Cascade Catalytic Efficiency with DNA Tetrahedron as Scaffold for Ultrasensitive Electrochemical Detection of DNA. *Analytical Chemistry*, 91, 3561-3566.
- WANG, G. & VASQUEZ, K. 2008. Non-B DNA structure-induced genetic instability in mammalian cells. *Environmental and Molecular Mutagenesis*, 49, 541-541.
- WANG, H., ZHANG, Y. H., MA, H. M., REN, X., WANG, Y. G., ZHANG, Y. & WEI, Q. 2016a. Electrochemical DNA probe for Hg<sup>2+</sup> detection based on a triple-helix DNA and Multistage Signal Amplification Strategy. *Biosensors & Bioelectronics*, 86, 907-912.
- WANG, J. 2006. Electrochemical biosensors: Towards point-of-care cancer diagnostics. *Biosensors & Bioelectronics*, 21, 1887-1892.
- WANG, J. 2008. Electrochemical glucose biosensors. *Chemical Reviews*, 108, 814-825.
- WANG, J. M., WANG, X. Y., WU, S., SONG, J., ZHAO, Y. Q., GE, Y. Q. & MENG, C. G. 2016b. Fabrication of highly catalytic silver nanoclusters/graphene oxide nanocomposite as nanotag for sensitive electrochemical immunoassay. *Analytica Chimica Acta*, 906, 80-88.
- WANG, X. H., LI, Y., WANG, J. D., WANG, Q. L., XU, L. J., DU, J., YAN, S. D., ZHOU, Y., FU, Q. X., WANG, Y. L. & ZHAN, L. S. 2012. A broad-range method to detect genomic DNA of multiple pathogenic bacteria based on the aggregation strategy of gold nanorods. *Analyst*, 137, 4267-4273.
- WANG, X. Z., JIANG, A. W., HOU, T. & LI, F. 2014. A sensitive and versatile "signal-on" electrochemical aptasensor based on a triple-helix molecular switch. *Analyst*, 139, 6272-6278.
- WATANABE, A., KAJITA, M., KIM, J., KANAYAMA, A., TAKAHASHI, K., MASHINO, T. & MIYAMOTO, Y. 2009. In vitro free radical scavenging activity of platinum nanoparticles. *Nanotechnology*, 20.
- WEI, Y. L., ZHOU, W. J., LI, X., CHAI, Y. Q., YUAN, R. & XIANG, Y. 2016. Coupling hybridization chain reaction with catalytic hairpin assembly enables non-enzymatic and sensitive fluorescent detection of microRNA cancer biomarkers. *Biosensors & Bioelectronics*, 77, 416-420.
- WILCOXON, J. P. & ABRAMS, B. L. 2006. Synthesis, structure and properties of metal nanoclusters. *Chemical Society Reviews*, 35, 1162-1194.
- WILLETS, K. A. & VAN DUYNE, R. P. 2007. Localized surface plasmon resonance spectroscopy and sensing. *Annual Review of Physical Chemistry*, 58, 267-297.

- WU, B. H., KUANG, Y. J., ZHANG, X. H. & CHEN, J. H. 2011. Noble metal nanoparticles/carbon nanotubes nanohybrids: Synthesis and applications. *Nano Today*, 6, 75-90.
- WU, L. L., WANG, L. Y., XIE, Z. J., PAN, N. & PENG, C. F. 2016. Colorimetric assay of L-cysteine based on peroxidase-mimicking DNA-Ag/Pt nanoclusters. *Sensors and Actuators B-Chemical*, 235, 110-116.
- WU, Z., LIU, G. Q., YANG, X. L. & JIANG, J. H. 2015. Electrostatic Nucleic Acid Nanoassembly Enables Hybridization Chain Reaction in Living Cells for Ultrasensitive mRNA Imaging. *Journal of the American Chemical Society*, 137, 6829-6836.
- XODO, L. E. 1995. CHARACTERIZATION OF THE DNA TRIPLEX FORMED BY D(TGGGTGGGTGGTTGGGTGGG) AND A CRITICAL R-CENTER-DOT-Y SEQUENCE LOCATED IN THE PROMOTER OF THE MURINE KI-RAS PROTOONCOGENE. *Febs Letters*, 370, 153-157.
- XODO, L. E., MANZINI, G. & QUADRIFOGLIO, F. 1990. SPECTROSCOPIC AND CALORIMETRIC INVESTIGATION ON THE DNA TRIPLEX FORMED BY D(CTCTTCTTTCTTTTCTTTCTTCTC) AND D(GAGAAGAAAGA) AT ACIDIC PH. *Nucleic Acids Research*, 18, 3557-3564.
- YAN, Z. Y., YANG, M., WANG, Z. H., ZHANG, F. F., XIA, J. F., SHI, G. Y., XIA, L., LI, Y. H., XIA, Y. Z. & XIA, L. H. 2015. A label-free immunosensor for detecting common acute lymphoblastic leukemia antigen (CD10) based on gold nanoparticles by quartz crystal microbalance. *Sensors and Actuators B-Chemical*, 210, 248-253.
- YANG, C. Y., SHI, K., DOU, B. T., XIANG, Y., CHAI, Y. Q. & YUAN, R. 2015. In Situ DNA-Templated Synthesis of Silver Nanoclusters for Ultrasensitive and Label-Free Electrochemical Detection of MicroRNA. *Acs Applied Materials & Interfaces*, 7, 1188-1193.
- YEH, Y. C., CRERAN, B. & ROTELLO, V. M. 2012. Gold nanoparticles: preparation, properties, and applications in bionanotechnology. *Nanoscale*, 4, 1871-1880.
- YU, Y. Y., CHEN, Z. G., JIAN, W. S., SUN, D. P., ZHANG, B. B., LI, X. C. & YAO, M. C. 2015. Ultrasensitive electrochemical detection of avian influenza A (H7N9) virus DNA based on isothermal exponential amplification coupled with hybridization chain reaction of DNAzyme nanowires. *Biosensors & Bioelectronics*, 64, 566-571.
- ZADEGAN, R. M. & NORTON, M. L. 2012. Structural DNA Nanotechnology: From Design to Applications. *International Journal of Molecular Sciences*, 13, 7149-7162.
- ZADEH, J. N., STEENBERG, C. D., BOIS, J. S., WOLFE, B. R., PIERCE, M. B., KHAN, A. R., DIRKS, R. M. & PIERCE, N. A. 2011a. NUPACK: Analysis and Design of Nucleic Acid Systems. *Journal of Computational Chemistry*, 32, 170-173.
- ZADEH, J. N., WOLFE, B. R. & PIERCE, N. A. 2011b. Nucleic Acid Sequence Design via Efficient Ensemble Defect Optimization. *Journal of Computational Chemistry*, 32, 439-452.

- ZHANG, Y., LEI, J. P., LING, P. H. & JU, H. X. 2015. Catalytic Hairpin Assembly-Programmed Porphyrin-DNA Complex as Photoelectrochemical Initiator for DNA Biosensing. *Analytical Chemistry*, 87, 5430-5436.
- ZERNECKE, A., BIDZHEKOV, K., NOELS, H., SHAGDARSUREN, E., GAN, L., DENECKE, B., HRISTOV, M., KOPPEL, T., JAHANTIGH, M. N., LUTGENS, E., WANG, S. S., OLSON, E. N., SCHOBER, A. & WEBER, C. 2009. Delivery of MicroRNA-126 by Apoptotic Bodies Induces CXCL12-Dependent Vascular Protection. *Science Signaling*, 2.
- ZHANG, D. Y. & SEELIG, G. 2011. Dynamic DNA nanotechnology using strand-displacement reactions. *Nature Chemistry*, 3, 103-113.
- ZHANG, J., SUN, Y., WU, Q., GAO, Y., ZHANG, H., BAI, Y. & SONG, D. Q. 2014. Preparation of graphene oxide-based surface plasmon resonance biosensor with Au bipyramid nanoparticles as sensitivity enhancer. *Colloids and Surfaces B-Biointerfaces*, 116, 211-218.
- ZHANG, Y., CHEN, Z. W., TAO, Y., WANG, Z. Z., REN, J. S. & QU, X. G. 2015a. Hybridization chain reaction engineered dsDNA for Cu metallization: an enzyme-free platform for amplified detection of cancer cells and microRNAs. *Chemical Communications*, 51, 11496-11499.
- ZHANG, Y., YAN, Y. R., CHEN, W. H., CHENG, W., LI, S. Q., DING, X. J., LI, D. D., WANG, H., JU, H. X. & DING, S. J. 2015b. A simple electrochemical biosensor for highly sensitive and specific detection of microRNA based on mismatched catalytic hairpin assembly. *Biosensors & Bioelectronics*, 68, 343-349.
- ZHANG, Z., WANG, Y. Y., ZHANG, N. B. & ZHANG, S. S. 2016. Self-assembly of nucleic acid molecular aggregates catalyzed by a triple-helix probe for miRNA detection and single cell imaging. *Chemical Science*, 7, 4184-4189.
- ZHAO, H. M., LI, Z. Q., LEE, N. Y., KIM, J. S. & LEE, E. C. 2012. Electrochemical DNA detection using Hoechst dyes in microfluidic chips. *Current Applied Physics*, 12, 1493-1496.
- ZHAO, Y. X., CHEN, F., LI, Q., WANG, L. H. & FAN, C. H. 2015. Isothermal Amplification of Nucleic Acids. *Chemical Reviews*, 115, 12491-12545.
- ZHENG, C., ZHENG, A. X., LIU, B., ZHANG, X. L., HE, Y., LI, J., YANG, H. H. & CHEN, G. N. 2014a. One-pot synthesized DNA-templated Ag/Pt bimetallic nanoclusters as peroxidase mimics for colorimetric detection of thrombin. *Chemical Communications*, 50, 13103-13106.
- ZHENG, J., HU, Y. P., BAI, J. H., MA, C., LI, J. S., LI, Y. H., SHI, M. L., TAN, W. H. & YANG, R. H. 2014b. Universal Surface-Enhanced Raman Scattering Amplification Detector for

Ultrasensitive Detection of Multiple Target Analytes. *Analytical Chemistry*, 86, 2205-2212.

ZHENG, J., LI, J. S., JIANG, Y., JIN, J. Y., WANG, K. M., YANG, R. H. & TAN, W. H. 2011. Design of Aptamer-Based Sensing Platform Using Triple-Helix Molecular Switch. *Analytical Chemistry*, 83, 6586-6592.

ZHENG, Y. K., LAI, L. M., LIU, W. W., JIANG, H. & WANG, X. M. 2017. Recent advances in biomedical applications of fluorescent gold nanoclusters. *Advances in Colloid and Interface Science*, 242, 1-16.

ZHOU, T., WANG, Y. J., DONG, Y. C., CHEN, C., LIU, D. S. & YANG, Z. Q. 2014. Tetrahedron DNA dendrimers and their encapsulation of gold nanoparticles. *Bioorganic & Medicinal Chemistry*, 22, 4391-4394.